

---

Electronic Thesis and Dissertation Repository

---

10-11-2012 12:00 AM

## Exploration of Three-dimensional Morphometrics of the Hip Joint and Reconstructive Technologies

Charys M. Martin

*The University of Western Ontario*

Supervisor

Timothy D. Wilson

*The University of Western Ontario* Joint Supervisor

Charles L. Rice

*The University of Western Ontario*

Graduate Program in Kinesiology

A thesis submitted in partial fulfillment of the requirements for the degree in Doctor of Philosophy

© Charys M. Martin 2012

Follow this and additional works at: <https://ir.lib.uwo.ca/etd>



Part of the [Medical Anatomy Commons](#)

---

### Recommended Citation

Martin, Charys M., "Exploration of Three-dimensional Morphometrics of the Hip Joint and Reconstructive Technologies" (2012). *Electronic Thesis and Dissertation Repository*. 904.

<https://ir.lib.uwo.ca/etd/904>

This Dissertation/Thesis is brought to you for free and open access by Scholarship@Western. It has been accepted for inclusion in Electronic Thesis and Dissertation Repository by an authorized administrator of Scholarship@Western. For more information, please contact [wlsadmin@uwo.ca](mailto:wlsadmin@uwo.ca).

EXPLORATION OF THREE-DIMENSIONAL MORPHOMETRICS OF THE HIP  
JOINT AND RECONSTRUCTIVE TECHNOLOGIES

(Spine title: 3D Morphometrics of the Hip and Reconstructive Technologies)

(Thesis format: Integrated Article)

by

Charys M. Martin

Graduate Program in Kinesiology

A thesis submitted in partial fulfillment  
of the requirements for the degree of  
Doctor of Philosophy

The School of Graduate and Postdoctoral Studies  
The University of Western Ontario  
London, Ontario, Canada

© Charys M. Martin 2012

THE UNIVERSITY OF WESTERN ONTARIO  
School of Graduate and Postdoctoral Studies

**CERTIFICATE OF EXAMINATION**

Supervisor

Examiners

\_\_\_\_\_  
Dr. Timothy Wilson

\_\_\_\_\_  
Dr. Anne Agur

Co- supervisor

\_\_\_\_\_  
Dr. Andrew Nelson

\_\_\_\_\_  
Dr. Charles L. Rice

Supervisory Committee

\_\_\_\_\_  
Dr. Jamie Melling

\_\_\_\_\_  
Dr. Jim Dickey

\_\_\_\_\_  
Dr. Tom Jenkyn

\_\_\_\_\_  
Dr. Aashish Goela

The thesis by

**Charys M. Martin**

entitled:

**Exploration of Three-dimensional Morphometrics of the Hip Joint  
and Reconstructive Technologies**

is accepted in partial fulfillment of the  
requirements for the degree of  
Doctor of Philosophy

\_\_\_\_\_  
Date

\_\_\_\_\_  
Chair of the Thesis Examination Board

## Abstract

This dissertation is an exploration of three-dimensional (3D) anatomy using the hip joint as the model of study. Very few studies have taken advantage of 3D modelling to assess the features of commercially available software, or to assess the validity and reliability of 3D morphometrics. This dissertation compared three reconstructive software programs to survey user appreciation concerning how 3D anatomical reconstructive software can be utilized and then established the advantages and limitations of 3D measurements in the hip joint. Three main studies are presented: the first, a comparison of three widely available 3D reconstructive software programs, Amira, OsiriX, and Mimics. This comparison used a decision matrix to outline which software is best suited for construction of 3D anatomical models, morphometric analysis, and building 3D visualization and learning tools. Mimics was the best-suited program for construction of 3D anatomical models and morphometric analysis. For creating a learning tool the results were less clear. OsiriX was very user-friendly; however, it had limited capabilities. Conversely, although Amira had endless potential and could create complex dynamic videos it had a challenging interface. Based on the overall results of study one, Mimics was used in the second and third studies to quantify 3D surface morphology of the hip joint. The second study assessed the validity and reliability of a novel 3D measurement approach of the femoral head (n=45). Study two highlighted the advantages of modelling a convex shape and the advantages of quantifying the proximal femur in 3D. This measurement approach proved to be valid and reliable. The third study assessed the validity and reliability of a similar 3D measurement approach applied to the acetabulum (n=45). This study illustrated the limitations and challenges encountered when quantifying the complex geometry of the concave acetabulum. This measurement approach was reliable, yet the differences between the digital and cadaveric measurements were large and clinically significant. The hip joint is a complex joint that benefits from 3D visualization and quantification; however, challenges surrounding measuring the acetabulum remain.

## Keywords

3D, Hip, Imaging, Femur, Acetabulum, Joint, Morphometrics, Reconstructive Software, Decision Matrix, CT



## Co-Authorship Statement

The written material in this thesis is the original work of the author. Charys Martin participated in all aspects of the work contained herein: conception of the hypotheses, conduction of the experiments, and authorship of the manuscripts. The roles of the co-authors are outlined below.

### Chapter 3:

This manuscript will be submitted to the Journal of Digital Imaging. C.M. Martin and T.D. Wilson shared in the conception of this research study. All authors on the manuscript, C.M. Martin, T.D. Wilson, C.L. Rice, V.A. Roach, and N. Nguyen, shared in the creation of the methodology of this study. The data for this study was collected, analyzed, and interpreted by C.M. Martin. C.M. Martin prepared the manuscript with inputs from all authors.

### Chapter 4:

This manuscript will be submitted to the Journal of Anatomy. C.M. Martin and T.D. Wilson shared in the conception of this research study. All authors on the manuscript, C.M. Martin, T.D. Wilson, C.L. Rice, J.G. Turgeon, and A. Goela, shared in the creation of the methodology. C.M. Martin and J.G. Turgeon collected data for this study; these data were analyzed and interpreted by C.M. Martin. C.M. Martin prepared the manuscript with inputs from all authors.

### Chapter 5:

This manuscript is in preparation. C.M. Martin and T.D. Wilson shared in the conception of this research study. All authors on the manuscript, C.M. Martin, T.D. Wilson, C.L. Rice, J.G. Turgeon, shared in the creation of the methodology. C.M. Martin and J.G. Turgeon collected data for this study; these data were analyzed and interpreted by C.M. Martin. C.M. Martin prepared the manuscript with inputs from all authors.

## Acknowledgments

My graduate career has been neither easy nor straightforward; however, along the way I have gained knowledge and experience well beyond the scope of this dissertation. The past four years would have been impossible without the guidance and support of many advisors and colleagues.

First I would like to thank my supervisors Dr. Timothy Wilson and Dr. Charles Rice. Your mentorship has been invaluable in my development as an academic, and for that I am thankful. Dr. Wilson, thank you for the opportunity to grow independently as a scientist while still providing me with the encouragement and support to succeed. Dr. Rice, thank you for always being available to support and guide me through this process.

To my advisors Dr. Aashish Goela and Dr. Jim Dickey, thank you for expert advice. Dr. Goela, your clinical expertise was invaluable. Dr. Dickey, your insightful comments and constructive criticisms always helped me to look at my work from a different angle and enabled me to broaden my knowledge base. It was a pleasure working with you and I hope that I will have that pleasure again in the future.

I also wish to express my gratitude to the Western University Body Bequeathal Program for the use of the cadaveric specimens; Dr. Cynthia Dunning for the use of your computer lab; Dr. Cesare Romagnoli for your clinical expertise early in the planning process; Kamal Agarwal, Gleb Naboka, and Erin Bussin for your assistance in preparing the cadaveric specimens; and Dr. Chris Lee for your guidance with regards to data analysis.

I am indebted to my student colleagues who have been involved with my projects over the years: James Turgeon, Victoria Roach, Dr. Ngan Nguyen, Jeremy Roth, Lauren Allen, Tamara Stock, and Mike Midgely. Thank you all for taking time to serve as observers, decision-makers, and recorders for my projects, I greatly appreciate it. A special thank you to Sid Bhattacharya for all of your technical support.

To the 2<sup>nd</sup> year B.Sc. Kin Students 2009-2011, thank you for being the best part of my week. Thank you for regularly reminding me why I chose to complete a doctoral degree. Teaching

anatomy is my passion and I hope that you all gained as much from the Kin 2221 labs as I did. To Gary Lapenski, Dr. Timothy Wilson, Dr. Marjorie Johnson, and Dr. Peter Haase, thank you for showing me what it means to be a great teacher. I aspire to be as engaging and inspiring as all of you one day. Additional thanks to Dr. Marjorie Johnson for being my unofficial advisor; your care and guidance is very much appreciated.

Thank you to the Department of Anatomy and Cell Biology for adopting me into your department for the past four years. To the department's clinical anatomy students from 2008-2011, thank you for creating such a fun work environment, especially Dr. Ngan Nguyen, Michele Barbeau, and Victoria Roach. You ladies helped me maintain my sanity over the past four years and I would have never been able to get this far without all of your support and love. Thank you for being there to share laughs, cries, and Friday dance parties.

I would like to express my heart-felt gratitude to my family, who has always believed in me, even when I didn't believe in my self. The love and encouragement provided to me by my whole family has been immeasurable, and has sustained me on my academic journey. Mom and Dad, thank you for instilling in me the drive and determination that enabled me to push through the hard times.

Finally, and most importantly, I wish to thank my husband, Dave. You are my rock and I could not have completed this dissertation without your love and unconditional support. Thank you for everything. To you I dedicate this dissertation.

# Table of Contents

<b>CERTIFICATE OF EXAMINATION .....</b>	<b>ii</b>
Abstract.....	iii
Co-Authorship Statement.....	iv
Acknowledgments.....	v
Table of Contents.....	vii
List of Figures .....	xiii
List of Appendices .....	xv
List of Abbreviations and Terms .....	xvi
Chapter 1 .....	1
1. General Introduction .....	1
1.1 Introduction to the Dissertation .....	1
1.2 3D Modelling.....	2
1.3 3D Reconstructive Software Programs.....	3
1.4 3D Modelling and Morphometrics of the Hip Joint.....	3
1.5 The Proximal Femur .....	4
1.6 The Acetabulum.....	5
1.7 Overall Objectives and Aims .....	6
1.8 References.....	6
Chapter 2.....	11
2 Literature Review.....	11
2.1 Anatomy of the Hip Joint.....	11
2.1.1 The Acetabulum.....	11
2.1.2 The Proximal Femur .....	12
2.2 Osteoarthritis.....	12

2.3 Hip Instability .....	13
2.3.1 Possible Causes of Hip Instability .....	14
2.3.2 Association of Osteoarthritis with Hip Instability .....	14
2.4 Femoroacetabular Impingement .....	15
2.4.1 Mechanisms of Impingement.....	15
2.4.2 Possible Causes of Femoroacetabular Impingement .....	19
2.4.3 Association of Osteoarthritis with Femoroacetabular Impingement .....	19
2.5 Diagnostic Measurement .....	20
2.5.1 Diagnostic Measurement for Hip Instability.....	20
2.5.2 Diagnostic Measurement for Femoroacetabular Impingement.....	22
2.5.3 Reliability of Measures .....	24
2.5.4 Challenges with Current Measures .....	24
2.6 Treatment .....	25
2.6.1 Treatment of Hip Instability.....	25
2.6.2 Treatment of Femoroacetabular Impingement.....	25
2.7 3D Modelling.....	26
2.7.1 3D Modelling in Measurement .....	26
2.7.2 3D Modelling in Education.....	27
2.8 Why is a Comparison Needed?.....	28
2.9 3D Reconstructive Software Programs .....	29
2.9.1 Amira .....	29
2.9.2 OsiriX.....	30
2.9.3 Mimics .....	31
2.9.4 Previous Assessment of the 3D Reconstructive Software Programs.....	32
2.10References.....	33
Chapter 3.....	41

3	Comparison of 3D Reconstructive Technologies used for Morphometric Research and the Translation of Knowledge.....	41
3.1	Introduction.....	41
3.2	Methods and Materials.....	44
3.2.1	Decision-Makers .....	44
3.2.2	3D Reconstructive Programs .....	45
3.2.3	Assessment.....	45
3.3	Results.....	47
3.3.1	Cost .....	47
3.3.2	System Requirements.....	48
3.3.3	Program Features .....	48
3.3.4	Decision Matrix - Morphometric Research Weighting Scale Results .....	50
3.3.5	Decision Matrix - Educational Features Weighting Scale Results .....	51
3.3.6	Open-ended Comments.....	54
3.3.7	Preference Questionnaire .....	55
3.4	Discussion .....	57
3.4.1	Program Features .....	57
3.4.2	Decision Matrix - Morphometric Research Weighting Scale.....	58
3.4.2.1	Morphometric Research Weighting Scale: 3D Modelling .....	58
3.4.2.2	Morphometric Research Weighting Scale: Measurement Tools .....	59
3.4.3	Decision Matrix - Educational Weighting Scale .....	60
3.4.3.1	Educational Weighting Scale: 3D Modelling.....	61
3.4.3.2	Educational Weighting Scale: Measurement Tools .....	62
3.4.3.3	Educational Weighting Scale: Educational Features.....	62
3.5	References.....	64
	Chapter 4.....	68

4	Validity and Reliability of a Novel 3D Measurement Approach for the Morphology of the Proximal Femur.....	68
4.1	Introduction.....	68
4.2	Methods and Materials.....	70
4.2.1	Cadaveric Measurements .....	71
4.2.2	Digital Measurements .....	72
4.2.3	Statistical Analysis.....	73
4.3	Results.....	74
4.3.1	Reliability of Femoral Head Surface Measurements .....	74
4.3.1.1	Intraobserver Reliability .....	74
4.3.1.2	Interobserver Reliability .....	75
4.3.2	Validity of Femoral Head Surface Measurements.....	77
4.4	Discussion .....	79
4.5	References.....	82
	Chapter 5.....	86
5	Validity and Reliability of a Novel 3D Measurement Approach for the Morphology of the Acetabulum .....	86
5.1	Introduction.....	86
5.2	Methodology .....	88
5.2.1	Cadaveric Acetabular Measurements .....	89
5.2.2	Digital Acetabular Measurements.....	90
5.2.3	Statistical Analysis.....	91
5.3	Results.....	92
5.3.1	Reliability of Acetabular Surface Measurements .....	92
5.3.1.1	Intraobserver Reliability .....	92
5.3.1.2	Interobserver Reliability .....	93
5.3.2	Validity of Acetabular Surface Measurements.....	95

5.4 Discussion .....	97
5.5 References .....	102
6 General Discussion .....	105
6.1 Introduction .....	105
6.2 3D Modelling .....	105
6.3 3D Reconstructive Software Programs .....	106
6.4 3D Modelling and Morphometrics of the Hip Joint .....	108
6.5 Future Directions .....	110
6.6 Conclusion .....	112
6.7 References .....	113
Appendices .....	115
Curriculum Vitae .....	155



## List of Tables

Table 3.1 - Program information and features .....	48
Table 3.2 - Decision-maker comments regarding each 3D reconstructive software program	54
Table 3.3 - Preference criteria combinations for creating an educational tool .....	56

## List of Figures

Figure 2.1 – Types of FAI.....	16
Figure 2.2 - FAI pathology during flexion.....	18
Figure 2.3 - Centre-edge (CE) angle.....	21
Figure 2.4 - Vertical-centre-anterior (VCA) angle.....	22
Figure 2.5 - Alpha angle.....	23
Figure 3.1: Overall novice and experienced scores for each 3D reconstructive program using the morphometric research weighting scale.....	50
Figure 3.2 - Novice and experienced scores, for each 3D reconstructive program using the morphometric research weighting scale, for (A) 3D modelling criteria and (B) measurement tools criteria .....	51
Figure 3.3 - Overall novice and experienced scores for each 3D reconstructive program using the educational features weighting scale.....	52
Figure 3.4 - Novice and experienced scores, for each 3D reconstructive program using the educational weighting scale, for (A) 3D modelling criteria, (B) measurement tools criteria, and (C) educational features criteria .....	53
Figure 3.5 - Final questionnaire preferences regarding program interface, 3D modelling features, measurement tools, and educational features.....	56
Figure 4.1 – Measurement of the femoral cadaveric specimens.....	71
Figure 4.2 - Measurement of the femoral digital models.....	73
Figure 4.3 - Polar graphs of intraobserver reliability measurements of femoral head surface.....	75

Figure 4.4 – Bland-Altman plot of intraobserver variability of the (A) femoral cadaveric measures and (B) femoral digital measures. ....	75
Figure 4.5 - Polar graphs of interobserver reliability measurements of the femoral head surface. ....	76
Figure 4.6 – Bland-Altman Plot of interobserver variability of the (A) femoral cadaveric measures and (B) femoral digital measures. ....	77
Figure 4.7 - Polar graph of mean femoral cadaveric and digital measurements.....	78
Figure 4.8 - Bland-Altman plot of the difference between the femoral cadaveric and the digital measurements. ....	78
Figure 5.1 - Measurement of the acetabular cadaveric specimens. ....	89
Figure 5.2 - Measurement of the acetabular digital models.....	91
Figure 5.3 - Polar graphs of intraobserver reliability measurements of the acetabular surface. ....	93
Figure 5.4 – Bland-Altman plots of intraobserver variability of the (A) acetabular cadaveric measures and (B) acetabular digital measures. ....	93
Figure 5.5 - Polar graphs of interobserver reliability measurements of the acetabular surface. ....	94
Figure 5.6 – Bland-Altman plots of interobserver variability of the (A) acetabular cadaveric measures and (B) acetabular digital measures. ....	95
Figure 5.7 - Polar graph of mean acetabular cadaveric measures and digital measures.....	96
Figure 5.8 - Bland-Altman plot of the difference between the acetabular cadaveric measurements and the acetabular digital measurements. ....	96

## List of Appendices

Appendix A: 3D Reconstructive Software Assessment Form and Final Questionnaire .....	115
Appendix B: Amira Instructional Guide.....	119
Appendix C: OsiriX Instructional Guide .....	128
Appendix D: Mimics Instructional Guide.....	137
Appendix E: Decision Matrix .....	146
Appendix F: Cadaveric Acetabular Measurements with Labra Removed.....	147
Appendix G: Permissions .....	150

## List of Abbreviations and Terms

### **Abbreviations:**

**AD** – Acetabular Dysplasia

**AP View** – Anteroposterior Radiographic View

**AW** – GE’s Advantage Workstation Volume Share 4

**CE** – Centre-edge Angle

**CI** – Confidence Interval

**CT** – Computed-Tomography

**DDH** - Developmental Dysplasia of the Hip

**DICOM** – Digital Imaging and Communications in Medicine

**FAI** – Femoroacetabular Impingement

**FEM** – Finite Element Modelling

**FP View** – False Profile Radiographic View

**MRI** – Magnetic Resonance Imaging

**N/A** – Not Applicable

**OA** – Osteoarthritis

**ROM** – Range of Motion

**TIVMI** - Treatment and Increased Vision for Medical Imaging

**VCA** – Vertical-centre-anterior Angle

### **Glossary of Terms:**

**Acetabular Depth** – Measures the relationship of the floor of the fossa acetabuli and the femoral head relative to the ilioischial line

*Profunda* – The floor of the fossa acetabuli touches or is medial to the ilioischial line

*Protrusio* – The medial edge of the femoral head is medial to the ilioischial line

**Acetabular Inclination** – Measures the angle between the face of the acetabular cup and the transverse pelvic axis

**Acetabular Version (crossover sign)** – Measures the relationship between the anterior and posterior wall of the acetabulum

*Anteverted Acetabuli* – The anterior wall does not cross the posterior wall of the acetabulum before reaching the lateral edge of the sourcil on an anterior-posterior radiograph

*Retroverted Acetabuli* – The anterior wall does cross over the posterior wall of the acetabulum before reaching the lateral edge of the sourcil on an anterior-posterior radiograph

**Anteroposterior (AP) View** – Focus-film distance is 100cm. If possible, the AP view should be obtained with the patient in a standing position with approximately 20° of internal rotation of the lower limbs, to compensate for femoral anteversion.

**Athropathy** – A disease of an abnormality of a joint

**Capsulorrhaphy** – Suture of a tear in a capsule, especially of a joint capsule to prevent recurring dislocation

**Centre-edge (CE) Angle** – Measures the superolateral acetabular coverage over the femoral head

**Coxa Vara** - a deformity of the hip, whereby the angle between the head and the shaft of the femur is reduced to less than 120°

**False Profile (FP) View** – This radiographic view is obtained with the patient standing and the affected side of the pelvis rotated 65° relative to the film

**Femoral Anteversion** - A condition where the femoral neck is angled more anteriorly causing the lower extremity to rotate internally

**Femoral Head Center** – Measures the center of the femoral head on an anterior-posterior radiograph

*Lateralized Head Center* – The medial aspect of the femoral head was greater than 10mm from the ilioischial line

**Femoral Head Sphericity** – Measured by applying a reference circle template (Mose templates) on an anterior-posterior radiograph, frog lateral radiograph and/or crosstable lateral radiograph

*Non Spherical* – The femoral epiphysis extends beyond the margin of the reference circle by 2mm or more

**Femoral Head-neck Offset** – Measures the concavity of the femoral head-neck junction on an anterior-posterior radiograph, frog lateral radiograph and/or crosstable lateral radiograph

**Ilioischial Line** – a line connecting the most lateral aspect of the pelvic brim and the most lateral aspect of the obturator foramen on an anterior-posterior radiograph

**Joint Congruency** – Measures the alignment of the arc of the femoral head in relationship to the arc of the acetabulum

**Learning** – the process of gaining knowledge and/or experience

**Legg-Calve-Perthes Disease** – Primary avascular necrosis of the capital femoral epiphysis

**Model** – A representation in three dimensions of an existing person or thing or of a proposed structure

**Morphometrics** – The quantitative analysis of form (size and shape)

**Osteoplasty** – Surgical repair or alteration of bone

**Osteotomy** – Surgical division or sectioning of bone

**Reliability** - or **Precision** or **Reproducibility** is defined as the degree to which the same method produces the same results on repeated measurements

**Segmentation** – Delineation of anatomical structures and other regions of interest on data sets from three-dimensional imaging modalities, such as computed-tomography and magnetic resonance imaging

**Slipped Capital Femoral Epiphysis** – refers to a fracture through the femoral head physis (growth plate), which results in slippage of the overlying epiphysis

**Tönnis Grade** – Classification system to grade osteoarthritic radiographic changes

**Validity** – or **Accuracy** is the degree to which an instrument measures the real value of a variable

**Vertical-centre-anterior (VCA) Angle** – Measures the anterior acetabular coverage over the femoral head



# Chapter 1

## 1. General Introduction

### 1.1 Introduction to the Dissertation

This dissertation is an exploration of three-dimensional (3D) anatomy using the hip joint as the main model of study. There are very few studies that have taken advantage of 3D modelling to test the validity and reliability of morphometrics of the hip joint as a basis for clinical applications, or to assess the features of commercially available software for analysis and knowledge transfer of 3D anatomy in general. In this dissertation I have combined these ideas by first taking a broad assessment of software available to aid in understanding how 3D anatomical software can be utilized, and then using the results of the software analysis I have assessed in detail some of the advantages and limitations of 3D measurements in a complex joint. Three main studies are presented: the first, a comparison of three widely available 3D reconstructive software programs and their ability to construct 3D anatomical models, conduct morphometric research with those models, and build 3D visualization and learning tools with the models; the second, a study analyzing the validity and reliability of a novel 3D measurement approach of the femoral head; and the third, a study analyzing the validity and reliability of a similar novel 3D measurement approach of the acetabulum. The order of presentation was chosen so the reader could appreciate the complexities of 3D software available to perform such measurements and to create learning tools to explain the new knowledge regarding the complex hip joint and morphometrics of the hip. Then using this knowledge regarding reconstructive software, the reader can comprehend the advantages and challenges surrounding 3D measurement of the hip joint. Thus, Chapter Three takes a broad approach to objectively compare and assess 3D reconstructed software available to

users who wish to perform these types of morphometric analyses. Chapter Four highlights the advantages of 3D modelling on a complex, essentially convex shape, the femoral head, and Chapter Five illustrates some of the challenges and limitations encountered with the congruent portion of the hip joint, the essentially concave and more irregular acetabulum, as compared to the femoral head. This dissertation provides a solid understanding of which 3D software is appropriate to use for morphometric research and education. It provides a foundation to establish a 3D measurement approach for the hip joint as well as enlightening the reader to the complexity of measuring the contours of human anatomy.

## 1.2 3D Modelling

Since the advent of computed-tomography (CT) and magnetic resonance imaging (MRI), the use of (3D) modelling for education, pre- and post-operative assessment, pre-surgical planning, and measurement has become more prevalent [1-3]. 3D modelling allows optimal visualization of complex anatomical structures and may afford novel and more precise measurement possibilities [4].

3D anatomical modelling has many advantages over traditional techniques, enabling complete visualization of complex anatomical morphology [4]. Traditional two-dimensional (2D) imaging techniques, such as plain radiographs and cross-sectional slices, are improving into 3D volume acquisitions reconstructed into 3D models of the anatomy [5]. In morphometrics, 3D modelling enables measurement of the entire 3D shape or morphology, as opposed to traditional measurements that are linear and are taken on 2D scans [6]. The transfer of knowledge with regard anatomical morphology, measurement, and surgical techniques is relying more and more on 3D modelling. These 3D models help learners conceptualize structures and spatial relationships that are difficult to visualize with other traditional learning tools [7].

### 1.3 3D Reconstructive Software Programs

In the last few decades, the increased speed and decreased cost of high quality computers has resulted in the greater availability of 3D reconstructive software programs becoming widely available [29]. These programs have been developed for all levels of training, from the general public to medical professionals [30]. A variety of 3D reconstructive software programs have been developed for scientific and educational use; however, no program has become the standard and all of the programs available differ in concept (surface-rendered or volume-rendered), operating system, features, and cost [4, 29].

As a result of the abundance of programs available, studies comparing available software programs have been conducted [4], [31, 32]. However, no study has been completed that evaluates the features of widely available medical imaging programs. Amira, OsiriX, and Mimics are three programs that are widely available, cost effective, and commonly used for morphometric research, building educational tools, pre-operative assessment, and pre-surgical planning [32-43]. A comparison study that objectively assesses these programs for usability, quality of models, features, and time efficiency is required.

### 1.4 3D Modelling and Morphometrics of the Hip Joint

Noninvasive morphometrics of the hip joint may benefit from 3D modelling. The hip joint is a complex anatomical structure comprised of many surfaces and contours that are three-dimensional in nature. Osteoarthritis (OA) is a major pathological condition that affects the hip joint and is associated with significant disability. Furthermore, morphological variations of the proximal femur and the acetabulum have been identified as potential factors contributing to osteoarthritis [8]. Radiographic examination is essential in screening patients to identify these underlying structural variations, in order to establish an accurate diagnosis, and develop a treatment strategy [9]. However, the

current methods used to define the geometry of the hip use pre-determined measures, typically lengths and angles, on 2D radiographic planes. Fitting these 2D measures to individual variations within a patient population is difficult. These linear measures may not assess the relevant clinical deviations because projecting 3D geometry on to 2D planes does not accurately account for the entire complex joint morphology [6, 10]. Additionally, given the large articular surface area of the hip joint, current 2D imaging methods result in an overlap of the femur and acetabulum and fail to analyze variations in osseous morphology that may be hidden by a hip in situ [11]. Creating 3D models of the morphology allows for the two anatomical structures of the hip joint, the proximal femur and the acetabulum, to be separated for visualization of the entire structure. A valid and reliable 3D measurement approach of the hip joint may assist further research in the area of the hip joint and may lead to a further understanding of the relationship between morphological variations of the hip joint and osteoarthritis. Further understanding of this relationship may lead to more timely diagnoses and treatments of morphological variations of the hip joint leading to a decrease in severe degenerative disease of the hip.

## 1.5 The Proximal Femur

One of the areas affected by morphological variations that can lead to OA is the proximal femur. The proximal femur consists of a spherical femoral head that articulates with the acetabulum [12]. Two conditions associated with proximal femur morphology variations are cam-femoroacetabular impingement (cam-FAI) and atraumatic hip instability [13-15].

Cam-FAI is characterized by a decreased head-neck offset of the anterosuperior-lateral aspect of the femoral-head neck junction [16-19]. Cam-FAI is assessed using the head-neck offset ratio [20] and the alpha angle [21]. Acetabular dysplasia (AD) is the primary cause of atraumatic hip instability and is characterized by insufficient anterolateral femoral head coverage by the acetabulum and superolateral inclination of the acetabular surface [22, 23]. Morphological changes in the dysplastic hip can result in a misshapen

femoral head and increased anteversion of the femoral neck [16, 23]. The centre-edge (CE) angle [24] and the vertical-centre-anterior (VCA) angle [25] are used to quantify acetabular coverage.

Early detection and appropriate treatment of hip instability and cam-FAI may help prevent the progression of OA [16, 17, 21, 26, 27]. However, the current radiographic parameters for diagnosing these conditions are unreliable [9, 15]. A clear set of measurements that quantify the entire 3D surface morphology of the proximal femur need to be defined to enable a more reliable diagnosis of early hip disease [15].

## 1.6 The Acetabulum

The other area affected by morphological variations that can lead to OA is the acetabulum. The acetabulum is comprised of all three pelvic bones; the ilium, the ischium, and the pubis. The acetabulum is deepened further via the acetabular labrum and the transverse acetabular ligament [23]. Two conditions that define the morphological variations of the acetabulum that are associated with OA are pincer-FAI and hip instability [13-15].

Pincer-FAI is defined as an abnormally deep acetabulum, which results in an overcoverage of the acetabulum over the femoral head [16-18, 28]. The CE angle, which is used to assess acetabular insufficiency (AD), can also assess acetabular overcoverage (pincer-FAI). Morphological changes caused by AD can also result in a shallow anteverted acetabulum [16, 23]. The CE angle [24] and the VCA angle [25] are used to quantify insufficient acetabular coverage.

Early detection and treatment of these morphological variations may help prevent the progression of degenerative disease [16, 17, 21, 26, 27]; however, the CE angle and the VCA angle have been found to be unreliable [9, 15]. A clear set of measurements that

quantify the entire 3D surface morphology of the acetabulum need to be defined to allow for more reliable diagnosis of early hip disease [15].

## 1.7 Overall Objectives and Aims

The overall objective of this dissertation is to explore the 3D reconstructive software programs available for morphometric and educational purposes and to explore the morphometrics of the hip joint in 3D. There are three main aims to this dissertation. One: to assess the features, quality, and usability of widely available, cost effective 3D reconstructive software programs that can be used to measure 3D morphology and help translate knowledge regarding 3D morphology. Two: to create and test the validity and reliability of a 3D measurement approach that quantifies the 3D morphology of the proximal femur. And finally three: to create and test the validity and reliability of a 3D measurement approach that quantifies the 3D morphology of the acetabulum in a way that can be used in conjunction with the proximal femur measurement approach. Thus, the two measurement approaches can quantify each bone separately but essentially can also quantify the articulating bones in relation to one another.

## 1.8 References

1. Humbert, L., H. Carlioz, A. Baudoin, W. Skalli, and D. Mitton, *3D Evaluation of the acetabular coverage assessed by biplanar X-rays or single anteroposterior X-ray compared with CT-scan*. Computer Methods in Biomechanics and Biomedical Engineering, 2008. **11**(3): p. 257 - 262.
2. Rosse, C., *The Potential of Computerized Representations of Anatomy in the Training of Health Care Providers*. Academic Medicine, 1995. **70**(6): p. 499-505.

3. Bale, R. and G. Widmann, *Navigated CT-guided interventions*. Minimally Invasive Therapy & Allied Technologies, 2007. **16**(4): p. 196-204.
4. Landes, C.A., F. Weichert, P. Geis, F. Helga, and M. Wagner, *Evaluation of two 3D virtual computer reconstructions for comparison of cleft lip and palate to normal fetal microanatomy*. The Anatomical Record Part A: Discoveries in Molecular, Cellular, and Evolutionary Biology, 2006. **288A**(3): p. 248-262.
5. Rosset, A., L. Spadola, and O. Ratib, *OsiriX: An Open-Source Software for Navigating in Multidimensional DICOM Images*. Journal of Digital Imaging, 2004. **17**(3): p. 205-216.
6. Waarsing, J.H., R.M. Rozendaal, J.A.N. Verhaar, S.M.A. Bierma-Zeinstra, and H. Weinans, *A statistical model of shape and density of the proximal femur in relation to radiological and clinical OA of the hip*. Osteoarthritis and Cartilage, 2010. **18**(6): p. 787-794.
7. Vernon, T. and D. Peckham, *The benefits of 3D modelling and animation in medical teaching*. The Journal of audiovisual media in medicine, 2002. **25**(4): p. 142-8.
8. Gregory, J.S., J.H. Waarsing, J. Day, H.A. Pols, M. Reijman, H. Weinans, and R.M. Aspden, *Early identification of radiographic osteoarthritis of the hip using an active shape model to quantify changes in bone morphometric features: Can hip shape tell us anything about the progression of osteoarthritis?* Arthritis & Rheumatism, 2007. **56**(11): p. 3634-3643.
9. Carlisle, J.C., L.P. Zebala, D.S. Shia, D. Hunt, P.M. Morgan, H. Prather, R.W. Wright, K. Steger-May, and J.C. Clohisy, *Reliability of various observers in determining common radiographic parameters of adult hip structural anatomy*. The Iowa Orthopaedic Journal, 2011. **31**: p. 52-58.
10. Beaulé, P.E., E. Zaragoza, K. Motamedi, N. Copelan, and F.J. Dorey, *Three-dimensional computed tomography of the hip in the assessment of femoroacetabular impingement*. J Orthop Res, 2005. **23**(6): p. 1286-92.
11. Audenaert, E., L. Vigneron, and C. Pattyn, *A method for three-dimensional evaluation and computer aided treatment of femoroacetabular impingement*. Computer aided surgery : official journal of the International Society for Computer Aided Surgery, 2011. **16**(3): p. 143-8.
12. Moore, K.L. and A.M.R. Agur, *Essential Clinical Anatomy*. Second Edition ed, ed. B. Sun 2002, Baltimore: Lippincott Williams & Wilkins. 691.
13. Lynch, J.A., N. Parimi, R.K. Chaganti, M.C. Nevitt, and N.E. Lane, *The association of proximal femoral shape and incident radiographic hip OA in elderly women*. Osteoarthritis and Cartilage, 2009. **17**(10): p. 1313-1318.

14. Harris-Hayes, M. and N.K. Royer, *Relationship of acetabular dysplasia and femoroacetabular impingement to hip osteoarthritis: a focused review*. PM & R : the journal of injury, function, and rehabilitation, 2011. **3**(11): p. 1055-1067 e1.
15. Clohisy, J.C., J.C. Carlisle, R. Trousdale, Y.J. Kim, P.E. Beaulé, P. Morgan, K. Steger-May, P.L. Schoenecker, and M. Millis, *Radiographic evaluation of the hip has limited reliability*. Clin Orthop Relat Res, 2009. **467**(3): p. 666-75.
16. Ganz, R., J. Parvizi, M. Beck, M. Leunig, H. Notzli, and K.A. Siebenrock, *Femoroacetabular impingement: a cause for osteoarthritis of the hip*. Clin Orthop Relat Res, 2003(417): p. 112-20.
17. Lavigne, M., J. Parvizi, M. Beck, K.A. Siebenrock, R. Ganz, and M. Leunig, *Anterior femoroacetabular impingement: part I. Techniques of joint preserving surgery*. Clin Orthop Relat Res, 2004(418): p. 61-6.
18. Beck, M., M. Kalhor, M. Leunig, and R. Ganz, *Hip morphology influences the pattern of damage to the acetabular cartilage: femoroacetabular impingement as a cause of early osteoarthritis of the hip*. J Bone Joint Surg Br, 2005. **87**(7): p. 1012-8.
19. Gosvig, K.K., S. Jacobsen, S. Sonne-Holm, and P. Gebuhr, *The prevalence of cam-type deformity of the hip joint: a survey of 4151 subjects of the Copenhagen Osteoarthritis Study*. Acta Radiologica, 2008. **49**(4): p. 436-41.
20. Eijer, H., Leunig, M., Mahomed, M., and Ganz, R., *Cross-table lateral radiographs for screening of anterior femoral head-neck offset in patients with femoro-acetabular impingement*. Hip International, 2001. **11**(1): p. 37-41.
21. Notzli, H.P., T.F. Wyss, C.H. Stoecklin, M.R. Schmid, K. Treiber, and J. Hodler, *The contour of the femoral head-neck junction as a predictor for the risk of anterior impingement*. J Bone Joint Surg Br, 2002. **84**(4): p. 556-60.
22. Violas, P., F. Fassier, R. Hamdy, M. Duhaime, and F.H. Glorieux, *Acetabular protrusion in osteogenesis imperfecta*. J Pediatr Orthop, 2002. **22**(5): p. 622-5.
23. Boykin, R.E., A.W. Anz, B.D. Bushnell, M.S. Kocher, A.J. Stubbs, and M.J. Philippon, *Hip instability*. Journal of the American Academy of Orthopaedic Surgeons, 2011. **19**(6): p. 340-349.
24. Wiberg, G., *Studies on dysplastic acetabula and congenital subluxation of the hip joint. with special reference to the complication of osteo-arthritis*. Acta Chirurgica Scandinavica, 1939. **83**(Suppl 58): p. 1-135.



25. Lequesne, M. and S. de, *[False profile of the pelvis. A new radiographic incidence for the study of the hip. Its use in dysplasias and different coxopathies.]*. Rev Rhum Mal Osteoartic, 1961. **28**: p. 643-52.
26. James, S.L., K. Ali, F. Malara, D. Young, J. O'Donnell, and D.A. Connell, *MRI findings of femoroacetabular impingement*. AJR Am J Roentgenol, 2006. **187**(6): p. 1412-9.
27. Kassarian, A., M. Brisson, and W.E. Palmer, *Femoroacetabular impingement*. European Journal of Radiology, 2007. **63**(1): p. 29-35.
28. Laude, F., T. Boyer, and A. Nogier, *Anterior femoroacetabular impingement*. Joint Bone Spine, 2007. **74**(2): p. 127-32.
29. Haas, A. and M.S. Fischer, *Three-dimensional reconstruction of histological sections using modern product-design software*. The Anatomical Record, 1997. **249**(4): p. 510-516.
30. Gehrman, S., K.H. Höhne, W. Linhart, B. Pflessner, A. Pommert, M. Riemer, U. Tiede, J. Windolf, U. Schumacher, and J.M. Rueger, *A novel interactive anatomic atlas of the hand*. Clinical Anatomy, 2006. **19**(3): p. 258-266.
31. Guyomarc'h, P., F. Santos, B. Dutailly, P. Desbarats, C. Bou, and H. Coqueugnot, *Three-dimensional computer-assisted craniometrics: A comparison of the uncertainty in measurement induced by surface reconstruction performed by two computer programs*. Forensic Science International, 2012. **219**(1-3): p. 221-7.
32. Matsumoto, T., Kanzaki, M., Amiki, M., Shimizu, T., Maeda, H., Sakamoto, K., Ookubo, Y., Onuki, T., *Comparison of three software programs for three-dimensional graphic imaging as contrasted with operative findings*. Eur J Cardiothorac Surg, 2012. **41**(5): p. 1098-103.
33. Brandt, R., T. Rohlfing, J. Rybak, S. Krofczik, A. Maye, M. Westerhoff, H.-C. Hege, and R. Menzel, *Three-dimensional average-shape atlas of the honeybee brain and its applications*. The Journal of Comparative Neurology, 2005. **492**(1): p. 1-19.
34. Wang, Z., F. Zeng, H. Li, Z. Ye, Y. Bai, W. Xia, and B. Liang, *Three-dimensional reconstruction on PC-Windows platform for evaluation of living donor nephrectomy*. Computer Methods and Programs in Biomedicine, 2007. **86**(1): p. 39-44.
35. Nguyen, N. and T.D. Wilson, *A head in virtual reality: development of a dynamic head and neck model*. Anatomical Sciences Education, 2009. **2**(6): p. 294-301.

36. Handzel, O., H. Wang, J. Fiering, J.T. Borenstein, M.J. Mescher, E.E. Swan, B.A. Murphy, Z. Chen, M. Peppi, W.F. Sewell, S.G. Kujawa, and M.J. McKenna, *Mastoid cavity dimensions and shape: method of measurement and virtual fitting of implantable devices*. Audiology & neuro-otology, 2009. **14**(5): p. 308-14.
37. Kramer, J., G. Laub, C. Czerny, and M.P. Recht, *MR and MR Arthrography*, in *Medical Radiology Diagnostic Imaging*, A.L. Baert and K. Sartor, Editors. 2008, Springer: Berlin, Heidelberg, New York. p. 31-48.
38. Kim, J., J. Wang, J. Ahn, H. Kim, and H. Lim, *Comparison of femoral tunnel length between transportal and retrograde reaming outside-in techniques in anterior cruciate ligament reconstruction*. Knee Surgery, Sports Traumatology, Arthroscopy, 2012: p. 1-9.
39. Rojas, C.A., H. Jawad, and J.H. Chung, *The new era of radiology teaching files*. AJR. American journal of roentgenology, 2012. **198**(4): p. 773-6.
40. Qing, K.-x., W.-k. Yiu, and S.W.K. Cheng, *A morphologic study of chronic type B aortic dissections and aneurysms after thoracic endovascular stent grafting*. Journal of Vascular Surgery, 2012. **55**(5): p. 1275-1276.
41. Tuan, H.S. and D.W. Hutmacher, *Application of micro CT and computation modelling in bone tissue engineering*. Computer-Aided Design, 2005. **37**(11): p. 1151-1161.
42. Mahaisavariya, B., B. Saekee, K. Sitthiseripratip, P. Oris, T. Tongdee, E.L. Bohez, and J. Vander Sloten, *Morphology of the radial head: A reverse engineering based evaluation using three-dimensional anatomical data of radial bone*. Proceedings of the Institution of Mechanical Engineers, Part H: Journal of Engineering in Medicine, 2004. **218**(1): p. 79-84.
43. Lu, S., Y.Q. Xu, Y.Z. Zhang, L. Xie, H. Guo, and D.P. Li, *A novel computer-assisted drill guide template for placement of C2 laminar screws*. European spine journal : official publication of the European Spine Society, the European Spinal Deformity Society, and the European Section of the Cervical Spine Research Society, 2009. **18**(9): p. 1379-85.

## Chapter 2

### 2 Literature Review

#### 2.1 Anatomy of the Hip Joint

The hip joint forms the connection between the lower limb and the pelvic girdle. It is a stable, synovial joint. The hip joint can move in flexion-extension, abduction-adduction, medial-lateral rotation, and circumduction. The articulating surfaces of the hip joint consist of the lunate surface of the acetabulum of the pelvis and the spherical head of the femur [1].

##### 2.1.1 The Acetabulum

The acetabulum is comprised of all three pelvic bones: the ilium, the ischium, and the pubis. The acetabulum is a deep socket, which creates the stability of the hip joint. It is oriented in an inferolateral position with an anterior tilt in the sagittal plane [2]. This orientation provides more posterior coverage of the femoral head than anterior coverage, thus allowing a greater range of motion (ROM), at the bony level, in flexion than extension. This orientation also creates a greater reliance on soft tissues for anterior stability [3].

The acetabulum is deepened further via the acetabular labrum and the transverse acetabular ligament. The labrum is a triangular fibrocartilaginous structure that circumferentially attaches to the outer rim of the bony acetabulum [3]. The labrum increases stability of the acetabulum by increasing the negative intraarticular pressure of

the joint, acting as a tension band, and participating in nociception and proprioception [5, 6]. The labrum is mostly avascular and thus has a limited ability to heal [3].

The acetabular fossa is located in the center of the medial aspect of the acetabulum and is surrounded by the lunate articular surface, which is covered by articular (hyaline) cartilage [1, 7]. The thickest cartilage is located on the anterior-superior aspect of the acetabular roof [8]. The acetabular fossa mainly contains fatty tissue and also contains numerous proprioceptive nerve endings. The transverse acetabular ligament attaches at the lower border of the fossa. This fibrous band separates the acetabular fossa from the inferior hip joint recess [7]. The ligamentum teres arises from the floor of the acetabulum and attaches to the fovea of the head of the femur. Hypertrophy of ligamentum teres has been reported in cases of acetabular dysplasia and osteonecrosis of the hip [9]. Arthroscopic evaluation reveals that the ligament is tight during external rotation and lax during internal rotation [10]. However, its role in hip stability is unclear [9, 11].

### 2.1.2 The Proximal Femur

The spheroidal head of the femur is also covered with articular (hyaline) cartilage, except for the fovea, where the ligamentum teres attaches [1]. Anteriorly, the cartilage extends laterally over a small area on the adjoining neck. The articular cartilage is generally thicker centrally than at the periphery [7]. The thickest cartilage is located on the anterosuperior-lateral aspect of the femoral head, which corresponds to the principle load-bearing area [7, 8]. The axis of the femoral neck is in  $10^\circ$  of anteversion from the transcondylar axis and is  $130^\circ$  of superior inclination from the axis of the femoral shaft [3].

## 2.2 Osteoarthritis

Osteoarthritis (OA) is one of the major pathological conditions of the hip joint. OA, also known as degenerative joint disease, is a noninflammatory disorder of diarthrotic joints characterized by the deterioration of articular cartilage and formation of new bone at the joint surfaces and margins [12]. OA of the hip joint is a multi-factorial disease that affects aging individuals and is associated with significant disability [13, 14]. Currently, the treatment consists of pain relief and improvement of function once the disease has already progressed, but little is known about the prevention of the disease [15]. While cartilage protection is a potential preventative therapy, changes in bone shape and structure may also contribute to the disease progression [15]. Trauma, age, physical activity, genetics, and a high body mass index (BMI) are identified as potential risk factors. Recently, morphological variations of the proximal femur and the acetabulum have been identified as potential risk factors [16]. Abnormal geometry of the proximal femur and acetabulum is thought to create abnormal loading patterns in the hip joint resulting in OA disease progression. However, it is not known when or how these morphological changes occur along the spectrum of the disease process [17]. The most common locations for bone geometry changes in the hip joint appear to be the acetabular rim and the femoral head and neck [17]. Two of the variations in morphology that have been associated with OA, are hip instability and femoroacetabular impingement (FAI) [15, 16, 18].

## 2.3 Hip Instability

Hip instability has been assumed to be isolated to cases where high-energy trauma to the hip has incurred, which is referred to as traumatic hip instability. However, research surrounding hip arthroscopy and hip related conditions has led to greater awareness of atraumatic hip instability [3]. Atraumatic hip instability is associated with developmental acetabular dysplasia (AD) of the hip, which represents a spectrum of abnormalities that cause an abnormal relationship between the acetabulum and the femoral head, such as: dysplasia, subluxation, and dislocation. AD is characterized by insufficient anterolateral

femoral head coverage by the acetabulum and superolateral inclination of the acetabular surface [19]. Typical morphological changes in the dysplastic hip include a misshapen femoral head, increased anteversion of the femoral neck, and a shallow, anteverted acetabulum [3, 20].

### 2.3.1 Possible Causes of Hip Instability

The etiology of AD may be related to congenital bony dysplasia, congenital ligament laxity, or may be idiopathic [3]. Individuals with bony disorders such as slipped capital femoral epiphysis, Legg-Calve-Perthes disease, and epiphyseal dysplasia can develop dysplasia [3, 21]. Individuals with soft-tissue disorders that cause laxity of the ligaments of the hip joint may be responsible for instability in the joint. In addition, individuals with connective tissue disorders may suffer from instability or spontaneous dislocation. However, true idiopathic instability may occur without the presence of congenital bony dysplasia, connective tissue disorders, overuse, or trauma [3].

### 2.3.2 Association of Osteoarthritis with Hip Instability

AD is often assumed to be associated with high-energy trauma. Thus, atraumatic AD may be missed clinically. Failure to recognize a subluxated or dislocated joint may lead to development of dysplasia as well as early OA [3]. AD results in an anterolateral acetabular rim overload, due to a decreased weight-bearing surface. This decreased weight-bearing surface and stability results in a migration of the femoral head to areas of less coverage. This migration may place excessive contact stresses on the supporting soft tissue and may lead to labral lesions, articular cartilage damage, and joint capsule deterioration. Labral lesions are thought to contribute to further damage of the associated structures [3, 16, 22]. Cartilage and labrum damage is believed to lead to more severe

degenerative disease of the joint, such as damage to the subchondral bone. It is accepted that severe AD leads to OA; however, less is known about the association of mild and moderate AD with OA [16].

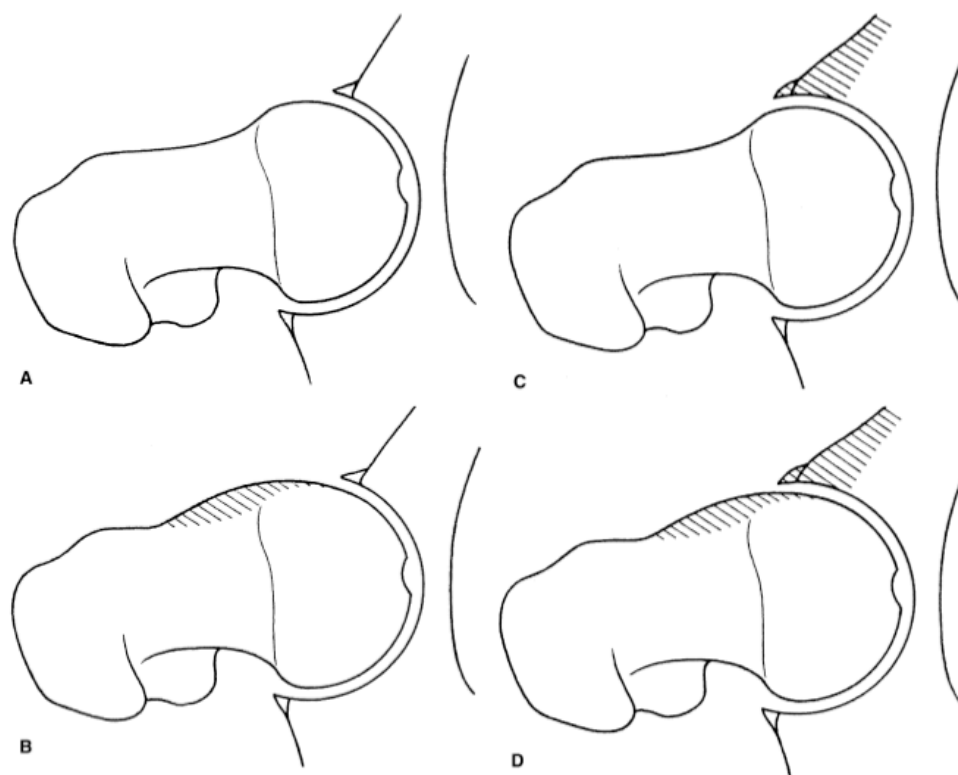
## 2.4 Femoroacetabular Impingement

FAI is a variation in hip morphology that presents in young active adults and may lead to abnormal contact between the neck of the femur and the acetabular rim of the pelvis [20]. These morphologic variations are suggested to lead to a reduction in joint clearance leading to repetitive contact between the femoral neck and the acetabular rim [20, 23]. This abnormal contact is likely to cause damage to the underlying labrum and cartilage of the joint and thus may be a cause of early OA [20, 23-25]. There are two morphologic variations that are suggested to lead to FAI: cam impingement, which affects the femoral neck, and pincer impingement, which affects the acetabular rim [20].

### 2.4.1 Mechanisms of Impingement

Cam impingement is characterized by a decreased head-neck offset of the anterosuperior or anterolateral portion of the femoral head-neck junction (Fig. 2.1B) [20, 24-26]. It is suggested that, during flexion, the aspherical femoral head rotates into the acetabulum and the protuberance on the head-neck junction applies compressive and shear forces to the anterosuperior acetabulum limiting ROM (Fig. 2.2C) [25, 27-29]. Repetitive osseous microtrauma of the abnormal femoral neck against the acetabulum can cause the formation of osteophytes on the anterior femoral neck, which in turn can exacerbate the problem [29]. These forces can also cause the labrum to be stretched and pushed outwards while the cartilage is being compressed and pushed centrally which can then cause the labrum and the cartilage to separate [20, 24, 25, 29]. This mechanism can result

in deep anterosuperior chondral lesions, extensive labral tears, or both of the acetabulum [20, 27, 29]. This proposed etiology is supported by a study conducted by Beck et al. [25] that evaluated plain radiographs of 26 patients (24 male) with isolated cam impingements. During surgical dislocation all hips demonstrated damage to the anterosuperior cartilage and separation of the labrum from the cartilage.

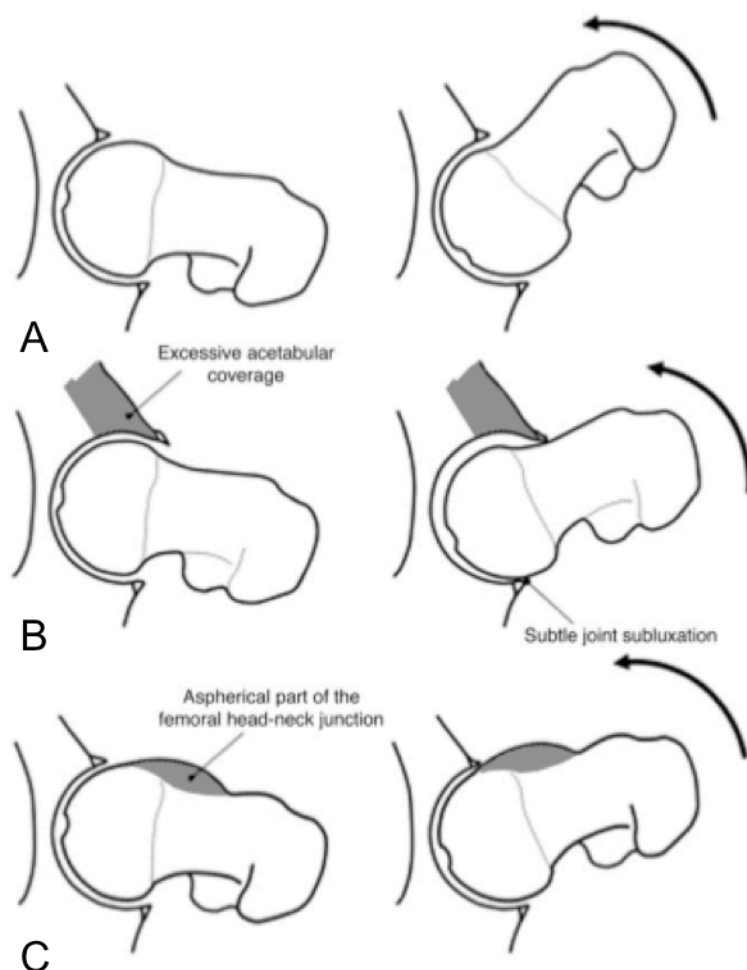


**Figure 2.1 – Types of FAI in a coronal view of the hip joint (A) Normal hip joint; (B) Cam-impingement: decreased head-neck offset; (C) Pincer Impingement: acetabulum over-covering the normal femoral head; (D) Mixed cam-pincer impingement: abnormal morphology of both the acetabular rim and the femoral head-neck junction [24]. Reprinted with permission from Lavigne, M., et al., *Anterior Femoroacetabular Impingement: Part I. Techniques of Joint Preserving Surgery, Current Orthopaedic Practice*, 418: p. 62.**

Pincer impingement is defined as an abnormally deep acetabulum, which causes excessive acetabular coverage over the anatomically normal femoral head (Fig. 2.1C)



[20, 24, 25, 30]. This excessive acetabular coverage is characterized by the femoral head sitting in a deep socket of the pelvis, such as coxa profunda and protrusio acetabulum [31]. Coxa profunda is a condition in which the most medial aspect of the acetabular fossa is touching or overlapping the ilioischial line and protrusio acetabulum is a condition in which the most medial margin of the femoral head protrudes medially with respect to the ilioischial line [32, 33]. The deep socket is suggested to limit ROM as the acetabular rim abuts against the femoral neck, which causes the labrum to become compressed (Fig. 2.2B). Repeated impact may result in damage to the labrum and the forces may be transmitted to the acetabular cartilage resulting in chondral damage. Continued abutment of the acetabular rim against the femoral head may result in the ossification of the underlying bone of the acetabular rim, anterior femoral neck, or both leading to exaggeration of the overcoverage and exacerbation of the impact [20, 24, 25, 29, 34, 35]. Cartilaginous damage associated with pincer impingement is usually small and located along the anterosuperior acetabular rim as a narrow strip. However, chondral damage can also be found in the posterior and posteroinferior aspect of the acetabulum due to a contre-coup injury [20, 24, 25, 27, 29, 35, 36].



**Figure 2.2 - FAI pathology during flexion in a coronal view of the hip. (A) Normal hip joint clearance and movement during flexion. (B) Pincer impingement limits ROM and results in the acetabular rim impacting against the femur and causes subtle joint subluxation, which can cause a posteroinferior contre-coup injury. (C) The head-neck protuberance of cam impingement rotates into the acetabulum causing compression and shear forces of the anterosuperior acetabulum and limits ROM. Reprinted with permission from the American Journal of Roentgenology [33].**

Mixed cam-pincer impingement is a combination of the two mechanisms of impingement and is more common than cam or pincer impingement occurring independently; although, one type usually predominates (Fig. 2.1D) [25, 29]. Beck et al. [25] radiographically evaluated 149 patients with FAI; 26 were observed to have isolated cam impingement (24 male) and only 16 presented with isolated pincer impingement (2 male). Additionally,

Phillippon et al. [37] studied 301 patients (153 males) who were undergoing surgery for FAI and only 50 patients were treated for pincer impingement, whereas 100 patients were treated for cam impingement and the majority, 151 patients, were treated for both cam and pincer impingement. Both patterns of labral and chondral damage are evident in individuals with mixed cam-pincer impingement [20].

## 2.4.2 Possible Causes of Femoroacetabular Impingement

Patients who present with FAI usually lack a clear history of hip disease. It has been suggested that the morphological variations may be caused by subtle developmental abnormalities such as Legg-Calvé Perthes disease and slipped capital femoral epiphysis for cam impingement and coxa profunda, acetabular retroversion, protrusio acetabuli, coxa vara, and os acetabuli for pincer impingement [20, 27, 29]. However, most cases are idiopathic [27].

## 2.4.3 Association of Osteoarthritis with Femoroacetabular Impingement

Abnormal morphology of the hip has been documented as a cause of early OA for some time; however, FAI has only recently been recognized as a clinical problem [38]. It is suggested that FAI primarily limits ROM due to the abnormal contact of the femoral neck and the acetabular rim. This repeated abnormal contact and resulting shearing forces caused by FAI are suggested to lead to labral lesions [24, 25, 27, 35, 39]. Studies show that labral lesions are the most common finding in individuals with FAI and occur in almost all cases [20, 23, 27, 40]. A study conducted by Phillippon et al. [37] found that 99% of 301 patients (153 male) undergoing surgical treatment for FAI had associated labral pathology and 82% had associated chondral pathology. Similarly, Pfirrmann et al.

[36] analyzed magnetic resonance arthrogram (MRA) findings in 50 patients (30 male) with FAI and found that 94% presented with anterosuperior labral lesions and that 84% had anterosuperior cartilage lesions. In agreement, Kassarian et al. [34] evaluated MRA findings of 40 patients (22 male) with FAI and found that 100% of the patients had an anterosuperior labral tear and 95% displayed anterosuperior cartilage abnormalities. Labral lesions predispose the adjacent cartilage to degeneration. Cartilage degeneration then leads to bone exposure, which will ultimately lead to the development of OA [20, 39, 40]. Thus, FAI is a potential mechanism for the development of OA [20, 37, 40].

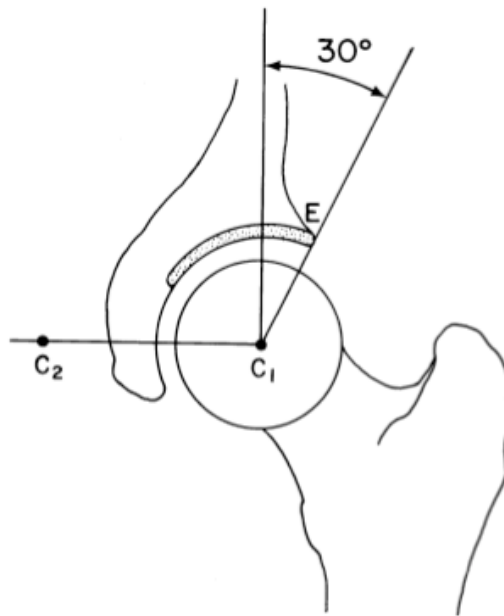
## 2.5 Diagnostic Measurement

### 2.5.1 Diagnostic Measurement for Hip Instability

Plain radiographs are typically the first tool used for the detection of acetabular dysplasia [41]. The centre-edge (CE) angle [21] and the vertical-centre-anterior (VCA) angle [21, 42] allow quantification of acetabular coverage. The CE angle, originally described by Wiberg [19], indirectly assesses the superolateral coverage of the acetabulum over the femoral head (Fig. 2.3) [43]. It is measured via two lines drawn from the centre of the femoral head on a centre cut coronal view of a magnetic resonance image (MRI) or an anteroposterior (AP) radiograph [21, 44]. One is a vertical line drawn from the centre of the femoral head through the acetabulum and the second is drawn from the centre of the femoral head through the lateral margin of the acetabulum. The angle formed between these lines is the CE angle [43]. A normal acetabulum is defined by a CE angle of greater than 25 degrees. A small CE angle is used to diagnose acetabular dysplasia ( $CE < 20^\circ$ ) [26, 40]. Whereas, the CE angle evaluates whether a lateral coverage deficiency is present, the VCA (Fig. 2.4) is used to evaluate anterior coverage. The VCA is measured using a false profile (FP) radiograph. Two lines are drawn, one vertical line through the center of the femoral head and an oblique line running from the centre of the head to the

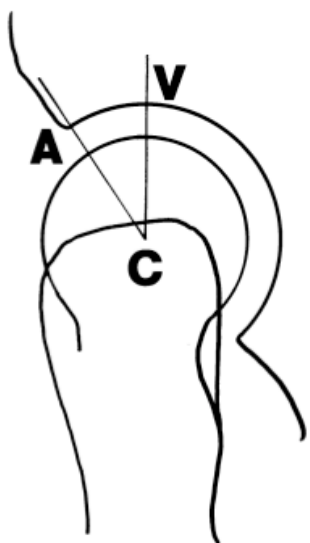
most anterior point of the acetabulum. The angle formed between these two lines represents the VCA angle. A VCA of  $>25^{\circ}$  is considered to be normal, while a VCA  $<25^{\circ}$  is associated with acetabular dysplasia [21, 42].

Due to the continuing development of three-dimensional (3D) imaging technologies, 3D assessment of the hip joint is an emerging area of interest for detecting acetabular pathologies [41]. However, 3D measurements are often linear, similar to the plain radiograph measures, using computed-tomography (CT) slices and do not necessarily utilize the inherent 3D capabilities of CT data sets [21, 41, 45]. In contrast, Nakamura et al. [46] introduced a “top view of the hip” using 3D reconstructed models from CT scans to evaluate posterolateral acetabular deficiency. However, no one has used 3D reconstructions to evaluate the surface morphology of the proximal femur and the acetabulum to better describe the entire surface morphology of the hip.



**Figure 2.3 - Centre-edge (CE) angle, as described by Wiberg [19], is measured on a centre cut coronal MRI. A vertical line is drawn perpendicular to the horizontal line ( $C_1$ ,  $C_2$ ) from the centre of the femoral head. A second line is drawn from the centre of the femoral head to the most lateral point of the acetabulum ( $E$ ). A normal centre-edge angle is associated with values  $>25^{\circ}$  and values  $<20^{\circ}$  are associated with**

**acetabular dysplasia [21].** *Springer and Skeletal Radiology*, 26 (2), 1997: p. 76, *Radiographic Measurements of Dysplastic Adult Hips*, S. Delaunay, Figure 1, is given to the publication in which the material was originally published; with kind permission from Springer Science and Business Media.

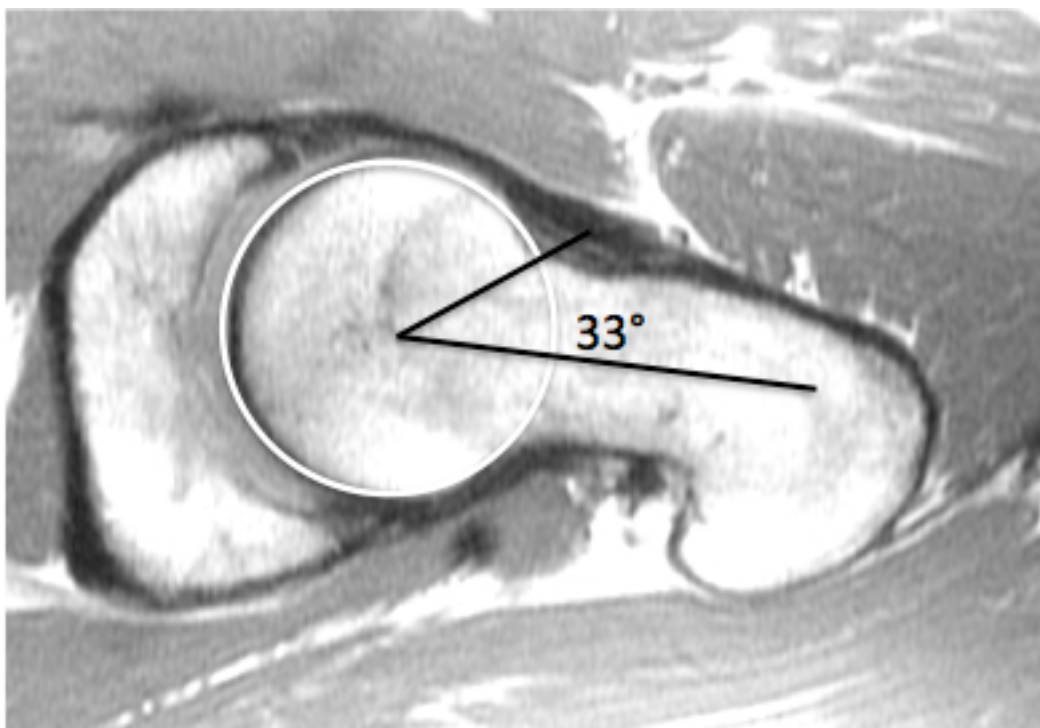


**Figure 2.4 - Vertical-centre-anterior (VCA) angle, as established by Lequesne [42], is assessed on a false-profile view radiograph. V = Vertical; C = Centre; A = Anterior. Normal VCA angles are  $>25^\circ$ , while dysplastic VCA angles are  $<25^\circ$  [21].** *Springer and Skeletal Radiology*, 26 (2), 1997: p. 77, *Radiographic Measurements of Dysplastic Adult Hips*, S. Delaunay, Figure 5, is given to the publication in which the material was originally published; with kind permission from Springer Science and Business Media.

## 2.5.2 Diagnostic Measurement for Femoroacetabular Impingement

The alpha angle, which is used to identify cam impingement, is considered to be the simplest and quickest method for measuring the femoral head-neck offset (Fig. 2.5) [29, 40]. The alpha angle is measured on centre cut axial oblique view MR images and is defined by a line drawn through the centre of the long axis of the femoral neck and head and a line drawn from the centre of the femoral head to the first point where the contour

of the femoral head exceeds the radius of the head [40]. There is no consensus of which alpha angle value is of diagnostic value for a hip with impingement.



**Figure 2.5 - Alpha angle.** A normal alpha angle measurement on an MR image of a 25-year-old male. As established by Notzli et al. [40], it is established on a centre cut axial oblique MRI. The alpha angle is measured between two lines. The first line is drawn from the centre of the femoral head through the centre of the long axis of the femoral neck. The second line is drawn from the femoral head to the point where the contour of the femoral neck exceeds the radius of the femoral head. Normal alpha angles range from 33 to 48 degrees. *Reprinted from authors MSc dissertation. Raynor, CM. 2008. Presence of markers of femoroacetabular impingement in the asymptomatic population. London: The University of Western Ontario. 88p.*

The CE angle discussed previously can also be used to assess acetabular overcoverage as well as insufficient coverage. A normal acetabulum is defined by a CE angle of greater than 25 degrees. A small CE angle is used to diagnose acetabular dysplasia ( $CE < 20^\circ$ ) [26, 40] and conversely a large CE angle can be used to identify pincer impingement.

### 2.5.3 Reliability of Measures

Early detection and treatment of hip instability and FAI may help prevent the progression of OA; however, the current radiographic parameters for diagnosing these conditions are unreliable. For instance Clohisy et al. [18], evaluated the reliability of six hip specialists identifying important radiographic features of the hip on plain radiographs. The readers identified: acetabular version, inclination and depth, position of femoral head center, head sphericity, head-neck offset, Tönnis grade, and joint congruency and were asked to make a diagnosis of normal, dysplastic, FAI or combined dysplastic and FAI on two separate occasions. The Clohisy group concluded that the standard radiographic parameters used to diagnose dysplasia and FAI are not reproducible [18]. Additionally, the same group, Carlisle et al. [47], further investigated the reliability of radiographic measurements of the hip by various musculoskeletal physicians. They found that while the measurements were reliable for a given observer, the measurements were less reliable across observers and were limited in determining a consistent radiographic diagnosis. A clear set of definitions and measurements must be developed to enable more reliable diagnosis of early hip disease [18].

### 2.5.4 Challenges with Current Measures

In current practice, the primary diagnostic tool used to diagnose structural hip disease is a plain radiograph; CT and MRI are often used to confirm the diagnosis and to further investigate the progress of disease [18]. Current measurement modalities that define the geometry of the hip use pre-determined measures, typically lengths and angles, on 2D planes. Attempting to measure 3D geometry on 2D planes with linear measurement approaches does not accurately account for the entire joint morphology [48]. Utilizing the



3D technologies inherent in CT and MR data allows for visualization and quantification of the complete surface morphology of the hip.

## 2.6 Treatment

### 2.6.1 Treatment of Hip Instability

Conservative, non-surgical, management of hip instability consists of protected weight bearing and physical therapy. In more severe cases of hip instability surgical intervention is often recommended. The type of surgical intervention is determined by the underlying pathology associated with the instability. Surgical treatments may consist of open reduction and internal fixation of a fracture, open or arthroscopic labral repair, osteoplasty, capsulorrhaphy, or osteotomy.

### 2.6.2 Treatment of Femoroacetabular Impingement

Orthopedic surgeons lack a consensus regarding the appropriate treatment of FAI. The classic radiographic findings for FAI consist of bony proliferation at the femoral head-neck junction, ossicle formation at the acetabular rim, labral tears, and cartilage flaps. Typically, orthopedic surgeons fall into three cohorts concerning the appropriate treatment for these radiographic findings. The most aggressive cohort of surgeons would diagnose FAI and recommend an open osteotomy or osteoplasty to correct the structural lesions, restore normal anatomy, and prevent the progression of degenerative disease. The second cohort of orthopedic surgeons, challenge the assertion of FAI as the primary diagnosis. These surgeons tend to place the diagnostic emphasis on the labral and chondral lesions and may recommend arthroscopy for the debridement of the soft tissue

lesions and removal of any loose bodies. Patients who receive this treatment are expected to experience short-term relief of symptoms, to notice a functional improvement, and to have a quick postoperative recovery. The third cohort of surgeons believes that degenerative disease of the hip cannot be prevented or delayed and suggest conservative treatment and eventual total hip replacement [49].

## 2.7 3D Modelling

Since the advent of 3D imaging, CT and MRI, the use of 3D modelling for education, measurement, pre-operative assessment, and pre-surgical planning has become a supplement to traditional techniques [41, 50, 51]. 3D modelling allows optimal noninvasive visualization of complex anatomical structures [52] and may afford new and more precise measurement possibilities.

Educational anatomical software has become increasingly available within the last decade. Programs have been developed for all levels of training, from the general public to medical professionals [53]. These programs have typically been in the form of an electronic book, presented with static anatomical images often enriched with animations and testing questions [53]. In contrast, 3D atlases offer the advantage of multiple views, interactivity, and visualization of real anatomical structures that are otherwise difficult to see [53].

The data sets acquired from 3D imaging can provide a 3D reconstruction of patient anatomy allowing personal and accurate measurement. This is an improvement from the standard 2D slice view and different colours can be allocated to different structures to replace the grey spectrum in the standard images [54].

### 2.7.1 3D Modelling in Measurement

Traditionally, clinical measurements for diagnoses have been based on plain radiographs, which are 2D measurements taken on a 2D scan. Quantifying 3D geometry on 2D planes with linear measurements does not accurately account for the entire joint morphology [48, 55]. Traditional 2D imaging techniques are evolving into 3D volume acquisitions with isotropic voxel sizes [56]. The increasing prevalence of 3D imaging has enabled 3D assessment of anatomical structures to become an area of interest [41].

### 2.7.2 3D Modelling in Education

Transfer of knowledge is very important in regards to anatomy and medicine. Historically the fundamental teaching tool for anatomical education was dissection [50, 57].

Dissection is still commonly used as an educational teaching tool; however, the hours allotted for anatomical education in the medical curriculum are drastically decreasing [58]. In order to compensate for this decrease in teaching time anatomical instructors are implementing other teaching methodologies such as 3D computer models [50].

Anatomical models have been used to assist anatomical learning for over a thousand years. However, more recent advances in technology have offered the ability to create visually rich and interactive 3D models [59]. Computer generated anatomy tools enable learners to work through self-directed learning modules at their own pace and the 3D models can often help learners conceptualize structures that are difficult to visualize in the gross anatomy lab [59].

Utilizing visual material is a highly effective method of teaching. Memory retention has been shown to increase when learning using visual aids compared to text-based learning aids. This result is due to the brain's greater capacity for retaining pictorial information [59]. 3D modelling in medical education is becoming more prevalent due to the relative affordability and the widened use of 3D computer graphics [59]. Multimedia anatomy 'text books' using 3D modelling have been published for student use; some of which

include interactive capabilities for student reference [53]. 3D modelling has also been used in virtual simulation programs for surgical residents. These simulators allow surgeons to gain surgical proficiency without risking the lives of patients [60]. In addition, using the same 3D technologies and measurements in education that are used in medicine helps with transferring knowledge from clinical practice to learner.

## 2.8 Why is a Comparison Needed?

3D virtual reconstructions have advantages over other types of imaging and modelling. Virtual reconstructions are not only visual representations of anatomical structures, these structures can be manipulated and dissected electronically, they can be measured and analyzed accurately, and the information can be stored, duplicated, and transferred among various computer platforms [52, 61]. If desired, stereolithography allows 3D reconstructions to be outputted as physical models [61]. Due to the decreased cost and the increased speed and features of computers a variety of 3D reconstructive software programs have been developed for scientific and educational use; however, no program has become the standard and the programs available differ in concept (voxel- or polymesh-based), operating system, features, and cost [52, 61]. Landes, et al. [52] conducted a comparison of two software programs, SeViSe and SURFdriver, that produced 3D reconstructions of histological slides. However, this study only outlined the differences between each program while conducting tasks, as opposed to utilizing a detailed evaluation form. Guyomarc'h et al. [62], conducted a comparative study between two software programs, Amira and Treatment and Increased Vision for Medical Imaging (TIVMI), investigating the measurement uncertainty created during data acquisition and surface reconstruction. They found that the 3D surface reconstruction created in TIVMI had higher precision and reproducibility than the reconstruction created in Amira; however, this study did not look at the other features, advantages, or disadvantages of the programs. Lastly Matsumoto et al. [63], compared the characteristics, advantages, disadvantages, and utility in the operative field of the images generated by three

programs, OsiriX, CTTRY, and Advantage Workstation Volume Share 4 (AW). They found that there were no notable differences in the vascular models at the segmental level and that all three programs were a useful reference during surgery [63]. However, AW is a program that is part of a General Electronic workstation that costs over 1.2 million Canadian dollars; thus, access to the AW software program is limited and not widely available for all research and educational purposes. Whereas the other two programs used are freeware. Furthermore, CTTRY is typically not used for medical imaging and is widely used for 3D movies and other applications. Thus it appears that, no study has been completed which evaluates the features of widely available medical imaging programs for usability, quality of model, and time efficiency.

## 2.9 3D Reconstructive Software Programs

Amira, Osirix, and Mimics are three programs that are widely available, cost effective, and are commonly used for anatomical research and educational purposes.

### 2.9.1 Amira

Amira (Mercury Computer Systems Inc., Chelmsford, USA) generates accurate reconstructions of anatomical structures automatically, semi-automatically, or by manually identifying regions of interest from serial sections. Anatomical models produced in Amira are capable of dynamic interaction and stereoscopic projection [64]. Amira is often used for educational purposes; for instance, Brandt et al. [65], used Amira to construct a digital atlas of a standard bee brain. Clinically, Amira has been used to create 3D representations of kidneys to evaluate renal vessel anatomy of potential kidney donors [66]. Additionally, Nguyen and Wilson [67] created a dynamic 3D model of the head and neck that is interactive and can be viewed in 2D, 3D, and stereoscopic 3D.

Amira also can be used in pre-surgical planning, for instance Handzel, et al. [68] used Amira to create a virtual reconstruction of the ‘canal wall up mastoidectomy space’, which is a space that is created to provide a cavity for temporal bone implants. This group also explored the use of these models for virtual fitting of the implant itself. Furthermore, Amira has been used for morphometric studies, Kramer, et al. [69] created 3D models of the orbit in 70 adult patients. Using these models they created a reference database of normal orbital volume, globe volume, globe to orbital volume ratio, and orbital cone angle to assist in the predictability of decompression surgery on exophthalmos reduction in Graves orbitopathy. Amira is commonly used for a variety of purposes in the medical field, typically education, pre-surgical planning, and morphometric research.

### 2.9.2 OsiriX

OsiriX (Apple Computer Inc., Cupertino, USA) was designed for radiologists and developed exclusively for the Mac OS X operating system. OsiriX is an open-source DICOM image processing workstation software. OsiriX is capable of viewing and manipulating digital anatomical data from various imaging modalities and quickly generating volume rendered anatomical structures [70]. OsiriX has been used in measurement studies such as a study conducted by Kim, et al. [71] who compared the femoral tunnel length, during anterior cruciate ligament reconstruction surgery, intraoperatively and post-operatively via OsiriX imaging software. In addition to being used for measurement, OsiriX has also been used to create educational tools. For example, Rojas [72], used OsiriX to create a comprehensive radiological teaching file that simulates day-to-day radiology practice. The file allows the user to navigate through an entire image dataset for a patient, and integrated into the file the user also has access to the patient’s clinical reports, imaging reports, test results, and pathology reports. OsiriX has also been used to create patient-specific models of lung vasculature that can be used for pre-surgical planning and as a reference during surgery itself. Matsumoto, et al. [63]

found that OsiriX was similar in lung vasculature images and usefulness as an in-surgery reference model as the other two programs used, CTTRY and AW. OsiriX has been used for morphometric research, educational purposes, and pre-surgical planning.

### 2.9.3 Mimics

Mimics (Materialise, Leuven, Belgium) can view and manipulate digital anatomical data from various imaging modalities. The data can be manually segmented or can be generated via volume rendering. Mimics has strong measuring and engineering capabilities that allow users to work directly on the 3D model as well as a wide range of output formats. This software allows you to accurately measure distances, diameters, angles, and densities on 2D scans and directly on the 3D models [73]. Qing, et al. [74] conducted a measurement study using Mimics software, that assessed aortic stent graft diameter changes and positional migration of the stent, on 3D models of patient CT scans, at 1, 6, 12, and 36 months post thoracic endovascular aortic repair. Mimics is also commonly used to prepare models for Finite Element Modelling (FEM). Mimics can create FEM meshes quickly from CT or MRI scans [75]. For example, Mahaisavariya, et al. [76] evaluated the 3D inner and outer geometry of the proximal radius using a reverse engineering technique. The group used Mimics software to create the 3D models of the radii before importing the models into reverse engineering computer aided design (CAD) software. Mimics has also been used in pre-surgical planning, Lu, et al. [77] used Mimics to create patient specific 3D models of C2 vertebra. Once a model was created it was exported to another workstation to establish a navigational template and laminar screw size. The template and screw were then used intraoperatively during a posterior occipitocervical fusion. Mimics is fundamentally used in morphometric research; however, it has also been used to create models for pre-surgical planning.

## 2.9.4 Previous Assessment of the 3D Reconstructive Software Programs

When conducting geometric morphometric analyses using reconstructed anatomical models, the models are subject to the influence of measurement uncertainty created during data acquisition and surface reconstruction. To assess this measurement uncertainty, Guyomarc'h, et al. [62], conducted a comparative study between two software programs, Amira and a program created by the authors (TIVMI). They measured intra- and interobserver variations in measurements of a known-size phantom and two crania. Although the 3D model created in Amira is more aesthetically pleasing, they found that the 3D surface reconstruction created in TIVMI had higher precision and reproducibility than the reconstruction created in Amira. Amira induced up to a 4% error in measurement of the phantom and up to a 5% uncertainty in measurement of the dry skulls [62].

To assess the accuracy of length measurements taken on reconstructed models created in OsiriX, Kim, et al. [78] compared measurements taken manually on pig knees to measurements taken on CT reconstructed models of the same pig knees with OsiriX. The mean differences between the OsiriX measurements and the manual measurements were less than 0.1mm and the Intraclass Coefficients (ICCs), for intra- and interobserver reliability, were very high.

Matsumoto, et al. [63] compared three 3D reconstructive software programs, OsiriX, CTTRY, and AW, to assess the characteristics, advantages, disadvantages, and utility in the operative field. They found that OsiriX was similar in lung vasculature images and usefulness as an in-surgery reference model as the other two programs used, CTTRY and AW. They also found that OsiriX easily generated and displayed 3D images and allowed for an easy understanding of spatial relationships. OsiriX was limited in that the 3D representation could not be altered after the model was created and thus could not be used for reference image simulation.



Tuan and Hutmacher [75], compared the Mimics software suite to two software programs (CTan and 3D Realistic Visualization) used in conjunction for bone tissue engineering, which were built into the Skyscan microtomographic scanner. They found that the Mimics software allowed a greater degree of image manipulation, visualization, and editing functions, which aid in the isolation of structures, compared to the Skyscan programs. ‘Region growing’ and measurements were also easy to perform using the Mimics software and were not possible using 3D realistic visualization and CTan. One disadvantage Tuan and Hutmacher found when analyzing Mimics was its inability to compute various structural bone parameters; however, the volume meshes are easily exported to be used in FEA software packages [73, 75].

## 2.10 References

1. Moore, K.L. and A.M.R. Agur, *Essential Clinical Anatomy*. Second Edition ed, ed. B. Sun 2002, Baltimore: Lippincott Williams & Wilkins. 691.
2. Köhnlein, W., R. Ganz, F. Impellizzeri, and M. Leunig, *Acetabular Morphology: Implications for Joint-preserving Surgery*. Clinical Orthopaedics and Related Research, 2009 **467**(3): p. 682-91.
3. Boykin, R.E., A.W. Anz, B.D. Bushnell, M.S. Kocher, A.J. Stubbs, and M.J. Philippon, *Hip instability*. Journal of the American Academy of Orthopaedic Surgeons, 2011. **19**(6): p. 340-349.
4. McCarthy, J.C., P.C. Noble, M.R. Schuck, J. Wright, and J. Lee, *The watershed labral lesion: Its relationship to early arthritis of the hip*. The Journal of Arthroplasty, 2001. **16**(8, Supplement 1): p. 81-87.
5. Crawford, M.J., C.J. Dy, J.W. Alexander, M. Thompson, S.J. Schroder, C.E. Vega, R.V. Patel, A.R. Miller, J.C. McCarthy, W.R. Lowe, and P.C. Noble, *The 2007 Frank Stinchfield Award. The biomechanics of the hip labrum and the stability of the hip*. Clinical Orthopaedics and Related Research, 2007. **465**: p. 16-22.
6. Kim, Y.T. and H. Azuma, *The nerve endings of the acetabular labrum*. Clin Orthop Relat Res, 1995(320): p. 176-81.

7. Standring, S., *Gray's Anatomy: The Anatomical Basis of Clinical Practice*. Fortieth ed, ed. S. Standring 2008: Churchill Livingstone Elsevier. 1551.
8. Oberlander, W., [*The stress of the human hip joint. VII. The distribution of cartilage thickness in the acetabulum and its functional explanation (author's transl)*]. *Anat Embryol (Berl)*, 1977. **150**(2): p. 141-53.
9. Chen, H.H., A.F. Li, K.C. Li, J.J. Wu, T.S. Chen, and M.C. Lee, *Adaptations of ligamentum teres in ischemic necrosis of human femoral head*. *Clinical Orthopaedics and Related Research*, 1996(328): p. 268-75.
10. Shindle, M.K., A.S. Ranawat, and B.T. Kelly, *Diagnosis and management of traumatic and atraumatic hip instability in the athletic patient*. *Clinics in sports medicine*, 2006. **25**(2): p. 309-326.
11. Bardakos, N.V. and R.N. Villar, *Predictors of progression of osteoarthritis in femoroacetabular impingement: A RADIOLOGICAL STUDY WITH A MINIMUM OF TEN YEARS FOLLOW-UP*. *J Bone Joint Surg Br*, 2009. **91-B**(2): p. 162-169.
12. Brown, D.E. and R.D. Neumann, *Orthopedic Secrets*. 3rd Edition ed 2004, Philadelphia: Hanley & Belfus An Affiliate of Elsevier. 450.
13. Felson, D., R. Lawrence, P. Dieppe, R. Hirsch, C. Helmick, J. Jordan, R. Kington, N. Lane, M. Nevitt, Y. Zhang, M. Sowers, T. McAlindon, T. Spector, A. Poole, S. Yanovski, G. Ateshian, L. Sharma, J. Buckwalter, K. Brandt, and J. Fries, *Osteoarthritis: New Insights. Part 1: The Disease and Its Risk Factors*. *Annals of Internal Medicine*, 2000. **133**(8): p. 635-646.
14. Chegini, S., Beck, M., Ferguson, S.J., *The effects of impingement and dysplasia on stress distributions in the hip joint during sitting and walking: A finite element analysis*. *Journal of Orthopaedic Research*, 2009. **27**(2): p. 195-201.
15. Lynch, J.A., N. Parimi, R.K. Chaganti, M.C. Nevitt, and N.E. Lane, *The association of proximal femoral shape and incident radiographic hip OA in elderly women*. *Osteoarthritis and Cartilage*, 2009. **17**(10): p. 1313-1318.
16. Harris-Hayes, M. and N.K. Royer, *Relationship of acetabular dysplasia and femoroacetabular impingement to hip osteoarthritis: a focused review*. *PM & R: the journal of injury, function, and rehabilitation*, 2011. **3**(11): p. 1055-1067 e1.
17. Gregory, J.S., J.H. Waarsing, J. Day, H.A. Pols, M. Reijman, H. Weinans, and R.M. Aspden, *Early identification of radiographic osteoarthritis of the hip using an active shape model to quantify changes in bone morphometric features: Can hip shape tell us anything about the progression of osteoarthritis?* *Arthritis & Rheumatism*, 2007. **56**(11): p. 3634-3643.

18. Clohisy, J.C., J.C. Carlisle, R. Trousdale, Y.J. Kim, P.E. Beaulé, P. Morgan, K. Steger-May, P.L. Schoenecker, and M. Millis, *Radiographic evaluation of the hip has limited reliability*. Clin Orthop Relat Res, 2009. **467**(3): p. 666-75.
19. Wiberg, G., *Studies on dysplastic acetabula and congenital subluxation of the hip joint. with special reference to the complication of osteo-arthritis*. Acta Chirurgica Scandinavica, 1939. **83**(Suppl 58): p. 1-135.
20. Ganz, R., J. Parvizi, M. Beck, M. Leunig, H. Notzli, and K.A. Siebenrock, *Femoroacetabular impingement: a cause for osteoarthritis of the hip*. Clin Orthop Relat Res, 2003(417): p. 112-20.
21. Delaunay, S., R.G. Dussault, P.A. Kaplan, and B.A. Alford, *Radiographic measurements of dysplastic adult hips*. Skeletal Radiol, 1997. **26**(2): p. 75-81.
22. Murphy, S.B., R. Ganz, and M.E. Muller, *The prognosis in untreated dysplasia of the hip. A study of radiographic factors that predict the outcome*. J Bone Joint Surg Am, 1995. **77**(7): p. 985-9.
23. Beck, M., M. Leunig, J. Parvizi, V. Boutier, D. Wyss, and R. Ganz, *Anterior femoroacetabular impingement: part II. Midterm results of surgical treatment*. Clin Orthop Relat Res, 2004(418): p. 67-73.
24. Lavigne, M., J. Parvizi, M. Beck, K.A. Siebenrock, R. Ganz, and M. Leunig, *Anterior femoroacetabular impingement: part I. Techniques of joint preserving surgery*. Clin Orthop Relat Res, 2004(418): p. 61-6.
25. Beck, M., M. Kalhor, M. Leunig, and R. Ganz, *Hip morphology influences the pattern of damage to the acetabular cartilage: femoroacetabular impingement as a cause of early osteoarthritis of the hip*. J Bone Joint Surg Br, 2005. **87**(7): p. 1012-8.
26. Gosvig, K.K., S. Jacobsen, S. Sonne-Holm, and P. Gebuhr, *The prevalence of cam-type deformity of the hip joint: a survey of 4151 subjects of the Copenhagen Osteoarthritis Study*. Acta Radiologica, 2008. **49**(4): p. 436-41.
27. Jaber, F.M. and J. Parvizi, *Hip pain in young adults: femoroacetabular impingement*. J Arthroplasty, 2007. **22**(7 Suppl 3): p. 37-42.
28. Ito, K., M.A. Minka, 2nd, M. Leunig, S. Werlen, and R. Ganz, *Femoroacetabular impingement and the cam-effect. A MRI-based quantitative anatomical study of the femoral head-neck offset*. J Bone Joint Surg Br, 2001. **83**(2): p. 171-6.
29. Kassarian, A., M. Brisson, and W.E. Palmer, *Femoroacetabular impingement*. European Journal of Radiology, 2007. **63**(1): p. 29-35.

30. Laude, F., T. Boyer, and A. Nogier, *Anterior femoroacetabular impingement*. Joint Bone Spine, 2007. **74**(2): p. 127-32.
31. Parvizi, J., M. Leunig, and R. Ganz, *Femoroacetabular Impingement*. J Am Acad Orthop Surg, 2007. **15**(9): p. 561-570.
32. Pomeranz, M.M. and R.A. Brand, *Intrapelvic protrusion of the acetabulum (Otto pelvis)*. Clinical Orthopaedics and Related Research, 2007(465): p. 6-15.
33. Tannast, M., K.A. Siebenrock, and S.E. Anderson, *Femoroacetabular impingement: radiographic diagnosis--what the radiologist should know*. AJR Am J Roentgenol, 2007. **188**(6): p. 1540-52.
34. Kassarian, A., L.S. Yoon, E. Belzile, S.A. Connolly, M.B. Millis, and W.E. Palmer, *Triad of MR arthrographic findings in patients with cam-type femoroacetabular impingement*. Radiology, 2005. **236**(2): p. 588-92.
35. Beall, D.P., C.F. Sweet, H.D. Martin, C.L. Lastine, D.E. Grayson, J.Q. Ly, and J.R. Fish, *Imaging findings of femoroacetabular impingement syndrome*. Skeletal Radiol, 2005. **34**(11): p. 691-701.
36. Pfirrmann, C.W., B. Mengiardi, C. Dora, F. Kalberer, M. Zanetti, and J. Hodler, *Cam and pincer femoroacetabular impingement: characteristic MR arthrographic findings in 50 patients*. Radiology, 2006. **240**(3): p. 778-85.
37. Philippon, M., R. Maxwell, T. Johnston, M. Schenker, and K. Briggs, *Clinical presentation of femoroacetabular impingement*. Knee Surgery, Sports Traumatology, Arthroscopy, 2007. **15**(8): p. 1041-1047.
38. Standaert, C.J., P.A. Manner, and S.A. Herring, *Expert Opinion and Controversies in Musculoskeletal and Sports Medicine: Femoroacetabular Impingement*. Archives of Physical Medicine and Rehabilitation, 2008. **89**(5): p. 890-893.
39. James, S.L., K. Ali, F. Malara, D. Young, J. O'Donnell, and D.A. Connell, *MRI findings of femoroacetabular impingement*. AJR Am J Roentgenol, 2006. **187**(6): p. 1412-9.
40. Notzli, H.P., T.F. Wyss, C.H. Stoecklin, M.R. Schmid, K. Treiber, and J. Hodler, *The contour of the femoral head-neck junction as a predictor for the risk of anterior impingement*. J Bone Joint Surg Br, 2002. **84**(4): p. 556-60.
41. Humbert, L., H. Carlioz, A. Baudoin, W. Skalli, and D. Mitton, *3D Evaluation of the acetabular coverage assessed by biplanar X-rays or single anteroposterior X-ray compared with CT-scan*. Computer Methods in Biomechanics and Biomedical Engineering, 2008. **11**(3): p. 257 - 262.

42. Lequesne, M. and S. de, *[False profile of the pelvis. A new radiographic incidence for the study of the hip. Its use in dysplasias and different coxopathies.]*. Rev Rhum Mal Osteoartic, 1961. **28**: p. 643-52.
43. Crockarell, J.R., Jr., R.T. Trousdale, and J.L. Guyton, *The anterior centre-edge angle. A cadaver study*. J Bone Joint Surg Br, 2000. **82**(4): p. 532-4.
44. Chen, L., M. Boonthathip, F. Cardoso, P. Clopton, and D. Resnick, *Acetabulum protrusio and center edge angle: new MR-imaging measurement criteria--a correlative study with measurement derived from conventional radiography*. Skeletal Radiol, 2009. **38**(2): p. 123-9.
45. Klaue, K., A. Wallin, and R. Ganz, *CT evaluation of coverage and congruency of the hip prior to osteotomy*. Clin Orthop Relat Res, 1988(232): p. 15-25.
46. Nakamura, S., J. Yorikawa, K. Otsuka, K. Takeshita, A. Harasawa, and T. Matsushita, *Evaluation of acetabular dysplasia using a top view of the hip on three-dimensional CT*. Journal of Orthopaedic Science, 2000. **5**(6): p. 533-539.
47. Carlisle, J.C., L.P. Zebala, D.S. Shia, D. Hunt, P.M. Morgan, H. Prather, R.W. Wright, K. Steger-May, and J.C. Clohisy, *Reliability of various observers in determining common radiographic parameters of adult hip structural anatomy*. The Iowa Orthopaedic Journal, 2011. **31**: p. 52-58.
48. Waarsing, J.H., R.M. Rozendaal, J.A.N. Verhaar, S.M.A. Bierma-Zeinstra, and H. Weinans, *A statistical model of shape and density of the proximal femur in relation to radiological and clinical OA of the hip*. Osteoarthritis and Cartilage, 2010. **18**(6): p. 787-794.
49. Palmer, W.E., *Femoroacetabular impingement: caution is warranted in making imaging-based assumptions and diagnoses*. Radiology, 2010. **257**(1): p. 4-7.
50. Rosse, C., *The Potential of Computerized Representations of Anatomy in the Training of Health Care Providers*. Academic Medicine, 1995. **70**(6): p. 499-505.
51. Bale, R. and G. Widmann, *Navigated CT-guided interventions*. Minimally Invasive Therapy & Allied Technologies, 2007. **16**(4): p. 196-204.
52. Landes, C.A., F. Weichert, P. Geis, F. Helga, and M. Wagner, *Evaluation of two 3D virtual computer reconstructions for comparison of cleft lip and palate to normal fetal microanatomy*. The Anatomical Record Part A: Discoveries in Molecular, Cellular, and Evolutionary Biology, 2006. **288A**(3): p. 248-262.
53. Gehrmann, S., K.H. Höhne, W. Linhart, B. Pflessner, A. Pommert, M. Riemer, U. Tiede, J. Windolf, U. Schumacher, and J.M. Rueger, *A novel interactive anatomic atlas of the hand*. Clinical Anatomy, 2006. **19**(3): p. 258-266.

54. De Paolis, L.T.a.A., G., *Visualization and Interaction System for Surgical Planning*, in *Engineering Interactive Computing Systems for Medicine and Health Care 2011* 2011: Pisa, Italy.
55. Beaulé, P.E., E. Zaragoza, K. Motamedi, N. Copelan, and F.J. Dorey, *Three-dimensional computed tomography of the hip in the assessment of femoroacetabular impingement*. J Orthop Res, 2005. **23**(6): p. 1286-92.
56. Rosset, A., L. Spadola, and O. Ratib, *OsiriX: An Open-Source Software for Navigating in Multidimensional DICOM Images*. Journal of Digital Imaging, 2004. **17**(3): p. 205-216.
57. Elizondo-Omaña, R.E., S. Guzmán-López, and M. De Los Angeles García-Rodríguez, *Dissection as a teaching tool: Past, present, and future*. The Anatomical Record Part B: The New Anatomist, 2005. **285B**(1): p. 11-15.
58. Drake, R.L., J.M. McBride, N. Lachman, and W. Pawlina, *Medical education in the anatomical sciences: The winds of change continue to blow*. Anatomical Sciences Education, 2009. **2**(6): p. 253-259.
59. Vernon, T. and D. Peckham, *The benefits of 3D modelling and animation in medical teaching*. The Journal of audiovisual media in medicine, 2002. **25**(4): p. 142-8.
60. Mantovani, F., G. Castelnovo, A. Gaggioli, and G. Riva, *Virtual reality training for health-care professionals*. Cyberpsychol Behav, 2003. **6**(4): p. 389-95.
61. Haas, A. and M.S. Fischer, *Three-dimensional reconstruction of histological sections using modern product-design software*. The Anatomical Record, 1997. **249**(4): p. 510-516.
62. Guyomarc'h, P., F. Santos, B. Dutailly, P. Desbarats, C. Bou, and H. Coqueugniot, *Three-dimensional computer-assisted craniometrics: A comparison of the uncertainty in measurement induced by surface reconstruction performed by two computer programs*. Forensic Science International, 2012. **219**(1-3): p. 221-7.
63. Matsumoto, T., Kanzaki, M., Amiki, M., Shimizu, T., Maeda, H., Sakamoto, K., Ookubo, Y., Onuki, T., *Comparison of three software programs for three-dimensional graphic imaging as contrasted with operative findings*. Eur J Cardiothorac Surg, 2012. **41**(5): p. 1098-103.
64. *Amira - Visualize Analyze Present*. 2012 [cited 2012 March]; Available from: <http://www.amira.com/>.
65. Brandt, R., T. Rohlfing, J. Rybak, S. Krofczik, A. Maye, M. Westerhoff, H.-C. Hege, and R. Menzel, *Three-dimensional average-shape atlas of the honeybee*

- brain and its applications*. The Journal of Comparative Neurology, 2005. **492**(1): p. 1-19.
66. Wang, Z., F. Zeng, H. Li, Z. Ye, Y. Bai, W. Xia, and B. Liang, *Three-dimensional reconstruction on PC-Windows platform for evaluation of living donor nephrectomy*. Computer Methods and Programs in Biomedicine, 2007. **86**(1): p. 39-44.
  67. Nguyen, N. and T.D. Wilson, *A head in virtual reality: development of a dynamic head and neck model*. Anatomical Sciences Education, 2009. **2**(6): p. 294-301.
  68. Handzel, O., H. Wang, J. Fiering, J.T. Borenstein, M.J. Mescher, E.E. Swan, B.A. Murphy, Z. Chen, M. Peppi, W.F. Sewell, S.G. Kujawa, and M.J. McKenna, *Mastoid cavity dimensions and shape: method of measurement and virtual fitting of implantable devices*. Audiology & neuro-otology, 2009. **14**(5): p. 308-14.
  69. Kamer, L., H. Noser, A. Schramm, B. Hammer, and E. Kirsch, *Anatomy-based surgical concepts for individualized orbital decompression surgery in graves orbitopathy. I. Orbital size and geometry*. Ophthalmic plastic and reconstructive surgery, 2010. **26**(5): p. 348-52.
  70. *OsiriX Imaging Software*. 2012 [cited 2012 March]; Available from: <http://www.osirix-viewer.com/AboutOsiriX.html>.
  71. Kim, J., J. Wang, J. Ahn, H. Kim, and H. Lim, *Comparison of femoral tunnel length between transportal and retrograde reaming outside-in techniques in anterior cruciate ligament reconstruction*. Knee Surgery, Sports Traumatology, Arthroscopy, 2012: p. 1-9.
  72. Rojas, C.A., H. Jawad, and J.H. Chung, *The new era of radiology teaching files*. AJR. American journal of roentgenology, 2012. **198**(4): p. 773-6.
  73. *Materialize Mimics Innovation Suite*. 2012 [cited 2012 March]; Available from: <http://www.materialise.com/BiomedicalRnD/application-areas>.
  74. Qing, K.-x., W.-k. Yiu, and S.W.K. Cheng, *A morphologic study of chronic type B aortic dissections and aneurysms after thoracic endovascular stent grafting*. Journal of Vascular Surgery, 2012. **55**(5): p. 1275-1276.
  75. Tuan, H.S. and D.W. Hutmacher, *Application of micro CT and computation modeling in bone tissue engineering*. Computer-Aided Design, 2005. **37**(11): p. 1151-1161.
  76. Mahaisavariya, B., B. Saekee, K. Sitthiseripratip, P. Oris, T. Tongdee, E.L. Bohez, and J. Vander Sloten, *Morphology of the radial head: A reverse*

*engineering based evaluation using three-dimensional anatomical data of radial bone*. Proceedings of the Institution of Mechanical Engineers, Part H: Journal of Engineering in Medicine, 2004. **218**(1): p. 79-84.

77. Lu, S., Y.Q. Xu, Y.Z. Zhang, L. Xie, H. Guo, and D.P. Li, *A novel computer-assisted drill guide template for placement of C2 laminar screws*. European spine journal : official publication of the European Spine Society, the European Spinal Deformity Society, and the European Section of the Cervical Spine Research Society, 2009. **18**(9): p. 1379-85.
78. Kim, G., H.-J. Jung, H.-J. Lee, J.-S. Lee, S. Koo, and S.-H. Chang, *Accuracy and Reliability of Length Measurements on Three-Dimensional Computed Tomography Using Open-Source OsiriX Software*. Journal of Digital Imaging, 2012: p. 1-6.



## Chapter 3

### 3 Comparison of 3D Reconstructive Technologies used for Morphometric Research and the Translation of Knowledge

#### 3.1 Introduction

Utilizing 3D models for education, pre-operative assessment, pre-surgical planning, and measurement has become increasingly prevalent since the advent of computed-tomography (CT) and magnetic resonance imaging (MRI) [1-3]. 3D modelling may afford advantages over traditional techniques through complete visualization of complex anatomical morphology [4]. Traditional 2D imaging techniques that involve superimposition or cross-sectional slices, are evolving into 3D models reconstructed from 3D volume acquisitions that allow visualization of the entire structures [5].

Three-dimensional volume acquisitions allow measurement of the entire 3D morphology, unlike traditional measurements that are linear and are taken on 2D scans [6]. Additionally, 3D volume acquisitions offer the potential creation of patient specific models, enabling patient-specific quantification and visualization of anatomical structures [7].

To accommodate advances in technology, educators are adapting the techniques employed to teach new health professionals morphology, measurement, and surgical skills, and these educational activities are beginning to rely more heavily on the use of 3D models. For learners, 3D models may help the conceptualization of structures and their spatial relationships that are difficult to otherwise visualize [8]. Through the utilization of the same 3D technologies and measurements used in medicine in education, the transition of transferring knowledge from clinical practice to learner becomes fluid.

Due, at least in part, to increased speed and decreased cost of high performance computer processors, many 3D reconstructive software programs have become widely available [9]. These programs are developed for all levels of training, from the general public to medical professionals [10]. A variety of 3D reconstructive software programs have been created for scientific and educational use; however, no program has emerged as the standard. Additionally, each program available varies greatly in its approach to reconstruction concepts (surface-rendered or volume-rendered), operating system requirements, features, and costs [4, 9].

As a result of the abundance of programs available, studies have compared available software programs. For instance, Landes et al. [4] compared two software programs, SeViSe and SURFdriver, used to produce 3D reconstructions of histological slides. However, this comparison outlined differences between the programs while conducting tasks and did not assess the programs in a systematic fashion. With regard to gross anatomy, Guyomarc'h et al., [11] compared 3D models between two software programs, Amira and an author-created program Treatment and Increased Vision for Medical Imaging (TIVMI). Although, they investigated the measurement uncertainty created during data acquisition and surface reconstruction, the investigators did not compare any other features, advantages, or disadvantages of the two programs that could be important to a wider anatomical user-base. Lastly, Matsumoto et al. [12] compared OsiriX, CTTRY, and Advantage Workstation Volume Share 4 (AW) models of lung vasculature, assessing the software programs with regard to their characteristics, advantages, disadvantages, and utility in the operative field. However, not all of the programs being compared in this study are widely available medical imaging software programs; AW is part of a GE clinical workstation that costs over 1.2 million Canadian dollars and thus is not widely available, and CTTRY is widely used in 3D cinema, but typically is not used for anatomical 3D modelling. Thus, no study has evaluated the overall advantages and disadvantages of widely available medical imaging software programs and their features, such as 3D segmentation tools, measurement tools, and educational features.

Amira, OsiriX, and Mimics are three programs that are widely available, relatively cost effective, and commonly used for morphometric research, to build educational tools, and

for pre-operative assessment and pre-surgical planning [12-23]. Although these software programs have not been systematically compared, other authors have assessed different features of these programs independently. For instance, Guyomarc'h et al. [11], discovered Amira-based models to be more aesthetically pleasing than TVVMI derived models, but yielded lower-precision reconstructions with limited reproducibility. Another study compared manual measurements taken on cadaveric pig knees to reconstructed models of the same knees produced with OsiriX, and established that the reproducibility of the measurements were very high and the mean differences were negligible [24]. Matsumoto et al. [12] compared models of lung vasculature and reported no notable differences in the 3D models created at the segmental level and that all three programs, including OsiriX, were useful as a reference during surgery. One limitation to OsiriX was that the 3D model could not be altered after it was created. Finally, Tuan and Hutmacher [21] compared Mimics to two software programs, CTan and 3D Realistic Visualization, used in conjunction for bone tissue engineering. Mimics exhibited greater degrees of image manipulation, visualization, and editing functions than the other two programs. One disadvantage of Mimics, with regard to finite element modelling (FEM), is its inability to compute various structural bone parameters (used to assess trabecular bone structure) inherently; however, volume meshes are easily exported to be used in FEM software programs.

As demonstrated by a comprehensive literature review, no comprehensive nor systematic comparison of consumer-level reconstructive software exists that informs a wide audience of anatomical researchers and educators. Therefore, the purpose of the current study was to conduct a systematic comparison of three widely available 3D reconstructive software programs, Amira, OsiriX, and Mimics, with respect to the software's ability to be used in morphometric research and in education to translate morphological knowledge. It is hypothesized that not one program will be adequate for both educational and research purposes. Cost, system requirements, and inherent features of each program are compared. A decision matrix was used to objectify the comparisons of usability of the interface, quality of the output, and efficiency of tools. A decision matrix is a concept selection tool commonly used in engineering [25]. Decision matrices inform a decision making process by transforming subjective rankings to meaningful

scores. Decision matrices have not been used in comparing 3D reconstructive software programs previously but may provide a novel method of deciding on a best-suited software program. The matrix consists of a set of criteria, which are then ranked by decision-makers. The criteria are weighted according to their level of importance in making a decision. Once the decision-maker completes an assessment, the rankings are multiplied by their weighting factor to produce a final score [26]. For this study, two different weighting methods were used, one to assess the morphometric research features and one to assess the educational features. 3D models can be used for an array of morphometric research and educational tools; this comparative exploration samples, demonstrates, and assesses the inherent features and tools available within each program.

## 3.2 Methods and Materials

### 3.2.1 Decision-Makers

Six anatomists were used as decision-makers in this study. Three of the decision-makers were novices and three were experienced. The novice decision-makers were a diverse group who did not have extensive experience using 3D reconstructive software programs. The first novice decision-maker conducts educational psychology research analyzing skill acquisition in medical students and residents. The second novice decision-maker was a new MSc student who had not yet started research using 3D reconstructive technologies. The third novice decision-maker had extensive knowledge regarding the application of the 3D reconstructive technologies, both for educational and research purposes; however, this decision-maker had never used the programs personally and thus, did not have any technical knowledge of the programs. The other three decision-makers were experienced, with previous involvement conducting one or more morphometric or educational study using 3D reconstructive software programs. The first expert decision-maker has extensive knowledge of the application of 3D reconstructive technologies and has extensive

experience creating 3D models and learning tools with Amira. The second expert decision-maker has extensive experience and technical knowledge of Amira and other 3D programs. The third expert decision-maker has extensive knowledge in the application of the 3D technologies and has experience conducting morphometric measurements using Mimics and Amira.

### 3.2.2 3D Reconstructive Programs

Three common software programs were chosen for the study: Amira 5.2 (Mercury Computer Systems Inc., Chelmsford, USA); OsiriX (Version 3.6) (Apple Computer Inc., Cupertino, USA); and Mimics (Version 14.11) (Materialise, Leuven, Belgium). The study components using Amira and Mimics were performed on a PC utilizing Microsoft Windows XP (64bit) with a 2.4 GHz Intel (R) Core (TM)2 Quad CPU (8GB ram). The OsiriX software was the 64bit version on a Mac Pro, OSX version 10.6.8 with a 2 x 3.2 GHz Quad-Core Intel Xeon processors (16GB ram).

### 3.2.3 Assessment

The software programs' websites were used to gather information regarding the available software features and costs; if necessary the companies were contacted. An assessment form consisting of three sections was developed (Appendix A) for the decision-makers to use when ranking the software. The sections were broad categories comprising multiple facets termed 'criteria'. The three sections consisted of 3D modelling tools (10 criteria), measurement tools (7 criteria), and educational features (6 criteria). Each criterion is rated on a 7-point Likert scale. A 7-point scale was chosen because it provides a more accurate measure of a participant's true evaluation than 5-point scales during unsupervised usability questionnaires when the participant must choose a whole number

[27]. Each criterion also included a ‘Not Applicable’ (N/A) box for decision-makers to use if a certain feature or tool was not available. Additionally, each part of the matrix had a section for open-ended comments.

An instructional guide was created for each software program (Appendix B, C, and D). The instructional guide consisted of tasks for the decision-maker to complete before ranking the criteria. The tasks chosen for the study involved undertakings commonly performed when conducting morphometric research or creating a learning tool, such as: building 3D models; segmenting structures; utilizing the available measurement tools; building and exporting dynamic views of the model in the form of a movie. The decision-makers ranked these criteria based on the process of completing the task and not necessarily focusing on the outcome of the task. Each program’s instructional guide outlined the same tasks and differed only by the available features and methodology of each program. Each decision-maker completed the program assessments in a different order to prevent exposure bias in the novice group. The experienced decision-makers also completed the assessments in a different order; however, these decision-makers had prior experience with at least one of the 3D reconstructive technologies available and thus exposure bias was not a concern.

Weightings for the criteria were established for both of the weighting scales, morphometric research and education, by classifying the importance of each criterion. The importance was classified on a 7-point likert scale. If the criterion was considered to be of high importance to the weighting scale, such as perceived accuracy of model creation in the morphometric research weighting scale, it received a 7-point classification. Similarly, if the criterion was of no importance to the weighting scale, such as the ability to create a movie for the morphometric research weighting scale, it received a 0-point classification and thus, that criterion would be removed from that weighting scale altogether. Some of the criterion’s importance classifications fell between high importance, 7-points, and no importance, 0-points. These criteria were allotted a classification along the 7-point scale, for instance, because measurement tools were included in the educational weighting scale but would not be important to all learning tools they were given an importance classification of 3-points. Thus, measurement tool

ratings were included in the educational weighting scale; however, their weightings decreased their importance in the overall scores. The percent importance of each classification became the weight for each criterion (Appendix E). To determine the final scores for each weighting scale, each decision-maker's rank was multiplied by the weight to calculate the score.

Following analysis of all three programs, decision-makers completed a final questionnaire to evaluate their overall preference of program interface, 3D modelling features, measurement tools, and educational features. The questions were open ended which allowed the decision-makers to answer freely (Appendix A).

### 3.3 Results

#### 3.3.1 Cost

In the current market, the basic Amira package costs \$5,400.00. In order for Amira to accommodate large DICOM file data sets, the 'Amira Very Large Data' option is suggested, which is an additional \$6,750.00. An annual maintenance fee of \$1,080.00 for the base package and \$1,350.00 for the Very Large Data package entitles the user to technical support and new product versions. OsiriX is the least expensive program, with the 32-bit version available as free-ware and \$426.00 for the 64-bit version for a single user. The base program for Mimics is \$6,900.00, the MedCad module, which provides the user with more 3D measurement tools, is an additional \$5,175.00. The Mimics license is perpetual; however, to receive program updates and program assistance the annual maintenance package is necessary at a cost of \$900.00 per year.

### 3.3.2 System Requirements

Amira is supported by Windows XP, Vista, and 7, Mac OS X 10.5 and higher, as well as Linux. OsiriX is a Mac only program and is supported by OS X 10.6 and higher. Finally, Mimics is supported by Windows XP, Vista, and 7; however, it is recommended to use Windows Vista or 7 with a minimum of 2GB of ram (8GBs for large data sets).

### 3.3.3 Program Features

All programs have multiple features that assist in the creation of 3D anatomical models from a variety of raw data sources, segmentation, performing measurement, and creation of 3D learning tools. The program features, system requirements, and main features are outlined in Table 5.1.

**Table 3.1 - Program information and features**

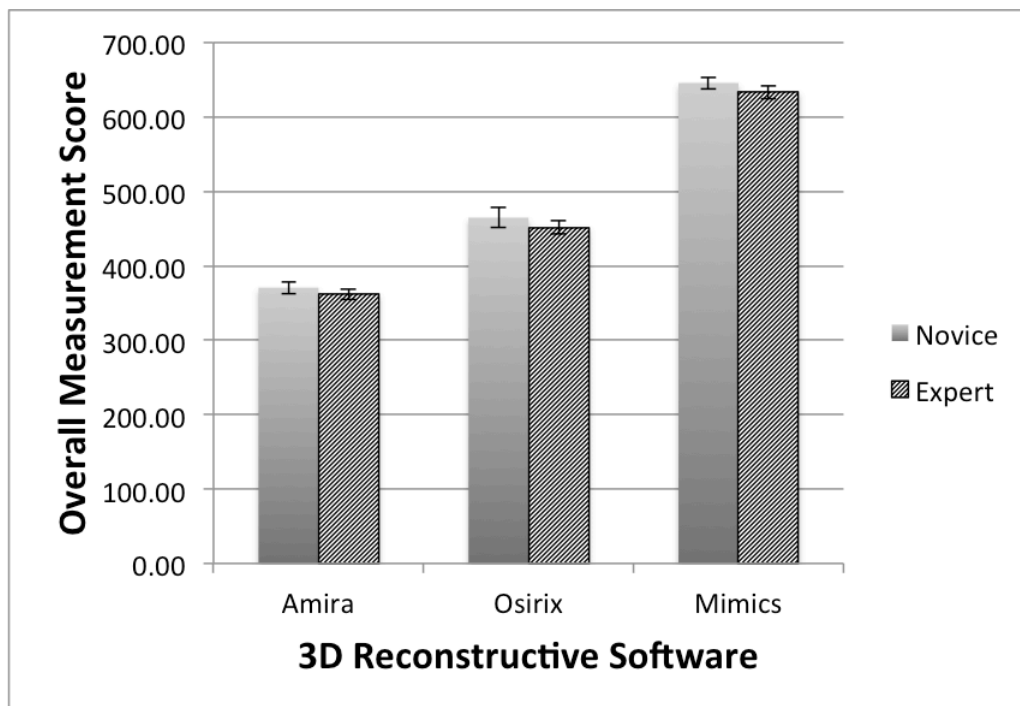
	<b>Amira 5.2</b>	<b>Osirix 3.6</b>	<b>Mimics 14.11</b>
<b>Cost</b>	\$5,400 Very Large Data Option \$6,750	Free for 32-bit \$426 for 64-bit	\$6,900 MedCad Module \$5,175
<b>System Requirements</b>	Windows – XP/Vista/7 Mac OS X – 10.5/10.6/10.7 Linux	Mac OS X – 10.6 +	Windows – XP/Vista/7
<b>Types of Models</b>	Surface-rendered Volume-rendered	Surface-rendered Volume-rendered	Surface-rendered Volume-rendered



	<b>Amira 5.2</b>	<b>Osirix 3.6</b>	<b>Mimics 14.11</b>
<b>Modelling Features</b>	Paintbrush Lassou Threshold Magic Wand Scissors Contour Fitting Interpolation Wrapping Smoothing Morphological Filters Opening/Closing Operations	Thresholding Grow Region Brush Scissors	Thresholding Region Growing Boolean Operations Cavity Fill Edit Masks Multiple Slice Edit Morphology Operations
<b>Measurement Features</b>	2D Length, Angle, Annotate 3D Length, Angle, Annotate Volume	2D Length, Oval, Angle, Rectangle, Text, Open Polygon, Pencil, Point	2D and 3D Measure Distance, Angle, Diameter, Density in Rectangle, Density in Ellipse Annotations CAD Module Objects Re-slicing Density
<b>Educational Features</b>	Movie Maker Exportation of Models Stereo (Anaglyph/Polarized)	Fly through (points of interest) Exportation of Models Stereo Anaglyph	Exportation of Models
<b>Additional Plug-ins/Modules Available</b>	Neuro Option Microscopy Option Developer Option Molecular Option Mesh Option Virtual Reality Option Very Large Data Option	Open-source software - Many 3 <sup>rd</sup> company plug-ins available	3-matic module

### 3.3.4 Decision Matrix - Morphometric Research Weighting Scale Results

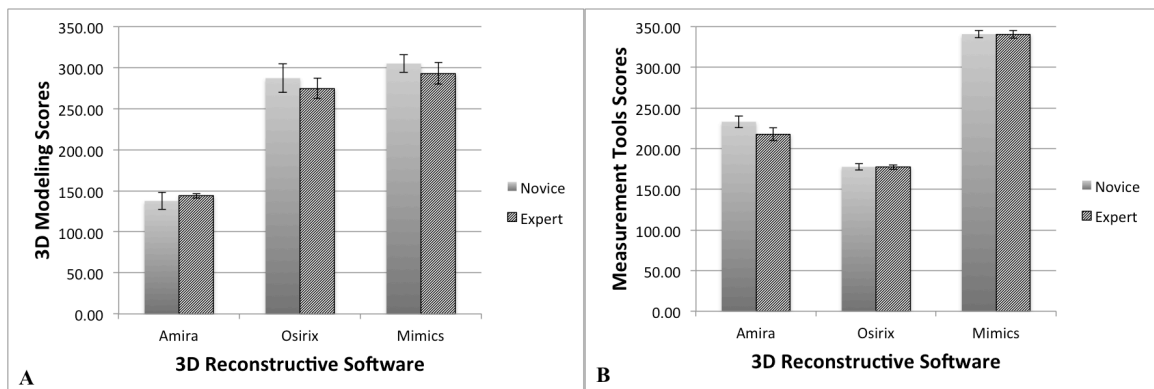
The morphometric research weighting scale applied greater emphasis to 3D modelling, perceived accuracy, and the availability of various measurement tools that can be applied to the created 3D model. The overall scores indicate that Mimics is the leading program for morphometric research (Fig. 3.1). The scores from both the novice decision-makers and the experienced decision-makers were similar.



**Figure 3.1: Overall novice and experienced scores for each 3D reconstructive program using the morphometric research weighting scale**

Examining only the criteria used to evaluate the 3D modelling features of the software both OsiriX and Mimics had high scores, whereas Amira scored lower comparatively (Fig. 3.2A). Once again, the novice and experienced decision-makers were similar in

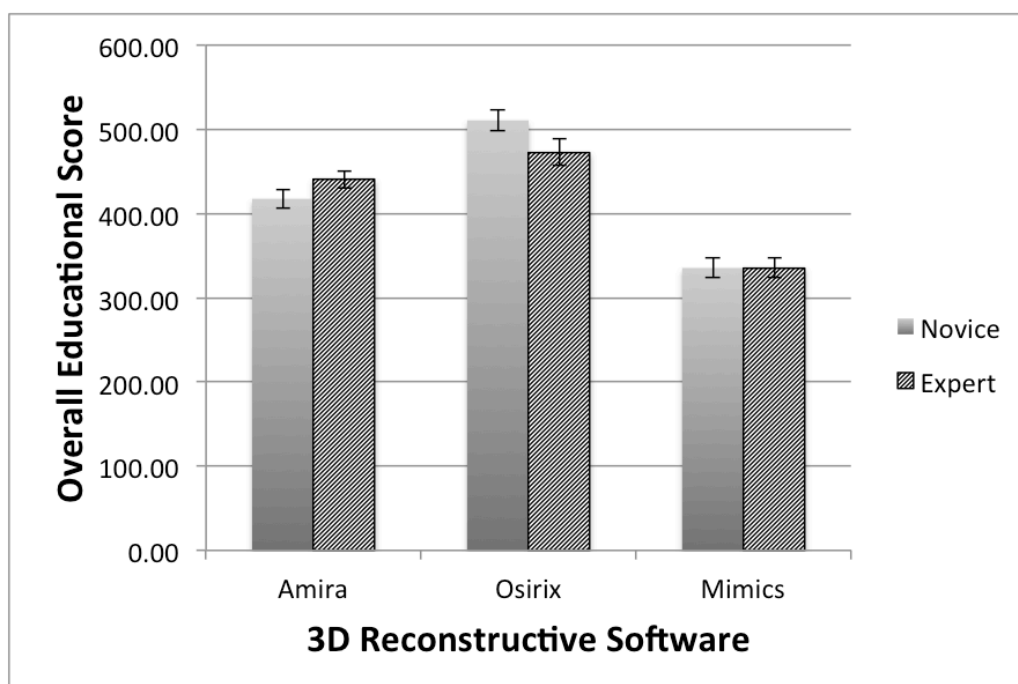
their scoring; however, the experienced decision-makers scored Amira slightly higher and scored OsiriX and Mimics slightly lower than the novice decision-makers. When looking at the criteria questions used to evaluate the available measurement tools, Mimics was scored the highest and both novice and experienced decision-makers scored the programs similarly (Fig. 3.2B).



**Figure 3.2 - Novice and experienced scores, for each 3D reconstructive program using the morphometric research weighting scale, for (A) 3D modelling criteria and (B) measurement tools criteria**

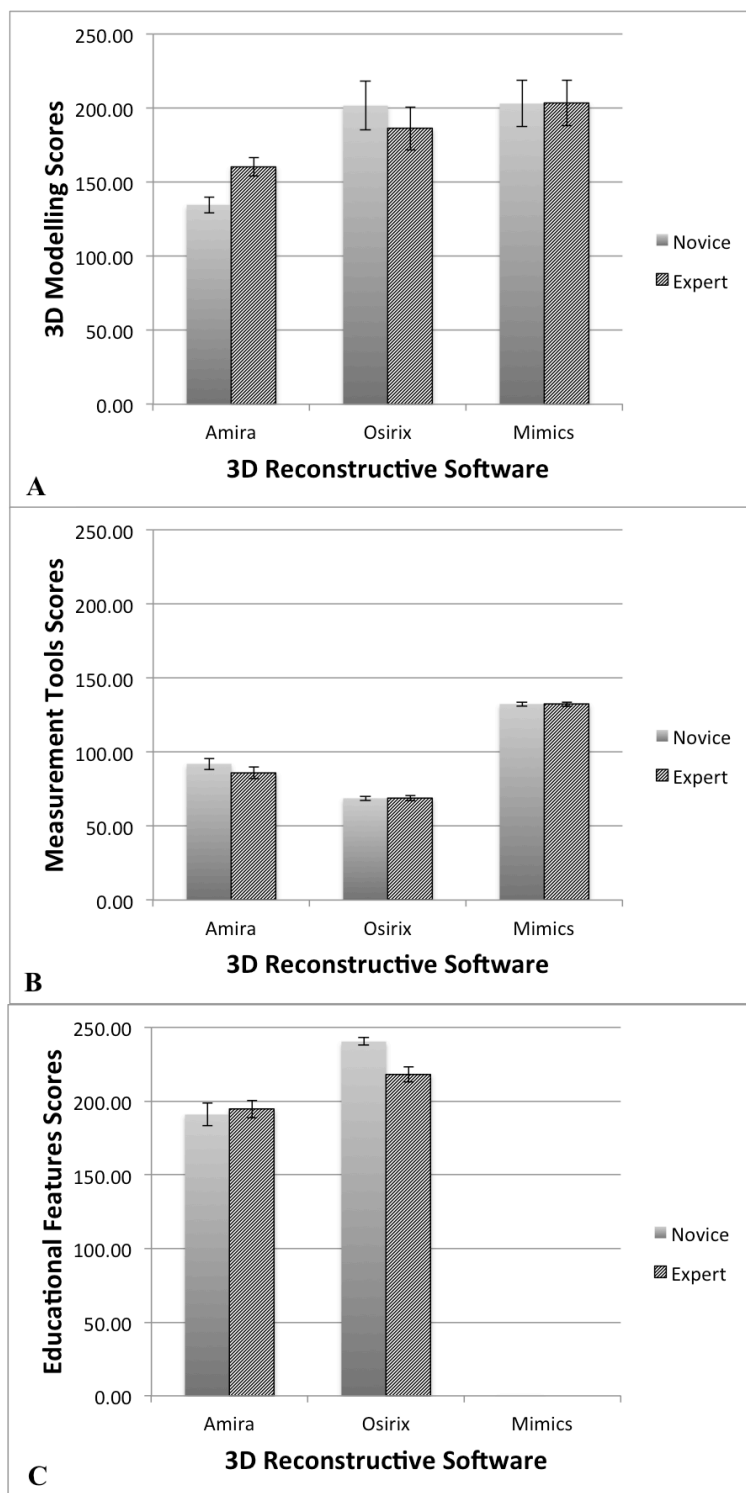
### 3.3.5 Decision Matrix - Educational Features Weighting Scale Results

The educational weighting scale applied a higher emphasis to 3D modelling, ease of use, and available educational features. The overall scores indicate that OsiriX is the leading program with Amira close behind for building 3D models for learning tools (Fig. 3.3). The scores from both the novice decision-makers and the experienced decision-makers were similar.



**Figure 3.3 - Overall novice and experienced scores for each 3D reconstructive program using the educational features weighting scale**

When examining the criteria that sampled 3D modelling features alone, OsiriX and Mimics were scored higher than Amira (Fig. 3.4A). The novice and experienced decision-makers scored Mimics very similarly, whereas the novices tended to score Amira lower and OsiriX higher than the experienced decision-makers. The measurement tool criteria were classified as having a lower importance and thus were weighted lower in the educational weighting scale; as a result these criteria had lower scores. Similarly to the results found with the morphometric research weighting scale, Mimics scored the highest for measurement tools and the novice and experienced decision-makers scored the programs the same (Fig. 3.4B). With regard to the criteria questions used to evaluate the programs' inherent educational features, both Amira and OsiriX were scored highly; however, OsiriX had higher scores than Amira (Fig. 3.4C). Mimics lacks inherent educational features and was not rated in this section. Novice decision-makers rated Amira similarly to the experienced users, but rated OsiriX higher than the experienced users.



**Figure 3.4 - Novice and experienced scores, for each 3D reconstructive program using the educational weighting scale, for (A) 3D modelling criteria, (B) measurement tools criteria, and (C) educational features criteria**

### 3.3.6 Open-ended Comments

All decision-makers provided comments on each section: 3D modelling, measurement tools, and educational features. The over-arching themes from these comments are summarized in Table 3.2.

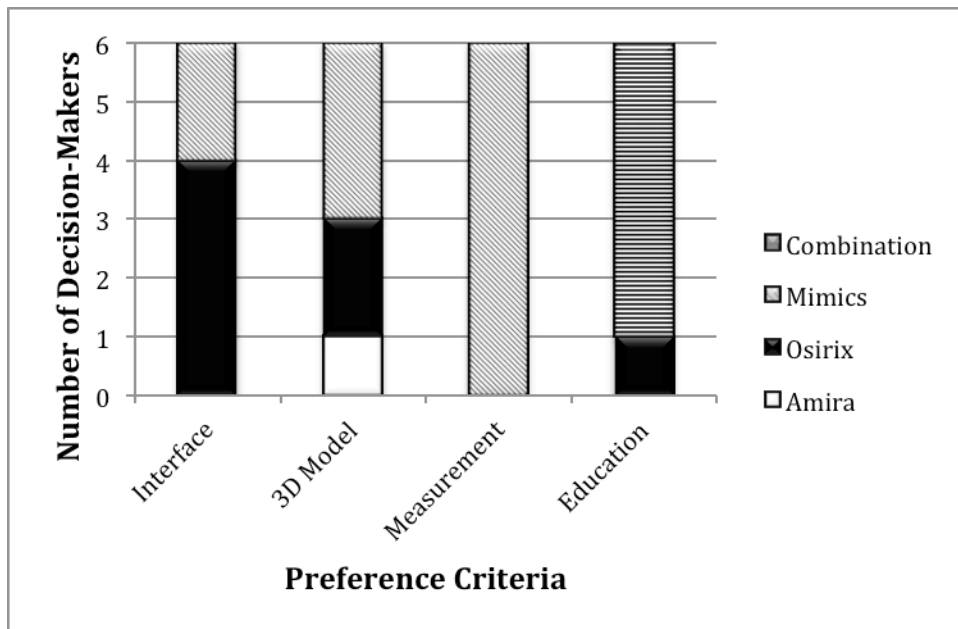
**Table 3.2 - Decision-maker comments regarding each 3D reconstructive software program**

	<b>3D Modelling</b>	<b>Measurement Tools</b>	<b>Educational Features</b>
<b>Amira</b>	<u>Advantages:</u> - A lot of features and potential - Esthetically pleasing models <u>Disadvantages:</u> - Not Intuitive - Time consuming	<u>Disadvantages:</u> - Cannot measure on 2D [data] slices - 2D measurements are not bound to model - Seems to be a high error rate in placing 3D measures	<u>Advantages:</u> - High potential for making dynamic movies - Making stereo models is easy <u>Disadvantages:</u> - Movie making interface is challenging - Quality of stereo anaglyph models is lower than expected
<b>OsiriX</b>	<u>Advantages:</u> - User friendly - Automated surface- and volume-rendered models are excellent quality and easy to make <u>Disadvantages:</u> - manual segmentation models (ROIs) have lower than ideal quality - Cannot add material to the automated models	<u>Advantages:</u> - Easy-to-use - Helpful to have references points that are visible in 2D and 3D <u>Disadvantages:</u> - Cannot perform measurements on 3D model - Limited tool choices and available tools perform simple actions	<u>Advantages:</u> - Easy-to-use - Movie is very smooth <u>Disadvantages:</u> - Stereoanaglyph is harsh - Movie capabilities are very limited
<b>Mimics</b>	<u>Advantages:</u> - Fast - Easy-to-use <u>Disadvantages:</u> - Time consuming to make a 3D model	<u>Advantages:</u> - User friendly - Excellent variety of measurement tools - Ability to map surfaces	<u>Advantages:</u> - With some creativity and screen capture the education value of demonstration with anatomical specimens

		- CAD objects are powerful for measurements <u>Disadvantages:</u> - Difficult to accurately place measurements in 3D	could be achieved. - Even more demonstrative would be the available measurements in this software to both anatomists and clinical colleagues
--	--	--	---

### 3.3.7 Preference Questionnaire

All preference results are shown in Figure 3.5. When asked which 3D program interface was preferred, four decision-makers (three novice and one experienced) chose OsiriX and two experienced decision-makers chose Mimics. With regard to 3D modelling, one experienced chose Amira, two decision-makers (one novice and one experienced) chose OsiriX, and three decision-makers (two novice and one experienced) chose Mimics as their preferred program. All decision-makers chose Mimics as their preferred program to conduct anatomical measurement. One experienced decision-maker chose OsiriX as the preferred program to create an educational tool. All of the other decision-makers said that they would use a combination of the three programs to create an educational tool. The other combinations divided by which program the decision-maker preferred to use to create the 3D model and which program the decision-maker preferred for its educational features. These combinations are outlined in Table 3.3.



**Figure 3.5 - Final questionnaire preferences regarding program interface, 3D modelling features, measurement tools, and educational features**

**Table 3.3 - Preference criteria combinations for creating an educational tool**

Decision-Maker	Build Model	Educational Features
Experienced 1	Mimics	Amira
Experienced 2	Amira	OsiriX
Experienced 3	OsiriX	OsiriX
Novice 1	Depends on the educational tool being created: <ul style="list-style-type: none"> <li>- Amira for complex movies but interface is not intuitive and exporting is timely</li> <li>- OsiriX for easy movies and exports</li> </ul>	
Novice 2	Mimics	Amira or OsiriX
Novice 3	OsiriX	OsiriX for movies Amira for blue/amber or polarized stereoanaglyph



## 3.4 Discussion

The purpose of this study was to compare three widely available 3D reconstruction software programs, Amira, OsiriX, and Mimics. Ranking of the software was performed with respect to each software's ability to be used in morphometric research and in education for the purpose of translating morphological knowledge. The software was ranked by both an experienced and novice cohort using an approach requiring users to perform specific tasks using standardized instructions tailored to each program.

### 3.4.1 Program Features

In terms of affordability, OsiriX is the least expensive program, with a free 32-bit version and \$426.00 for a 64-bit version. OsiriX is an open-source program and thus third-party individuals can create their own plug-ins to manipulate the program to suit their personal research, clinical, and educational needs; this results in the basic OsiriX program being limited in its features, tools, and abilities. For a researcher or a person designing a learning tool this may be a limitation, as he or she may want to use the basic program without spending time and effort designing a plug-in. Many third-party plug-ins are available to the public; however, most plug-ins are designed for a very specific purpose and often are not suitable for general use. Conversely, Amira and Mimics have similar costs for the base program, have many similar innate features designed to assist in measuring and building 3D models, and Amira also has inherent educational features. Both Amira and Mimics have the ability to add on different options for specific uses at an additional cost.

### 3.4.2 Decision Matrix - Morphometric Research Weighting Scale

The morphometric research weighting scale placed heavier emphasis on 3D modelling, perceived accuracy of the anatomical model, measurement, as well as the availability and usability of the measurement tools. Overall scores from the morphometric research weighting scale (Fig. 3.1), demonstrate that Mimics scored the highest, with OsiriX coming in second, and Amira scoring the lowest.

#### 3.4.2.1 Morphometric Research Weighting Scale: 3D Modelling

The 3D modelling criteria questions, using the morphometric research weighting scale, resulted in Mimics scoring the highest with OsiriX trailing slightly behind (Fig. 3.2A). Amira scored quite low in this area. Mimics scored the highest due to the ease of use of its interface and wide availability of tools for segmenting. Manually segmenting anatomical structures is time consuming in all programs; however, one experienced decision-maker mentioned that "... [segmenting] in all three programs was cumbersome but I found that Mimics had the best tools to help with the process." These findings are supported by Tuan and Hutmacher's study that found that Mimics afforded a greater degree of image manipulation, visualization, and editing functions, when compared to two other programs used for bone tissue engineering [21]. OsiriX's high scores in the area of 3D modelling can be attributed to its user-friendly interface, time efficiency, and the high quality of the automatic surface- and volume-rendered models it creates. However, OsiriX did not achieve scores as high as Mimics because of its limited abilities in manual segmentation. Manual segmentation of structures can be achieved in OsiriX, by creating a region of interest (ROI) model; however, the decision-makers found that these ROI models were lower quality than the automatic volume-rendered models. Another limitation to 3D modelling in OsiriX is that the automated models cannot be altered after they are created. Matsumoto et al. [12] also found that the inability to alter

the 3D model after creation was a major limitation in OsiriX, when comparing OsiriX to two other programs, CTTRY and AW, with respect to their characteristics, advantages, disadvantages, and utility in the operating room. Amira's low scores in the area of 3D modelling appear to be due to its non-intuitive interface and the tools and features requiring time to achieve a desired outcome. One decision-maker commented that "[Amira] is useful and does output useful models but its interface and user controls are painstaking and challenging to operate; I would avoid using it despite its output quality." Another decision-maker stated "... the process to come to a surface generated 3D model is long and not intuitive with some steps not well demarcated. These poor work flow ergonomics make it long to get to a suitable/acceptable final product." Thus, due to their user-friendly interfaces and 3D modelling features Mimics and OsiriX scored high in the 3D modelling section of the Morphometric weighting scale; Amira's low scores, on the other hand, were a result of a challenging interface despite model quality.

#### 3.4.2.2 Morphometric Research Weighting Scale: Measurement Tools

Mimics scored the highest with Amira and OsiriX scoring lower in the measurement tool category of the morphometric research weighting scale (Fig. 3.2B). Mimics' strong score in this area is a result of its variety of available measurement tools and its user-friendly interface. One decision-maker commented that: "the measurement tools are fantastic and not only appear to measure what I want but in some instances encourage new dimensions/perspectives to the data at hand." Another decision-maker commented on a specific measurement tool available stating that: "the ability to map convex and concave [anatomical] structures is invaluable for clinical/research activities." Amira scored quite a bit lower than Mimics but slightly higher than OsiriX. Once again the lower scores were due, at least in part, to the challenging program interface but there were also some comments surrounding the disadvantages of the measurement tools themselves, such as "[not being able to make] measurements on 2D slices is a limitation to research" and "the

3D [measurements], though anchored [unlike the 2D measurements] are ill-representations of anatomical measures as they fail to align with surface contour and are thus greatly hindered.” OsiriX was scored the lowest of the three programs. The decision-makers found that the measurement tools were easy-to-use but that they were limited and only performed simple actions. Another major disadvantage in OsiriX was that the measurements could only be performed on the 2D slices and not on the 3D model itself. Mimics scored higher than OsiriX and Amira, in the area of measurement tools, because of the variety and versatility of the measurement tools available.

### 3.4.3 Decision Matrix - Educational Weighting Scale

The educational weighting scale was designed to assess the inherent educational features of the program, such as making educational movies and visualizing models in stereo 3D. Any program that creates 3D models may be used as part of an educational tool, via exporting images; however, for the current study, only inherent movie making and stereo 3D tools were assessed. The educational weighting scale applied a higher emphasis on aesthetics and ease of use. Depending on the audience and the learning objectives, a 3D model does not necessarily need to be an accurate representation of the raw data; however, it must appear to be the appropriate anatomical structure and the models must be easy to make in order for it to be worthwhile for an educator to take the time to create a 3D model as a learning tool. Although the ‘perceived anatomical accuracy’ criterion was given a lower importance classification, it was not removed from the educational weighting scale, because surgical training tools would require high anatomical accuracy. Thus, the necessity for anatomical accuracy depends on the educational tool being created. The educational weighting scale assessment criteria were divided into three categories: 3D modelling, measurement tools, and educational features. The criteria assessing measurement tools were included in the educational weighting scale with a lower importance classification. Measurement tools were included because learning tools created with 3D anatomical models can be used to transfer knowledge of clinical

measurements, diagnoses, and treatments, and thus the measurements themselves can be visualized within the learning tool. However, the actual measurements taken on a demonstrative model might be less critical than those used in actual clinical practice. Overall results for the educational weighting scale are displayed in Figure 3.3. OsiriX scored the highest with Amira trailing slightly behind and Mimics scored the lowest. OsiriX's high scores can be attributed to the program's easy-to-use features and interface. Mimics' low scores likely result from its lack of movie making or stereo 3D functions; however, it was rated high in both the 3D modelling and measurement tool sections. It should be noted that Mimics does have the ability to screen capture and record a video. However, visualization of this recording is only available within the Mimics program itself and exporting of this video would require third-party software to capture it for export.

#### 3.4.3.1 Educational Weighting Scale: 3D Modelling

In analysis of criteria pertaining to the evaluation of 3D modelling performance, both OsiriX and Mimics accumulated high scores (Fig. 3.4A). Both the novice and experienced decision-makers scored Mimics similarly, whereas the novice decision-makers scored OsiriX slightly higher than the experienced decision-makers. Mimics' high scores can be attributed to the program's user-friendly interface and its variety of segmentation tools. OsiriX's easy-to-use interface and the aesthetics of the program's automated surface- and volume-rendered 3D models resulted in high scores in the area of 3D modelling. Because a user cannot manually alter the automated models and the limited manual segmentation/model creation in OsiriX likely attributed to the experienced users bestowing a lower 3D modelling score to OsiriX than the novices. Amira was rated the lowest of all three programs in the 3D modelling section. Although, the decision-makers were pleased with the 3D models that Amira creates the scores dropped due to the challenging segmentation process and interface. The experienced decision-makers rated Amira higher than the novice decision-makers, likely due to

previous experience that the experienced users had with Amira and other 3D reconstructive software programs. Similar to Guyomarc'h et al., the decision-makers were satisfied with the aesthetics of the models that Amira creates [11].

### 3.4.3.2 Educational Weighting Scale: Measurement Tools

The results of the measurement tools category of the educational weighting scale mirrored those of the morphometric research weighting scale, with Mimics scoring highest and OsiriX scoring lowest (Fig. 3.4B). The reasons behind these scores are the same as the reasons described above from the morphometric research weighting scale results. They differ only in the increased or decreased weight based on perceived importance; thus resulting in lower overall scores.

### 3.4.3.3 Educational Weighting Scale: Educational Features

For assessing the programs' inherent educational features, OsiriX scored the highest followed by Amira. Although Mimics was not scored in this section because it lacked inherent educational features, one decision-maker commented on its educational potential; "I think with some creativity and screen capture, the educational value of demonstration with anatomical specimens [created in Mimics] could be achieved. Even more demonstrative would be the wonderful measurements available in this software to both anatomists and clinical colleagues". OsiriX's high scores are attributed to the program's user-friendly interface and easy-to-use movie and stereo functions. Although easy-to-use, OsiriX's movie function is limited by its ability to only record simple actions and its inability to include 2D slices within the recording. Additionally, the decision-makers found OsiriX's stereo function to be unforgiving on the eyes. Some of the comments addressed these advantages and disadvantages: "if the generated models made

it to the desired quality, the educational and demonstrational possibilities increase as the rapidity and ease of use is high”; “it is easy to create a movie; however, it is very limited in what you can do with the video”. Amira’s scores were high, but lower than OsiriX’s scores. Amira scored high because the program has seemingly unlimited potential in terms of complexity and dynamism of movies and stereo models. However, the scores did not surpass OsiriX’s scores due to the challenging interface of the movie-making function. One decision-maker commented on this stating, “[Amira] has boundless potential but the interface challenges are far too great and too frequent to be useful to a researcher, professor, or clinician. Using it is painful. Though final products could be useful in teaching, most educators lack the time investment that understanding this program demands for even basic use.”

From the results discussed above, the overall program preferences were not surprising. Both OsiriX, with four votes, and Mimics, with two votes, were the programs of choice for interface. For 3D modelling, two decision-makers chose OsiriX, three chose Mimics, and one experienced decision-maker, with prior experience with Amira, chose Amira. All six decision-makers chose Mimics for the preferred program to conduct morphometric research. The preferred program for creating a learning tool was not as obvious. One decision-maker chose OsiriX; however, the other decision-makers did not make a definitive choice, stating they would prefer to use a combination of programs as opposed to a single program. The combinations of programs are listed in Table 3.3. These combinations tended to avoid using Amira to create the 3D model, due to the challenging interface, and would use either Amira or OsiriX for their educational features depending on the task at hand.

This study aimed to provide a general comparison of the features, usability, and quality of output of three different 3D reconstructive software programs available to a wide set of potential users. Although the assessment was designed to cover the majority of the features required for general morphometric research and learning tool design, it was limited in that it did not include all available features in each program. This study did assess the variety, usefulness, ease of use, and perceived accuracy of the available measurement tools. However, not testing the accuracy or precision of the models and

measurements, by reconstructing a model of known dimensions, was a limitation.

Previous studies assessing precision and accuracy have compared some of these software programs to other available programs [11, 24]. Comparing the precision and accuracy of the widely available programs assessed in this study would be an asset; however, that was beyond the scope of this particular study. In addition, this comparison included software programs that are widely available and commonly used for morphometric research and educational purposes. However, it would be advantageous to include additional programs available to assess and compare all available programs.

In conclusion, Mimics seems to be the best suited for a variety of morphometric research projects. Mimics is user-friendly, creates anatomical models easily, and has a variety of useful measurement tools available. For creating an educational learning tool the results were less clear. If the data being used of high quality and can be adapted into a learning tool from an automatic surface- or volume-rendered model, OsiriX is a great program. Any operator can easily create simple, high quality movies from 3D representations of anatomical structures. If the learning tool designer is interested in manually segmenting complex structures, wants to create complex dynamic videos, and has time to learn an intricate program, then Amira would be the best choice.

### 3.5 References

1. Humbert, L., H. Carlioz, A. Baudoin, W. Skalli, and D. Mitton, *3D Evaluation of the acetabular coverage assessed by biplanar X-rays or single anteroposterior X-ray compared with CT-scan*. Computer Methods in Biomechanics and Biomedical Engineering, 2008. **11**(3): p. 257 - 262.
2. Rosse, C., *The potential of computerized representations of anatomy in the training of health care providers*. Academic Medicine, 1995. **70**(6): p. 499-505.
3. Bale, R. and G. Widmann, *Navigated CT-guided interventions*. Minimally Invasive Therapy & Allied Technologies, 2007. **16**(4): p. 196-204.



4. Landes, C.A., F. Weichert, P. Geis, F. Helga, and M. Wagner, *Evaluation of two 3D virtual computer reconstructions for comparison of cleft lip and palate to normal fetal microanatomy*. The Anatomical Record Part A: Discoveries in Molecular, Cellular, and Evolutionary Biology, 2006. **288A**(3): p. 248-262.
5. Rosset, A., L. Spadola, and O. Ratib, *OsiriX: An open-sourcesoftware for navigating in multidimensional DICOM images*. Journal of Digital Imaging, 2004. **17**(3): p. 205-216.
6. Waarsing, J.H., R.M. Rozendaal, J.A.N. Verhaar, S.M.A. Bierma-Zeinstra, and H. Weinans, *A statistical model of shape and density of the proximal femur in relation to radiological and clinical OA of the hip*. Osteoarthritis and Cartilage, 2010. **18**(6): p. 787-794.
7. De Paolis, L.T. and G. Aloisio, *Visualization and interaction system for surgical planning*, in *Engineering Interactive Computing Systems for Medicine and Health Care 2011* 2011: Pisa, Italy.
8. Vernon, T. and D. Peckham, *The benefits of 3D modelling and animation in medical teaching*. The Journal of audiovisual media in medicine, 2002. **25**(4): p. 142-8.
9. Haas, A. and M.S. Fischer, *Three-dimensional reconstruction of histological sections using modern product-design software*. The Anatomical Record, 1997. **249**(4): p. 510-516.
10. Gehrmann, S., K.H. Höhne, W. Linhart, B. Pflessner, A. Pommert, M. Riemer, U. Tiede, J. Windolf, U. Schumacher, and J.M. Rueger, *A novel interactive anatomic atlas of the hand*. Clinical Anatomy, 2006. **19**(3): p. 258-266.
11. Guyomarc'h, P., F. Santos, B. Dutailly, P. Desbarats, C. Bou, and H. Coqueugniot, *Three-dimensional computer-assisted craniometrics: A comparison of the uncertainty in measurement induced by surface reconstruction performed by two computer programs*. Forensic Science International, 2012. **219**(1-3): p. 221-7.
12. Matsumoto, T., Kanzaki, M., Amiki, M., Shimizu, T., Maeda, H., Sakamoto, K., Ookubo, Y., Onuki, T., *Comparison of three software programs for three-dimensional graphic imaging as contrasted with operative findings*. Eur J Cardiothorac Surg, 2012. **41**(5): p. 1098-103.
13. Brandt, R., T. Rohlfing, J. Rybak, S. Krofczik, A. Maye, M. Westerhoff, H.-C. Hege, and R. Menzel, *Three-dimensional average-shape atlas of the honeybee brain and its applications*. The Journal of Comparative Neurology, 2005. **492**(1): p. 1-19.

14. Wang, Z., F. Zeng, H. Li, Z. Ye, Y. Bai, W. Xia, and B. Liang, *Three-dimensional reconstruction on PC-Windows platform for evaluation of living donor nephrectomy*. Computer Methods and Programs in Biomedicine, 2007. **86**(1): p. 39-44.
15. Nguyen, N. and T.D. Wilson, *A head in virtual reality: development of a dynamic head and neck model*. Anatomical Sciences Education, 2009. **2**(6): p. 294-301.
16. Handzel, O., H. Wang, J. Fiering, J.T. Borenstein, M.J. Mescher, E.E. Swan, B.A. Murphy, Z. Chen, M. Peppi, W.F. Sewell, S.G. Kujawa, and M.J. McKenna, *Mastoid cavity dimensions and shape: method of measurement and virtual fitting of implantable devices*. Audiology & neuro-otology, 2009. **14**(5): p. 308-14.
17. Kramer, J., G. Laub, C. Czerny, and M.P. Recht, *MR and MR Arthrography*, in *Medical Radiology Diagnostic Imaging*, A.L. Baert and K. Sartor, Editors. 2008, Springer: Berlin, Heidelberg, New York. p. 31-48.
18. Kim, J., J. Wang, J. Ahn, H. Kim, and H. Lim, *Comparison of femoral tunnel length between transportal and retrograde reaming outside-in techniques in anterior cruciate ligament reconstruction*. Knee Surgery, Sports Traumatology, Arthroscopy, 2012: p. 1-9.
19. Rojas, C.A., H. Jawad, and J.H. Chung, *The new era of radiology teaching files*. AJR. American journal of roentgenology, 2012. **198**(4): p. 773-6.
20. Qing, K.-x., W.-k. Yiu, and S.W.K. Cheng, *A morphologic study of chronic type B aortic dissections and aneurysms after thoracic endovascular stent grafting*. Journal of Vascular Surgery, 2012. **55**(5): p. 1275-1276.
21. Tuan, H.S. and D.W. Hutmacher, *Application of micro CT and computation modeling in bone tissue engineering*. Computer-Aided Design, 2005. **37**(11): p. 1151-1161.
22. Mahaisavariya, B., B. Saekee, K. Sitthiseripratip, P. Oris, T. Tongdee, E.L. Bohez, and J. Vander Sloten, *Morphology of the radial head: A reverse engineering based evaluation using three-dimensional anatomical data of radial bone*. Proceedings of the Institution of Mechanical Engineers, Part H: Journal of Engineering in Medicine, 2004. **218**(1): p. 79-84.
23. Lu, S., Y.Q. Xu, Y.Z. Zhang, L. Xie, H. Guo, and D.P. Li, *A novel computer-assisted drill guide template for placement of C2 laminar screws*. European spine journal : official publication of the European Spine Society, the European Spinal Deformity Society, and the European Section of the Cervical Spine Research Society, 2009. **18**(9): p. 1379-85.

24. Kim, G., H.-J. Jung, H.-J. Lee, J.-S. Lee, S. Koo, and S.-H. Chang, *Accuracy and reliability of length measurements on three-dimensional computed tomography using open-source OsiriX software*. Journal of Digital Imaging, 2012: p. 1-6.
25. Al-Najjar, B.a.A., Imad, *Selecting the most efficient maintenance approach using fuzzy multiple criteria decision making*. Int. J. Production Economics, 2003. **84**: p. 85-100.
26. Müller, R. and P. Büttner, *A critical discussion of intraclass correlation coefficients*. Statistics in Medicine, 1994. **13**(23-24): p. 2465-2476.
27. Finstad, K., *Response Interpolation and Scale Sensitivity: Evidence Against 5-Point Scales*. Journal of Usability Studies, 2010. **5**(3): p. 104-110.

## Chapter 4

### 4 Validity and Reliability of a Novel 3D Measurement Approach for the Morphology of the Proximal Femur

#### 4.1 Introduction

Osteoarthritis (OA) of the hip joint is a multi-factorial disease that affects a large number of aging individuals and is associated with significant disability [1, 2]. Morphological variations of the proximal femur and the acetabulum have been identified as potential factors contributing to OA. Altered geometry of the proximal femur, the acetabulum, or both, is thought to create abnormal loading patterns in the hip joint resulting in OA disease progression [3]. However, it is not known where these morphological changes occur along the spectrum of the disease process [3] and specifically whether they precede disease onset. Importantly, to help in assessing morphological changes and their impact on disease progression, normative values first need to be established. The most common locations for variations in bone geometry of the hip joint are the acetabular rim and the femoral head and neck [3].

Hip instability and femoroacetabular impingement (FAI) are two of the conditions that define morphological variations of the hip joint [4, 5]. Acetabular dysplasia (AD) is the primary cause of atraumatic hip instability and is characterized by insufficient anterolateral femoral head coverage by the acetabulum and superolateral inclination of the acetabular surface [6, 7]. AD can result in morphological changes to the femoral head, such as a misshapen femoral head and increased anteversion of the femoral neck [7, 8]. Acetabular dysplasia results in anterolateral acetabular rim overload, excessive shear stresses, and instability, which is thought to lead to joint degeneration [9]. FAI is characterized by abnormal contact between the anterosuperior-lateral aspect of the

femoral neck and the anterosuperior acetabular rim. AD is assessed radiographically by the centre-edge (CE) [6] angle and the vertical-centre-anterior (VCA) angle [10, 11]. One specific type of FAI is cam impingement. Cam impingement is characterized by a decreased head-neck offset of the anterosuperior or anterolateral portion of the femoral head-neck junction [8, 12-14]. During hip flexion this cam-lesion rotates into the acetabulum and applies compressive and shear forces to the anterosuperior acetabulum limiting range of motion (ROM) and resulting in labrum and articular cartilage damage [8, 13, 15]. Currently, cam impingement is identified using the head-neck offset ratio [16] and the alpha angle [17].

Detecting and providing early treatment to patients with hip instability and FAI may slow the progression of OA [8, 14, 17-19]; however, the current two-dimensional (2D) radiographic parameters for detecting these morphological variations are unreliable. Clohisy J.C. et al. [4], evaluated the reliability of six hip specialists identifying important radiographic features of the hip on plain radiographs. The diagnostic measures for AD, CE angle and VCA angle, and the diagnostic measures for cam-FAI, head-neck offset ratio and alpha angle, were included in these radiographic features of the hip. They found that these standard radiographic parameters used to diagnose these bony variations are not reproducible [4]. The same group conducted another study investigating the reliability of radiographic measurements of the hip by various physicians, who are musculoskeletal specialists. Similarly, they found that the measurements were not reliable among observers and were limited in their ability to determine a constant radiographic diagnosis [20]. A clear set of definitions and measurements are necessary for reliable detection of early hip disease [4].

In addition to the radiographic methods of measurement lacking reproducibility, these methods also attempt to define the geometry of the hip using pre-determined measures, typically lengths and angles, from two-dimensional (2D) radiographic planes. Projecting three-dimensional (3D) geometry on to 2D planes does not accurately account for the entire joint morphology and quantifying the morphology with linear measures on a 2D scan may not assess the relevant pathologies [21, 22]. In addition, given the large articular surface area, 2D methods result in visual apposition, or overlap, of the femur

and acetabulum and fail to analyze variations in osseous morphology that may otherwise be hidden [23]. A reliable and accurate measurement modality that quantifies the entire 3D surface morphology of the hip may assist in early detection and treatment of early hip disease.

Measurement modalities of the hip joint are implemented and used to diagnose pathologies without having been validated or tested for reliability. Unfortunately, this has led to clinical practice relying on potentially invalid and unreliable hip metrics to plan patient interventions. In addition these measurements rely on 2D linear measures to assess 3D geometry. Thus, the purpose of this study was to develop and test the validity and reliability of a 3D measurement approach for proximal femur morphometry. The novel measurement quantifies the entire 3D morphology of the femoral head.

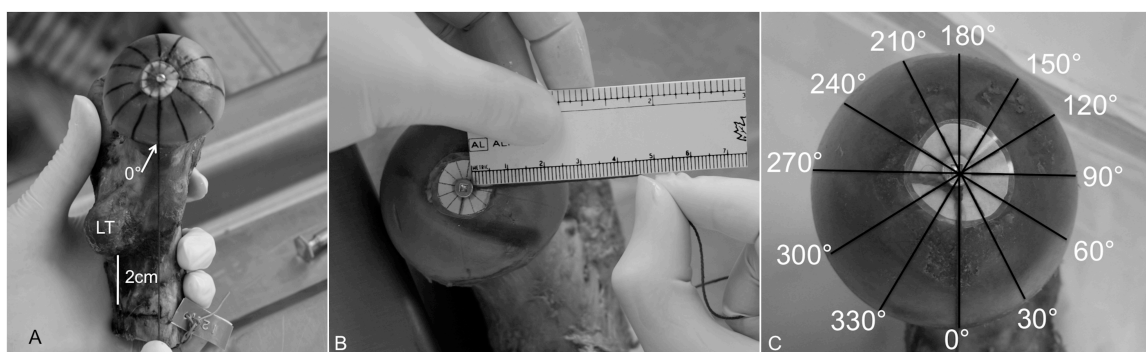
Measurements are taken every 30° around the sphere from the centre of the fovea to the point at which the convexity of the femoral head meets the concavity of the femoral neck. This measurement approach was selected such that measurement would be inclusive of any and all bony lesions present at the head-neck junction. The novel measurement approach was applied to both cadaveric specimens and to 3D digital models created from CT scans of the same specimens. It is hypothesized that the mean difference between the digital measures and the measures taken on the cadaveric specimens will be minimal. Additionally, it is hypothesized that there will be strong reliability between observers and trials.

## 4.2 Methods and Materials

Forty-seven cadaveric femurs were obtained with permission from the Western University Body Bequeathal program. Two specimens were excluded from the study, one was excluded due to the presence of a metal prosthesis and the other specimen was excluded from the inability to manually separate the femur from the pelvis due to severe degenerative disease. The 45 specimens included in the study (23 right; 22 left and 8

female; 37 male) had an average age of  $77.6 \pm 11.5$  years (age range 51-104 years) and consisted of 19 bilateral and 7 unilateral femurs. As this is primarily an evaluation of the method, bilateral femurs were included in the study and each individual femur was considered as a separate specimen.

All specimens underwent CT scanning in a GE Lightspeed VCT (*GE Healthcare, WI., USA*) at University Hospital, London, Ontario. The images had a slice thickness of 0.6mm and a pixel matrix of 512 by 512. After scanning, the cadaveric specimens were manually dissected, stripping them of all soft tissue with the exception of articular (hyaline) cartilage. To prepare for measurement, a 1.5cm circular template consisting of 12 radiating lines, each separated by 30 degrees, was created for each specimen (Fig. 4.1B).



**Figure 4.1 – Measurement of the femoral cadaveric specimens. (A) Establishment of the 0° angle marker. (B) Linear surface measurement of the femoral head from the center of the fovea marker to the point where the neck extends from the femoral head using suture string. (C) Linear surface measurements are taken at each of the 12 angle markers.**

#### 4.2.1 Cadaveric Measurements

The flexible angle template was applied to the center of the fovea and screwed into the bone for stability. Femoral midline was established while in a medial view of the fovea

by measuring the diameter of the shaft 2cm inferior to the lesser trochanter. A line drawn from the midline point to the fovea established the 0-degree angle (Fig. 4.1A). Linear surface measurements were performed using a suture string along the surface of the femoral head from the center of the fovea to the point where the convexity of the femoral head meets with the concavity of the femoral neck. The length of the string at each of the 12 angles, representing femoral surface dimension, was then measured with a ruler (Fig. 4.1B).

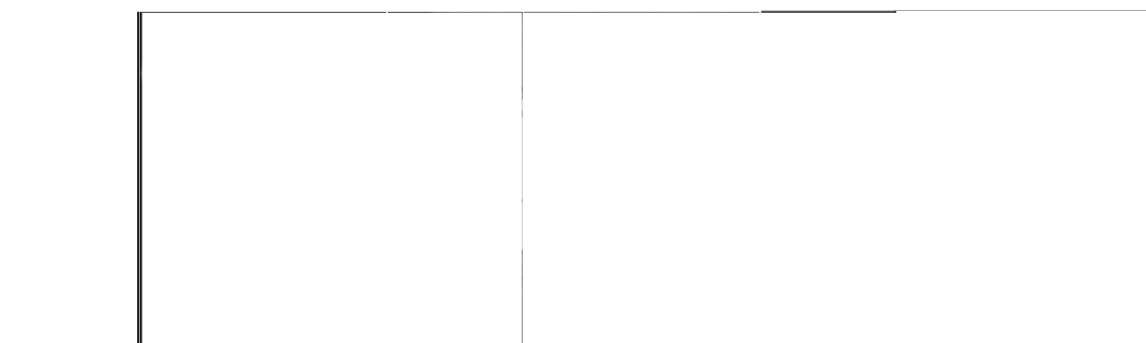
### 4.2.2 Digital Measurements

The CT, digital imaging and communications in medicine (DICOM), files for all specimens were imported into the computer software *Mimics 14.11* (*Materialise, Leuven, Belgium*). Standardized image thresholding was performed to separate the bone contrast from the surrounding soft tissue contrast levels (Hounsfield threshold values: minimum = 226; maximum = 2606). Manual segmentation was performed on each model to separate the femur from the pelvis. In order to accurately measure the surface of the 3D model, the surface must be continuous and devoid of any holes; thus, each model went through a *cavity fill* process. This process ensures a continuous surface; however, it does not ‘smooth’ the surface of the model nor does it adversely affect the calculation of the surface.

In order to create a virtual angle template that is identical to the cadaveric angle template, a 2D circle with a 1.5cm diameter was applied to center of the fovea. A 3D marker was placed in the center of the 2D circle to indicate the center of the fovea. The location of the femoral midline was established by measuring the diameter of the shaft 2cm inferior to the lesser trochanter, while in a medial view of the fovea. A line extending from the femoral midline point to the fovea established the 0-degree angle; a 3D marker was applied to indicate the 0-degree angle (Fig. 4.2A). A 2D plane was created at the level of the fovea, which included both the center of the fovea marker and the 0-degree angle



marker. The remaining 11 angles were designated, using the *measure angle* tool, every 30 degrees from the 0-degree line. 3D markers were placed to indicate each angle (Fig. 4.2B). Measurements were made, on the 3D model using the *measure distance over surface* tool, from the center of the fovea marker to the point where the convexity of the femoral head meets the concavity of the femoral neck at each of the 12 angles (Fig. 4.2C).



**Figure 4.2 - Measurement of the femoral digital models. (A) Establishment of the center of the fovea and the 0° angle marker. (B) Creation of the angle template on a 2D plane. (C) Measurement of the femoral head from the center of the fovea marker to the point where the neck extends from the femoral head. Measurements are taken at each of the 12 angle markers.**

### 4.2.3 Statistical Analysis

To assess validity of the measurement approach, one anatomist (CM) performed all of the cadaveric and digital measurements. To assess intraobserver reliability, the main observer (CM) repeated the measurements, in a randomized order, on the entire dataset ( $n = 45$ ), with a minimum of 48 hours separating measurement trials. In order to assess interobserver reliability, a subset ( $n = 18$ ) of specimens was randomly selected. Two independent blinded anatomists (CM & JT) performed all measurements on this subset in random order. The observers were not provided with any feedback while measuring and were blinded to their previous measurements and the other observers.

Statistical analysis was performed using *SPSS 16* (SPSS Inc., Chicago, Illinois) and *Prism 5* (GraphPad Software, Inc. La Jolla, California). The mean difference between the methods was assessed by the Bland-Altman method. Interobserver and intraobserver reproducibility were assessed by the intra-class correlation coefficient (ICC) and the Bland-Altman method.

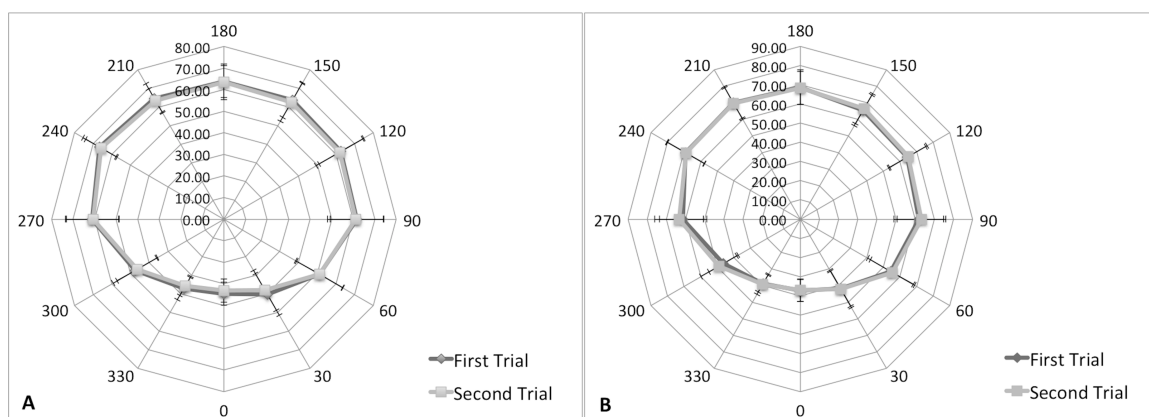
## 4.3 Results

### 4.3.1 Reliability of Femoral Head Surface Measurements

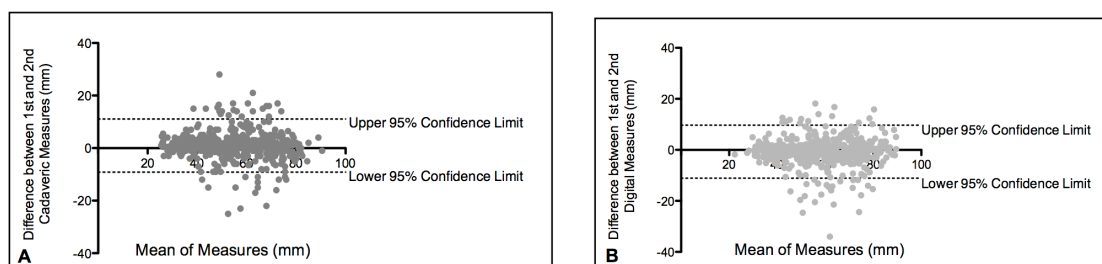
#### 4.3.1.1 Intraobserver Reliability

High intraobserver reliability ( $n = 45$ ) was observed between the first and second cadaveric measurements with an intraclass correlation coefficient (ICC) of 0.99 (95% confidence interval (CI) 0.91 to 1.0). Figure 4.5A displays the mean cadaveric measurements at each degree point for the first and second measures taken by observer one (CM) on a polar graph. The points on the polar graph correspond to the points measured on the femoral head (Fig. 4.1C). The Bland-Altman plot (Fig. 4.6A) illustrates the difference between the mean cadaveric measurements at each measurement point for the first and second measures. The mean difference between the two measurements was -5.16mm and the upper and lower 95% confidence limits were 11.05mm and -9.17mm respectively. The intraobserver reliability for the first and second digital measurements ( $n = 45$ ) was also observed to be high with an intraclass correlation coefficient of 0.99 (95% CI 0.98 to 0.99). The polar graph Figure 4.5B, displays the mean digital measurements for the first and second measures taken by observer one (CM). The points on the polar diagram correspond to the points measured on the femoral head (Fig. 4.1C). The Bland-Altman Plot in Figure 4.6B illustrates the difference between the first and second

measures at each measurement point. The mean difference (SD) between the two measurements was -5.30mm and the upper and lower 95% confidence limits were 9.66mm and -11.11mm respectively.



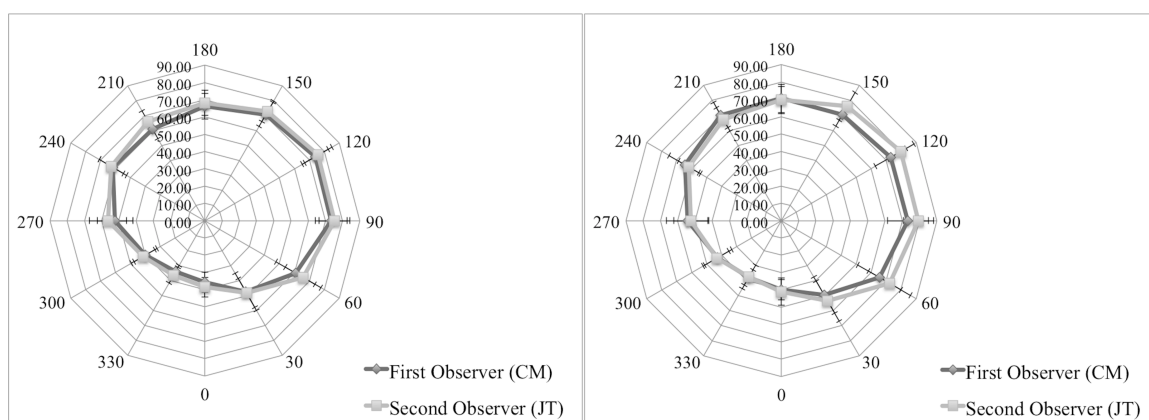
**Figure 4.3 - Polar graphs of intraobserver reliability measurements of femoral head surface. The 12 axes represent the 12-degree points where the measurements were taken. The mean measurement (mm  $\pm$  SD) for each degree point is plotted for the first and second measures. (A) Mean cadaveric first and second measurements. (B) Mean digital first and second measurements.**



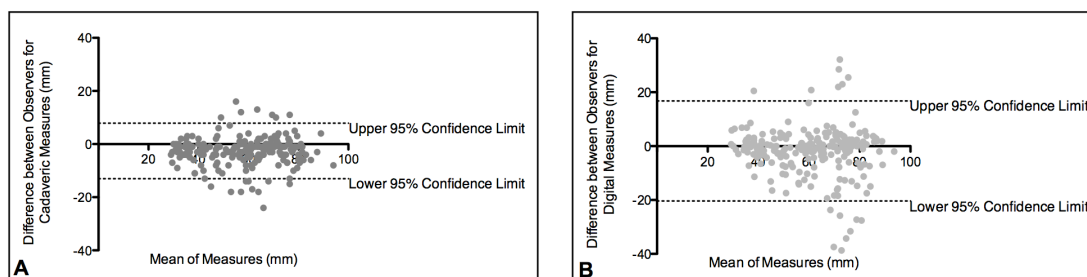
**Figure 4.4 – Bland-Altman plot of intraobserver variability of the (A) femoral cadaveric measures and (B) femoral digital measures. The x-axis plots the mean measurement between observations against the difference between the measures (mm) on the y-axis (First Measure – Second Measure).**

#### 4.3.1.2 Interobserver Reliability

A high agreement was observed between observers when measuring the cadaveric specimens (ICC = 0.99, 95% CI 0.99 to 0.99) and when measuring the digital model measurements (ICC of 0.98, 95% CI 0.93 to 0.99). Polar graphs display the mean measures for each observer for cadaveric measures (Fig. 4.7A) and digital measures (Fig. 4.7B). The points on the polar diagram correspond to the points measured on the femoral head (Fig. 4.1C). The Bland-Altman plots illustrate the difference between the mean measures at each measurement point for the cadaveric measures (Fig. 4.8A) and digital measures (Fig. 4.8B). The mean difference between the two observers' cadaveric measurements was -5.33mm and the upper and lower 95% confidence limits were 7.84mm and -13.05mm respectively. For the digital measures, the mean difference between the two measurements was -9.47mm and the upper and lower 95% confidence limits were 16.74mm and -20.39mm respectively.



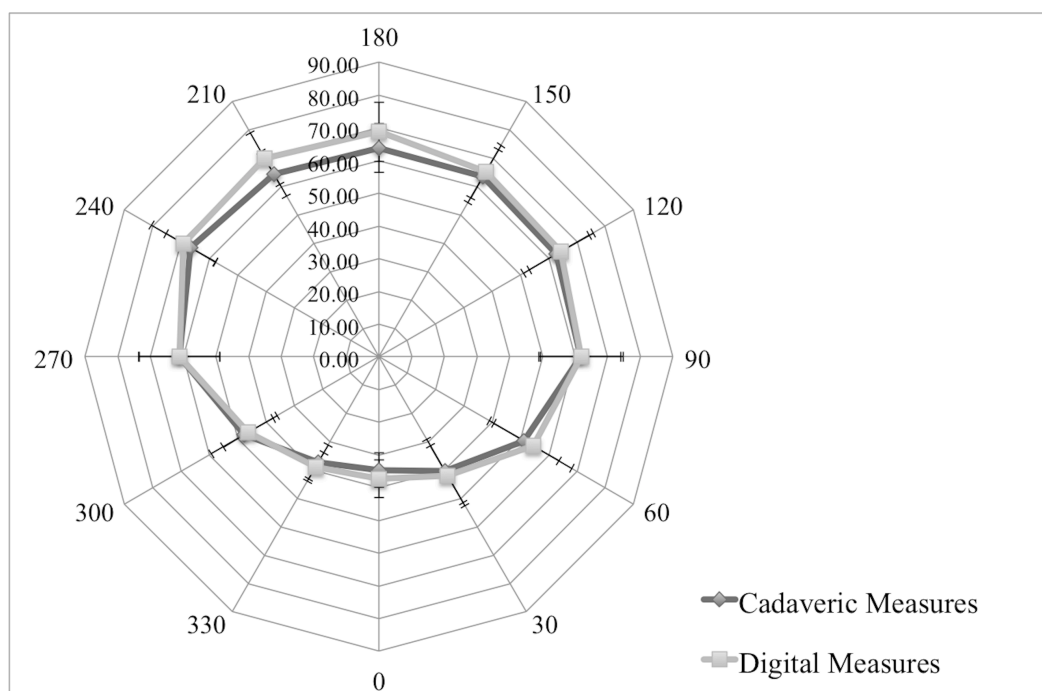
**Figure 4.5 - Polar graphs of interobserver reliability measurements of the femoral head. The 12 axes represent the 12-degree points where the measurements were taken and the mean measurement (mm  $\pm$  SD) for each degree point is plotted for both observers. (A) Cadaveric measures for observer 1 (CM) and observer 2 (JT). (B) Digital measures for observer 1 (CM) and observer 2 (JT).**



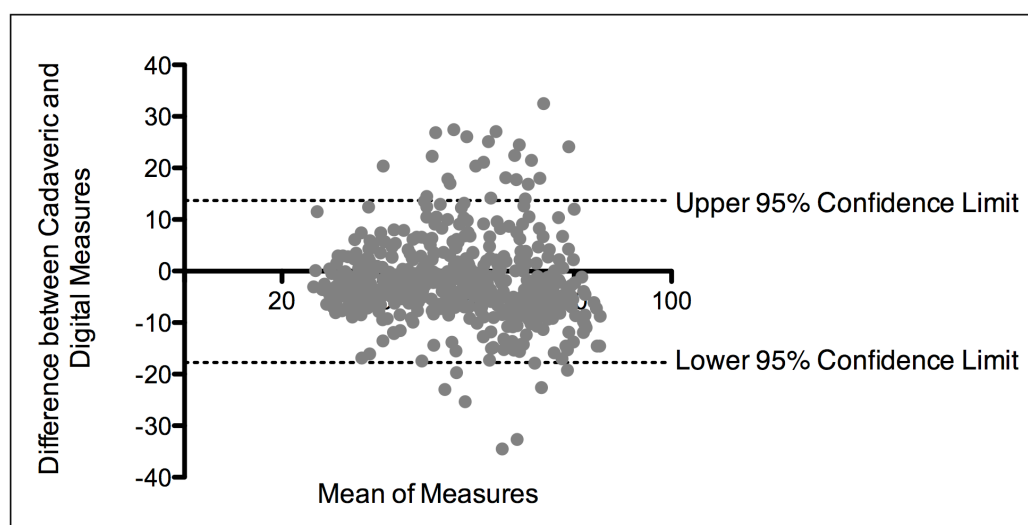
**Figure 4.6 – Bland-Altman Plot of interobserver variability of the (A) femoral cadaveric measures and (B) femoral digital measures. The x-axis plots the mean measurement between observations against the difference between the measures (mm) on the y-axis (First Observer (CM) – Second Observer (JT)).**

#### 4.3.2 Validity of Femoral Head Surface Measurements

The mean difference between the cadaveric and digital measures of the same femur was -2.04mm. The Bland-Altman plot (Fig. 4.4), illustrates the difference between the mean cadaveric measures and the mean digital measures at each measurement point. The upper and lower 95% confidence limits were 13.67mm and -17.75mm respectively. The polar graph, Figure 4.3, displays mean femoral head measurements for both cadaveric and digital modalities at each of the 12 angle markers. The degree points on the polar graph correspond to the angle markers measured on the femoral head (Fig. 4.1C). This graph illustrates that the largest femoral head surface measurements were found between 150 and 240 degrees corresponding to the anterosuperior-lateral femoral head surfaces. The smallest surface measurements were found between 330 and 30 degrees corresponding to the inferomedial surface of the femoral head.



**Figure 4.7 - Polar graph of mean femoral cadaveric and digital measurements (mm  $\pm$  SD). The 12 axes represent the degree ( $^{\circ}$ ) points (see Fig. 4.1C) identifying measurement position. Mean measurements for each degree point are plotted for the cadaveric and digital measures.**



**Figure 4.8 - Bland-Altman plot of the difference between the femoral cadaveric and the digital measurements for the same femur. The x-axis plots the mean of two measurements against the difference between the measurement modalities (cadaveric - digital) on the y-axis.**

## 4.4 Discussion

The limited reliability of current radiographic approaches used to diagnose hip instability and FAI has created a necessity for a valid and reliable measurement methodology for early detection of hip disease [4]. Current hip measurement modalities define the geometry using pre-determined 2D linear measures. These measures fail to quantify the entire 3D surface morphology of the femoral head and may not assess relevant clinical deviations [21]. Thus, utilizing a technique, as described here, that accurately and reliably accounts for the entire 3D surface morphology of the femoral head may assist in early detection and treatment of hip disease.

The digital measurement approach presented was found to be reliable and when compared to the cadaveric measurements the measurements were consistent with a mean difference of -2.04mm. The digital measurement approach had excellent intraobserver reliability (ICC = 0.99, CI 0.98 to 0.99) and interobserver reliability (ICC = 0.98, CI 0.93 to 0.99). Originally, it was thought that the presence of hyaline cartilage on the cadaveric specimens, and the inability to visualize hyaline cartilage on the digital models due to the limitation of CT imaging of cartilage, would create a discrepancy in the measurements. However, in general the digital measurements tended to be slightly larger than the cadaveric measurements at most degree points, thus including hyaline cartilage in the cadaveric measurements produced minimal and unlikely clinically relevant error. The larger digital measurements may be due to an increased accuracy when using the digital measurement algorithm. The digital model surfaces were attained using the *measure distance over surface* tool, which detects minute changes in the surface morphology of the 3D model, whereas the cadaveric specimens were measured along the surface with string. The string would not have accounted for the small indentations on the femoral head surface that would have been detected using the digital approach. Hence, it may be reasonable to suggest the digital measure should be more accurate. A systematic difference in the observer's digital versus cadaveric measurement approach may be another potential explanation for the digital measures tending to be larger than the cadaveric measures.

The digital measurement approach affords visualization and measurement of the entire joint surface of the femoral head. Typically the largest length of the femoral head is located anterosuperior-laterally, whereas the smallest length of the femoral head is found inferolaterally [24]. This study's measurements were consistent with normal femoral head geometry. The largest femoral head surfaces corresponded to the anterosuperior-lateral aspect of the femoral head, found between 150 and 240 degrees, and the smallest femoral head surface measurements corresponded to the inferolateral aspect of the femoral head, found from 330 to 30 degrees. Additionally, the anterosuperior-lateral aspect of the femoral head is the common location for cam-FAI bony abnormalities. Cam-FAI is characterized by a 'bump' or 'lesion' that decreases the head-neck offset at the anterosuperior-lateral portion of the femoral head-neck junction [8, 12-14]. The alpha angle is considered to be the simplest and quickest method for measuring the femoral head-neck offset [17, 19]. The alpha angle is measured on centre cut axial oblique view MR images and is defined as the angle between a line drawn through the centre of the long axis of the femoral neck and head and a line drawn from the centre of the femoral head to the first point where the contour of the femoral head exceeds the radius of the head [17]. A consensus of which alpha angle value is diagnostic of a hip with impingement does not exist in the literature as many criteria values are used [17, 19, 25].

In addition, because the alpha angle is measured on one slice, the cam lesion may be incompletely visualized or not captured at all. The measurement approach presented herein enables measurement of the same cam lesion in a 3D manner, allowing complete lesion visualization. Longer femoral head lengths found between 150 and 240 degrees may be indicative of a cam lesion. A range of normal values and a range of values indicative of cam lesions need to be established for this measurement approach. Furthermore, reliability is increased in the 3D approach, as the operator no longer physically selects the center cut axial oblique view. Due to the specimens being obtained from older individuals for this study it is possible that structural hip pathologies, including cam lesions, may have been present. On some specimens, bony calcifications were easily visualized on both the cadaveric specimens and the digital models; these bony calcifications were included in the measurements via longer lengths measured at the



anterosuperior-lateral aspect of the femoral head, illustrating that the digital measurement approach is robust, valid, and reliable regardless of variation in femoral head anatomy.

The segmentation protocol used to create the 3D models may be a source of small error due to partial-volume effects where bone meets soft tissue. Partial-volume effects occur when multiple tissue types contribute to the digital composition of a single voxel (a 3D pixel). The voxel is expressed as an average of the attenuation properties of all contributing tissues, resulting in blurred tissue boundaries [26]. However, the potential for partial volume errors was minimized with thin CT slice thicknesses, 0.6mm, as it is less likely multiple structures will occupy the same voxel. When creating the 3D models a cavity-fill process was performed to ensure a continuous surface. Deviations in the surface were created from a lack of cortical bone thickness in areas of the proximal femur, thus these areas were not identified as bone on the CT scans. The cavity-fill process was done manually to ensure that deviations in the model surface were filled, yet no excess bone was added to the surface. Although the cavity-fill was performed carefully and manually, this process may have created a source of error in the digital measurements. The placement of the measurement template may also provide to be a challenge when performing these measurements. The angle template was applied to the centre of the fovea; however, a slight change in location of the template may alter the measurement results. Thus, if the placement of the template was different on a cadaveric specimen than it was on a digital model a difference between measurements may have resulted. However, due to the high agreement between measurements one would expect the placement location of the template produced minimal error. To accurately achieve a mean difference of -2.04mm the required sample size would be 168 specimens, thus the included 45 specimens limited this study. Similarly, Bland-Altman analyses require a sample size of 50 and thus, the sample of 45 in this study may have produced slightly wider 95% confidence limits [27]. Additionally, another limitation to the digital measurement approach was the time required to build a 3D model and conduct the measurements. If such a measurement approach was introduced into clinical practice the creation of the model and the measurement approach would need to be automated for time efficiency.

With novel approaches such as those described here, greater use of 3D imaging can be exploited to measure 3D femoral geometry. Future studies should be completed to establish a range of normal and pathological measures. These values could then be used to determine precise normal and pathological criteria values. Creating pathological criteria values using a valid and reliable measurement modality may lead to early diagnoses and treatment of structural hip disease, which may lead to a decrease in morbidity associated with OA [8, 14, 17-19]. Once pathological criteria values have been established, the measurement approach could be automated and widely available for use on imaging visualization stations. The novel digital measurement approach could also be applied to the acetabulum to assess similar morphometrics. Structural hip disease affects both the proximal femur and the acetabulum. It is important to examine the 3D morphology disarticulated for the presence of structural lesions that may be hidden when articulated [23]; however, it would be beneficial to assess the femoral structural lesions in relation to the acetabular structural lesions.

In conclusion, the presented measurement approach is reliable, provides consistent measures between methods within -2.04mm, and was able to measure discrete characteristics of the femoral head. This novel digital measurement approach allows for the quantification of the entire 3D geometry of the femoral head and is able to measure individual variations and potentially detect abnormalities.

## 4.5 References

1. Felson, D., R. Lawrence, P. Dieppe, R. Hirsch, C. Helmick, J. Jordan, R. Kington, N. Lane, M. Nevitt, Y. Zhang, M. Sowers, T. McAlindon, T. Spector, A. Poole, S. Yanovski, G. Ateshian, L. Sharma, J. Buckwalter, K. Brandt, and J. Fries, *Osteoarthritis: New Insights. Part 1: The disease and its risk factors*. Annals of Internal Medicine, 2000. **133**(8): p. 635-646.
2. Chegini, S., Beck, M., Ferguson, SJ., *The effects of impingement and dysplasia on stress distributions in the hip joint during sitting and walking: A finite element analysis*. Journal of Orthopaedic Research, 2009. **27**(2): p. 195-201.

3. Gregory, J.S., J.H. Waarsing, J. Day, H.A. Pols, M. Reijman, H. Weinans, and R.M. Aspden, *Early identification of radiographic osteoarthritis of the hip using an active shape model to quantify changes in bone morphometric features: Can hip shape tell us anything about the progression of osteoarthritis?* Arthritis & Rheumatism, 2007. **56**(11): p. 3634-3643.
4. Clohisy, J.C., J.C. Carlisle, R. Trousdale, Y.J. Kim, P.E. Beaulé, P. Morgan, K. Steger-May, P.L. Schoenecker, and M. Millis, *Radiographic evaluation of the hip has limited reliability.* Clin Orthop Relat Res, 2009. **467**(3): p. 666-75.
5. Lynch, J.A., N. Parimi, R.K. Chaganti, M.C. Nevitt, and N.E. Lane, *The association of proximal femoral shape and incident radiographic hip OA in elderly women.* Osteoarthritis and Cartilage, 2009. **17**(10): p. 1313-1318.
6. Wiberg, G., *Studies on dysplastic acetabula and congenital subluxation of the hip joint. with special reference to the complication of osteo-arthritis.* Acta Chirurgica Scandinavica, 1939. **83**(Suppl 58): p. 1-135.
7. Boykin, R.E., A.W. Anz, B.D. Bushnell, M.S. Kocher, A.J. Stubbs, and M.J. Philippon, *Hip instability.* Journal of the American Academy of Orthopaedic Surgeons, 2011. **19**(6): p. 340-349.
8. Ganz, R., J. Parvizi, M. Beck, M. Leunig, H. Notzli, and K.A. Siebenrock, *Femoroacetabular impingement: a cause for osteoarthritis of the hip.* Clin Orthop Relat Res, 2003(417): p. 112-20.
9. Murphy, S.B., R. Ganz, and M.E. Muller, *The prognosis in untreated dysplasia of the hip. A study of radiographic factors that predict the outcome.* J Bone Joint Surg Am, 1995. **77**(7): p. 985-9.
10. Lequesne, M. and S. de, *[False profile of the pelvis. A new radiographic incidence for the study of the hip. Its use in dysplasias and different coxopathies.]* Rev Rhum Mal Osteoartic, 1961. **28**: p. 643-52.
11. Delaunay, S., R.G. Dussault, P.A. Kaplan, and B.A. Alford, *Radiographic measurements of dysplastic adult hips.* Skeletal Radiol, 1997. **26**(2): p. 75-81.
12. Gosvig, K.K., S. Jacobsen, S. Sonne-Holm, and P. Gebuhr, *The prevalence of cam-type deformity of the hip joint: a survey of 4151 subjects of the Copenhagen Osteoarthritis Study.* Acta Radiologica, 2008. **49**(4): p. 436-41.
13. Beck, M., M. Kalhor, M. Leunig, and R. Ganz, *Hip morphology influences the pattern of damage to the acetabular cartilage: femoroacetabular impingement as a cause of early osteoarthritis of the hip.* J Bone Joint Surg Br, 2005. **87**(7): p. 1012-8.

14. Lavigne, M., J. Parvizi, M. Beck, K.A. Siebenrock, R. Ganz, and M. Leunig, *Anterior femoroacetabular impingement: part I. Techniques of joint preserving surgery*. Clin Orthop Relat Res, 2004(418): p. 61-6.
15. Jaber, F.M. and J. Parvizi, *Hip pain in young adults: femoroacetabular impingement*. J Arthroplasty, 2007. **22**(7 Suppl 3): p. 37-42.
16. Eijer, H., Leunig, M., Mahomed, M., and Ganz, R., *Cross-table lateral radiographs for screening of anterior femoral head-neck offset in patients with femoro-acetabular impingement*. Hip International, 2001. **11**(1): p. 37-41.
17. Notzli, H.P., T.F. Wyss, C.H. Stoecklin, M.R. Schmid, K. Treiber, and J. Hodler, *The contour of the femoral head-neck junction as a predictor for the risk of anterior impingement*. J Bone Joint Surg Br, 2002. **84**(4): p. 556-60.
18. James, S.L., K. Ali, F. Malara, D. Young, J. O'Donnell, and D.A. Connell, *MRI findings of femoroacetabular impingement*. AJR Am J Roentgenol, 2006. **187**(6): p. 1412-9.
19. Kassarian, A., M. Brisson, and W.E. Palmer, *Femoroacetabular impingement*. European Journal of Radiology, 2007. **63**(1): p. 29-35.
20. Carlisle, J.C., L.P. Zebala, D.S. Shia, D. Hunt, P.M. Morgan, H. Prather, R.W. Wright, K. Steger-May, and J.C. Clohisy, *Reliability of various observers in determining common radiographic parameters of adult hip structural anatomy*. The Iowa Orthopaedic Journal, 2011. **31**: p. 52-58.
21. Waarsing, J.H., R.M. Rozendaal, J.A.N. Verhaar, S.M.A. Bierma-Zeinstra, and H. Weinans, *A statistical model of shape and density of the proximal femur in relation to radiological and clinical OA of the hip*. Osteoarthritis and Cartilage, 2010. **18**(6): p. 787-794.
22. Beaulieu, P.E., E. Zaragoza, K. Motamedi, N. Copelan, and F.J. Dorey, *Three-dimensional computed tomography of the hip in the assessment of femoroacetabular impingement*. J Orthop Res, 2005. **23**(6): p. 1286-92.
23. Audenaert, E., L. Vigneron, and C. Pattyn, *A method for three-dimensional evaluation and computer aided treatment of femoroacetabular impingement*. Computer aided surgery : official journal of the International Society for Computer Aided Surgery, 2011. **16**(3): p. 143-8.
24. Standring, S., *Gray's Anatomy: The Anatomical Basis of Clinical Practice*. Fortieth ed, ed. S. Standring 2008: Churchill Livingstone Elsevier. 1551.
25. Gosvig, K.K., S. Jacobsen, H. Palm, S. Sonne-Holm, and E. Magnusson, *A new radiological index for assessing asphericity of the femoral head in cam impingement*. J Bone Joint Surg Br, 2007. **89**(10): p. 1309-16.

26. Pham, D.L., C. Xu, and J.L. Prince, *Current methods in medical image segmentation*. Annu Rev Biomed Eng, 2000. **2**: p. 315-37.
27. Rankin, G. and M. Stokes, *Reliability of assessment tools in rehabilitation: an illustration of appropriate statistical analyses*. Clinical rehabilitation, 1998. **12**(3): p. 187-99.

## Chapter 5

### 5 Validity and Reliability of a Novel 3D Measurement Approach for the Morphology of the Acetabulum

#### 5.1 Introduction

Osteoarthritis (OA) progression in the hip joint may be the result of abnormal loading patterns on the articular surfaces of the joint caused by variants of hip morphology. Morphological variations of the proximal femur and acetabulum have been identified as potential factors leading to the development of osteoarthritis [1]. However, normative values for hip morphometry have yet to be established. Further, it is unknown at which time points in the spectrum of the degenerative disease process these morphological changes occur [1].

Two conditions that are associated with OA and define morphological variations of the joint include hip instability and femoroacetabular impingement (FAI) [2, 3]. Atraumatic hip instability is primarily caused by acetabular dysplasia (AD), and is characterized by insufficient anterolateral femoral head coverage by the acetabulum and superolateral inclination of the acetabular surface [4]. AD results in anterolateral acetabular rim overload, excessive shear stresses, and instability which is thought to lead to joint degeneration [5]. Radiographically, AD is assessed by the centre-edge (CE) [4] angle and the vertical-centre-anterior (VCA) angle [6, 7]. FAI is characterized by abnormal contact between the superoanterior-lateral femoral neck and the superoanterior acetabular rim. The type of impingement that is associated with morphological variations of the acetabular rim is known as pincer-FAI. Pincer-FAI is characterized by an abnormally deep acetabulum, which results in excessive acetabular coverage over the anatomically normal femoral head [8-11]. The deep acetabulum is suggested to limit range of motion

(ROM) as the acetabular rim abuts against the femoral neck, causing labrum compression. Repetitive trauma to the area may result in damage to the labrum and the surrounding articular cartilage [8-10]. The CE angle, which is typically used to assess insufficient acetabular coverage, as in cases of AD, is also used to assess acetabular overcoverage.

Early detection and treatment of hip instability and FAI may help prevent the progression of OA [8, 9, 12-14]; however, the current radiographic parameters for diagnosing these conditions are unreliable. Clohisy et al. (2009), evaluated the reliability of six observers identifying important radiographic features of the hip on plain radiographs on two separate occasions. The important radiographic features were: acetabular version, inclination and depth, position of femoral head center, head sphericity, head-neck offset, Tönnis grade, and joint congruency. Observers were also asked to make a diagnosis of normal, dysplastic, FAI, or combined dysplastic and FAI. The Clohisy group concluded that the standard radiographic parameters that are used to diagnose dysplasia and FAI were not reproducible. A clear set of definitions and measurements must be developed to allow for more reliable diagnosis of early hip disease [2].

Currently, the primary tool used to diagnose structural hip disease is a plain radiograph, with computed-tomography (CT) and magnetic resonance imaging (MRI) typically used to confirm the diagnosis and further investigate the disease progression [2]. Current metrics that define the geometry of the hip use pre-determined measures, typically lengths and angles derived from two-dimensional (2D) radiographic planes. Fitting these 2D measures to three-dimensional (3D) geometry on 2D planes may not accurately account for the relevant clinical morphology [15-16]. Additionally, these current modalities assess the hip while it is articulated failing to analyze the femur and acetabulum separately for bony variations that may be otherwise hidden [17]. An accurate and reliable metric that quantifies the entire 3D surface morphology of the hip may assist in early detection and treatment of subclinical hip disease.

Most metrics of hip joint morphology are utilized to detect underlying pathologic conditions without verification of validity and reliability. Unfortunately, this has led to

clinical practice relying on potentially invalid and unreliable quantitative parameters. In Chapter Four a 3D measurement approach was established for the morphology of the proximal femur. This approach consisted of defining the geometry of the femoral head based on a convex radial grid consisting of 12 points over the femoral head surface. Using these points, 12 lines were measured from the centre of the fovea to the point where the femoral head extends from the femoral neck. This measurement approach was established to measure the femoral morphology accurately in the digital realm, within  $\pm 2.04\text{mm}$ , with high reproducibility.

The purpose of this current study was to apply a similar measurement approach to measure acetabular morphometry and to test the validity and reliability of the 3D measurement approach. Ideally, the acetabular measurement approach could be used in conjunction with the femoral head measurement approach to describe the morphometrics of the entire bone-to-bone interface at the hip joint. Measurements of the acetabulum will consist of 12 measures from the centre of the acetabulum. These measures will quantify the entire 3D surface morphology of the acetabulum while measuring along the contours of the socket. The novel measurement approach will be applied to the cadaveric specimens and to 3D digital models created from CT scans of the same specimens. It is hypothesized that the digital measures will be the same as those taken on the cadaveric specimens. Furthermore, it is hypothesized that there will be a strong reliability will exist between observers and trials.

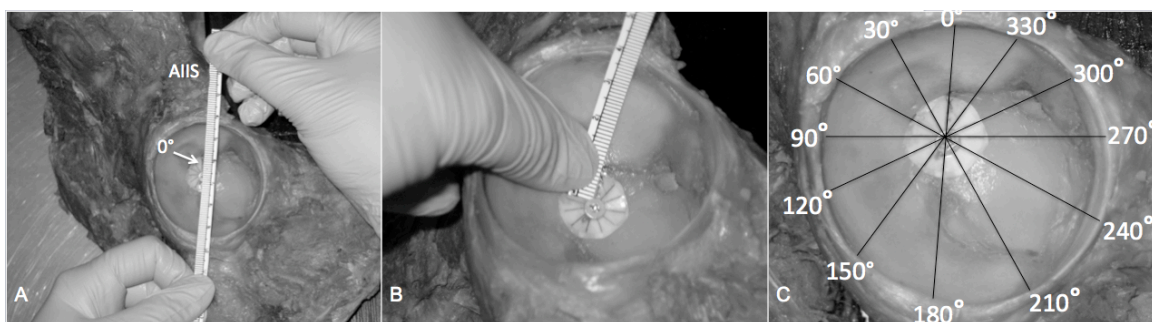
## 5.2 Methodology

The University of Western Ontario Body Bequeathal program approved the use of forty-five cadaveric hemisected pelvises for this study. Two specimens were not included in the study sample because one specimen had a metal prosthesis and the other specimen was severely diseased resulting in the inability to manually separate the femur from the pelvis. The 45 specimens included in the study (23 right; 22 left and 8 female; 37 male) had an



average age of  $77.58 \pm 11.46$  years (age range 51-104 years) and consisted of 19 bilateral and 7 unilateral pelvises. As this was primarily an evaluation of the method, bilateral acetabuli were included in the study and each individual acetabulum was considered as a separate specimen.

All specimens underwent CT scanning in a GE Lightspeed VCT (*GE Healthcare, WI, USA*) at University Hospital, London, Ontario. The images had a slice thickness of 0.6mm with a matrix of 512 by 512. After scanning, the cadaveric specimens were manually dissected, stripping them of all soft tissue with the exception of articular (hyaline) cartilage and the acetabular labrum. To prepare for measurement, a 1.5cm circular angle template consisting of 12 lines radiating from the center, separated by 30 degrees, was created for each specimen (Fig. 5.1C)



**Figure 5.1 - Measurement of the acetabular cadaveric specimens. A) Establishment of the center of the acetabulum and the 0° angle marker. B) Measurement of the acetabulum from the center of the acetabulum along the surface to the acetabular rim/labrum. Measurements are taken at each of the 12 angle markers.**

### 5.2.1 Cadaveric Acetabular Measurements

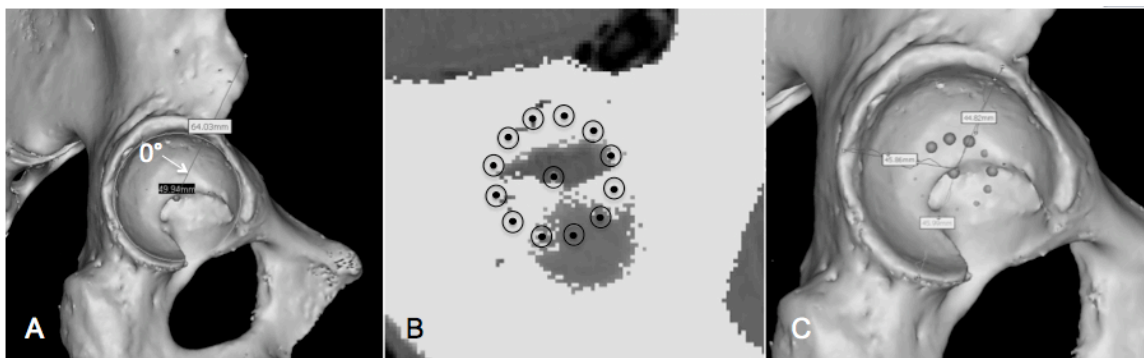
The acetabular center was established on the floor of the acetabulum by calculating the point of intersection of a horizontal and vertical maximal diameter. The flexible angle template was applied to the acetabular center. A line drawn from the most anteroinferior

portion of the anterior inferior iliac spine to the center of the acetabulum marker established the 0° angle (Fig. 5.1A). Measurements were made from the acetabular center to the acetabular rim and labrum at each of the 12-degree markers using a flexible ruler (Fig. 5.1B).

The CT, digital imaging and communications in medicine (DICOM), files for all specimens were imported into *Mimics 14.11* (*Materialise, Leuven, Belgium*). Image thresholding was performed to separate the bone from the surrounding soft tissue (Hounsfield threshold values: minimum: 226; maximum: 2606). Manual segmentation was performed on each model to separate the femur from the pelvis. In order to accurately measure the surface of the 3D model, the surface must be continuous and devoid of any holes. To ensure there were no holes in the 3D mesh, each model went through a *cavity fill* process. This process ensures a continuous surface; however, it does not ‘smooth’ the surface of the model nor does it adversely affect the calculation of the surface morphology.

### 5.2.2 Digital Acetabular Measurements

Utilizing a best-fit circle of the acetabular rim, the diameter of the acetabulum was used to establish the acetabular center; a 3D marker was applied to this point. A line drawn from the most anterior portion of the anterior inferior iliac spine to the center of the acetabulum marker established the 0-degree angle; a 3D marker was applied to indicate the 0-degree angle (Fig. 5.2A). A plane was created at the level of the acetabular notch to create the angle template. The 11 other angles were measured, using the ‘*measure angle tool*’, every 30 degrees from the 0-degree marker. 3D markers were placed to indicate each angle (Fig. 5.2B). Measurements were made on the 3D model, using the ‘*measure distance over surface tool*’, from the center of the acetabulum marker to the acetabular rim/labrum at each of the 12-degree markers (Fig. 5.2C).



**Figure 5.2 - Measurement of the acetabular digital models. A) Establishment of the center of the acetabulum and the 0° angle marker. B) Creation of the acetabular angle template on a 2D plane of the acetabular floor. C) Measurement of the acetabulum from the center of the acetabulum along the surface to the acetabular rim/labrum. Measurements are taken at each of the 12 angle markers.**

### 5.2.3 Statistical Analysis

To assess validity of the measurement approach one anatomist (CM) performed all of the cadaveric and digital measurements. To assess intraobserver reliability, the main observer (CM) repeated the measurements on the entire dataset ( $n = 45$ ), in a random order with a minimum of 48 hours separating measurement trials. In order to assess interobserver reliability, a subset ( $n = 18$ ) of specimens was randomly selected. Two independent blinded anatomists (CM & JT) performed all measurements of this subset in random order. The observers were not provided with any feedback while measuring and were blinded to their previous measurements and the other observer's measurements.

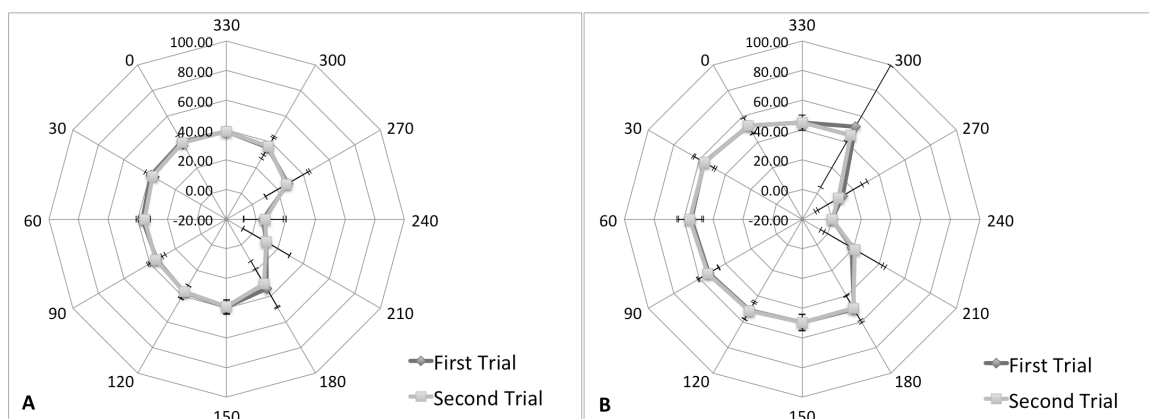
Statistical analysis was performed using *SPSS 16 (SPSS Inc., Chicago, Illinois, USA)* and *Prism 5 (GraphPad Software Inc. La Jolla, California, USA)*. The mean difference between the methods was assessed by the Bland-Altman method. Interobserver and intraobserver reproducibility was assessed by the intra-class correlation coefficient (ICC) and the Bland-Altman method.

## 5.3 Results

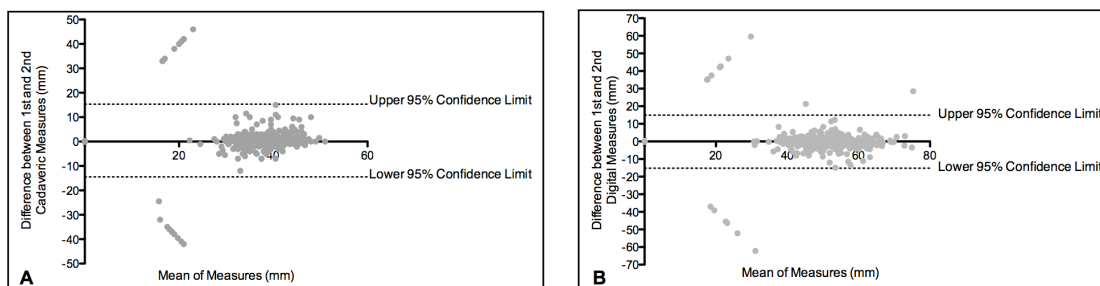
### 5.3.1 Reliability of Acetabular Surface Measurements

#### 5.3.1.1 Intraobserver Reliability

Excellent intraobserver reliability ( $n = 45$ ) was observed between the first and second cadaveric measurements with an intraclass correlation coefficient of 0.99 (95% confidence interval (CI) 0.98 to 0.99). The polar graph, Figure 5.5A, displays the mean cadaveric measures for each trial. The points on the polar graph correspond to the points measured on the acetabulum (Fig. 5.1C). Figure 5.6A illustrates the difference between the cadaveric first and second measures. The mean difference was 0.41mm, with an upper 95% confidence limit of 15.31mm and a lower limit of -14.49mm. The intraobserver reliability for the first and second digital measurements ( $n = 45$ ) was also observed to be excellent with an intraclass correlation coefficient of 0.99 (95% CI 0.98 to 0.99). A polar graph, Figure 5.5B, displays the mean digital measures for each trial. Figure 5.6B illustrates the difference between measures of the two trials. The mean difference between trials was -0.15mm; with upper and lower 95% confidence limits of 14.92mm and -15.22mm respectively.



**Figure 5.3 - Polar graphs of intraobserver reliability measurements of the acetabular surface. The 12 axes represent the 12-degree points where the measurements were taken. The mean measurement (mm) for each degree point is plotted for the first and second measures. (A) Cadaveric first and second mean measures. (B) Digital first and second mean measures.**

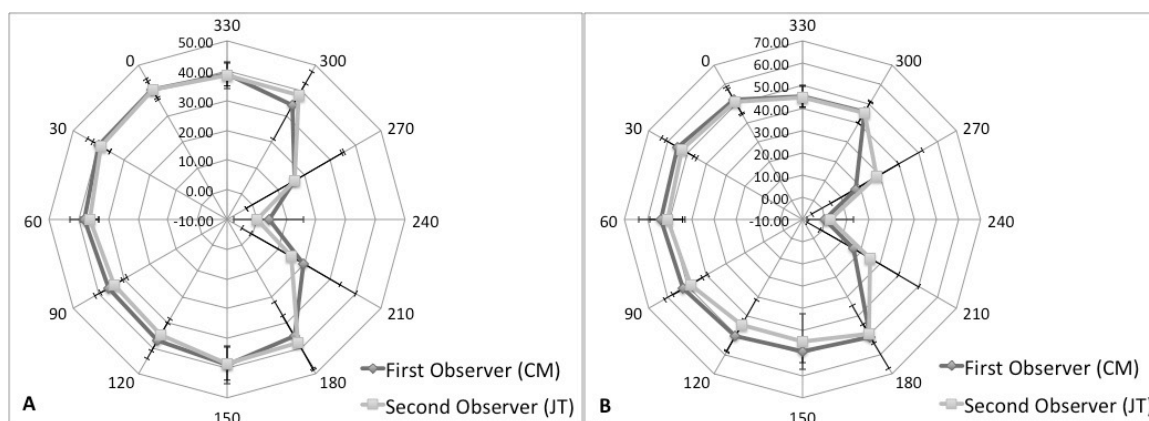


**Figure 5.4 – Bland-Altman plots of intraobserver variability of the (A) acetabular cadaveric measures and (B) acetabular digital measures. The x-axis plots the mean measurement between observations against the difference between the measures (mm) on the y-axis (First Measure – Second Measure). The outlying points represent inconsistent measures at the acetabular notch.**

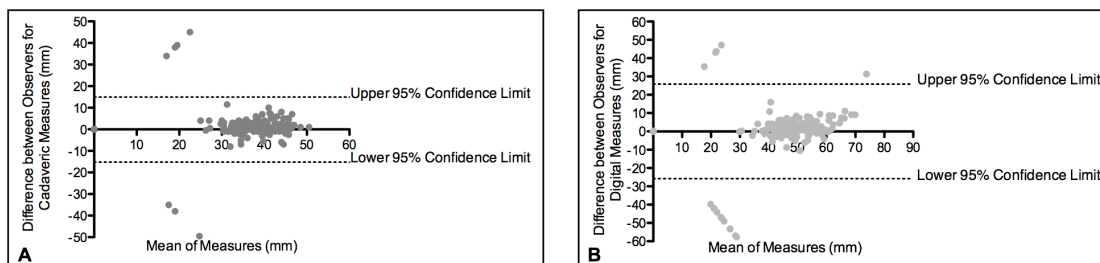
### 5.3.1.2 Interobserver Reliability

A random subset of the specimen population (n=18) was used to assess interobserver reliability. An excellent agreement was observed between observers when measuring the

cadaveric specimens with an intraclass correlation coefficient of 0.99 (95% CI 0.96 to 0.99). When measuring the digital models, an excellent interobserver reliability between observers was also noted with an intraclass coefficient of 0.97 (95% CI 0.91 to 0.99). Polar graphs display the mean measures for each observer for cadaveric measures (Fig. 5.7A) and digital measures (Fig. 5.7B). The Bland-Altman plots illustrate the difference between the mean measures by each observer for the cadaveric measures (Fig. 5.8A) and digital measures (Fig. 5.8B). The mean difference between the observers' cadaveric measures was 0.90mm, with an upper 95% confidence limit of 15.87mm and a lower limit of -14.08mm. For the digital measures the mean difference between observers was -0.02mm and the upper and lower 95% confidence limits were 25.79mm and -25.83mm respectively.



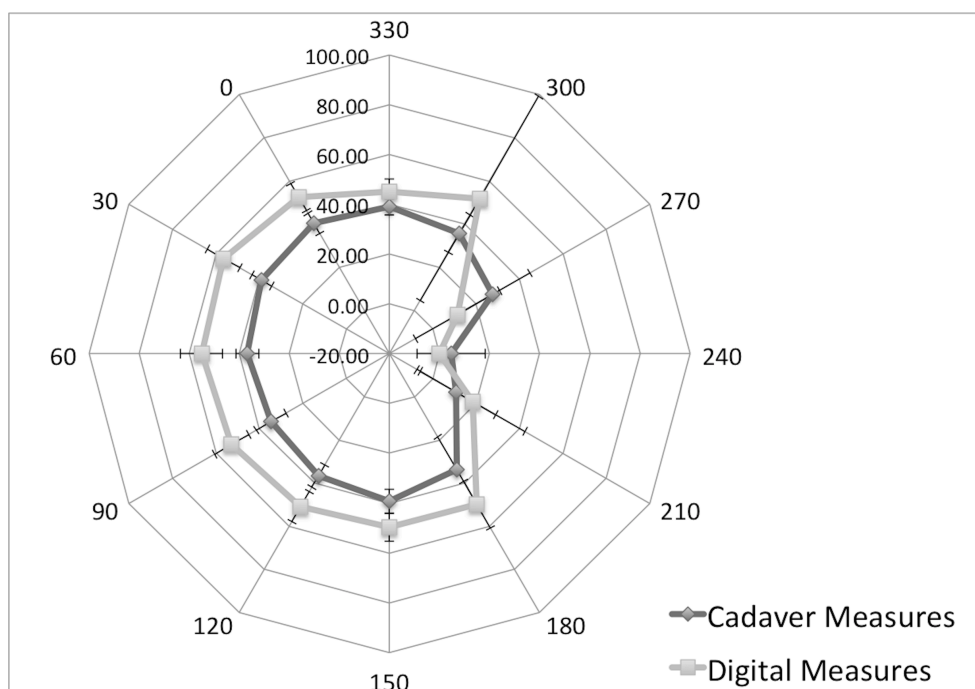
**Figure 5.5 - Polar graphs of interobserver reliability measurements of the acetabular surface. The 12 axes represent the 12-degree points where the measurements were taken and the mean measurement (mm) for each degree point is plotted for both observers. (A) Cadaveric measures for observer 1 (CM) and observer 2 (JT). (B) Digital measures for observer 1 (CM) and observer 2 (JT).**



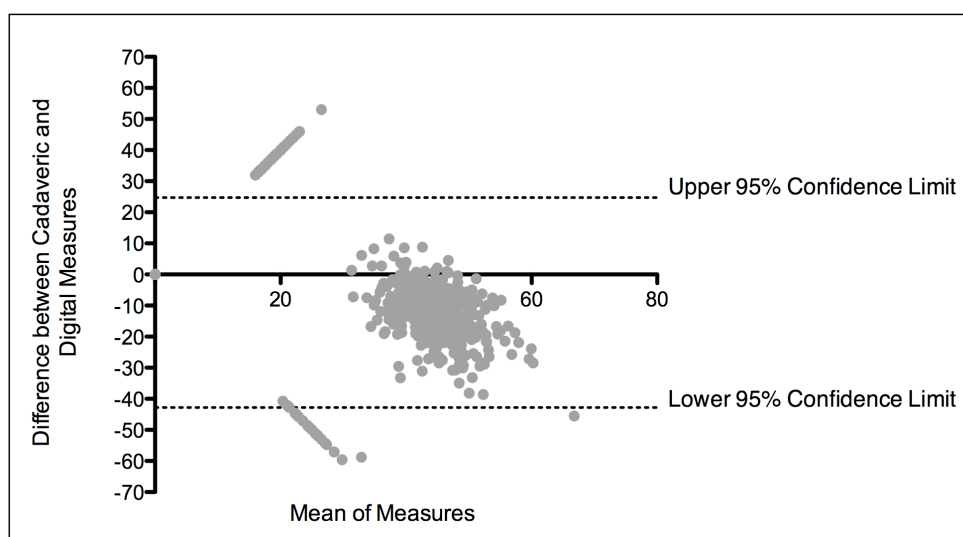
**Figure 5.6 – Bland-Altman plots of interobserver variability of the (A) acetabular cadaveric measures and (B) acetabular digital measures. The x-axis plots the mean measurement between observations against the difference between the measures (mm) on the y-axis (First Observer (CM) – Second Observer (JT)). The outlying points represent inconsistent measures at the acetabular notch.**

### 5.3.2 Validity of Acetabular Surface Measurements

The mean difference between the cadaveric measures and the digital measures was -9.06mm (Fig 5.4). The upper and lower 95% confidence limits were 24.70mm and -42.82mm respectively. The polar graph, Figure 5.3, displays mean acetabular measurements for each modality, cadaveric and digital, at each of the 12 degree points. The points on the polar graph correspond to the points measured on the acetabulum (Fig. 5.1C). This graph illustrates that the largest acetabular surfaces were found between 330 and 180 degrees corresponding to the lunate surface of the acetabulum. The smallest surface measurements were found between 210 and 270 degrees, with large error bars, corresponding to the acetabular notch and surrounding surfaces.



**Figure 5.7 - Polar graph of mean acetabular cadaveric measures and digital measures. The 12 axes represent the 12-degree (°) points (see Fig. 5.1C) where the measurements were taken and the mean measurement (mm  $\pm$  SD) for each degree point is plotted for the cadaveric and digital measures.**



**Figure 5.8 - Bland-Altman plot of the difference between the acetabular cadaveric measurements and the acetabular digital measurements. The x-axis plots the mean of the measurements by each modality against the difference between the measurement modalities (cadaveric - digital) on the y-axis. The outlying points represent inconsistent measures at the acetabular notch.**



## 5.4 Discussion

Due to the poor reliability of currently available measurement approaches for diagnosing hip instability and FAI, a valid and reliable measurement tool for early detection of hip disease is needed [2]. Current radiographic parameters measure the morphometry using pre-determined 2D measures on 2D projections. These measures are used to indirectly infer 3D geometry making it difficult to account for normal individual anatomic variation. Additionally, relevant 3D geometry may be missed when selecting the 2D scan [15]. A valid and reliable measurement technique that quantifies the entire 3D surface morphology is necessary in order to assist in early detection and treatment of hip disease.

Similar to the results found in Chapter Four, where a similar measurement approach was applied to the femoral head, the digital measurement approach used to define acetabular surfaces also had high intraobserver reliability (ICC = 0.99, CI 0.98 to 0.99) and interobserver reliability (ICC = 0.97, CI 0.91 to 0.99). However, unlike the results found in Chapter Four, the digital measurement approach for acetabular morphometry had some large differences between the measurements. The mean difference in measurements for the acetabulum was -9.06mm; however, the 95% confidence limits were wide and some differences between measurements were as large as 61.29mm. Differences this large are clinically significant considering the size of the acetabulum itself and surrounding tissues. In addition to this, the results in Figure 5.3 and 5.4 suggest that the digital measurements are systematically larger than the cadaveric measurements. These inconsistencies in the measurements may have potentially come from a variety of error sources, such as the presence of the labrum in the cadaveric specimens, calcified labrum appearing and being measured as bone on the digital models, difficulty measuring along the concavity of the acetabulum in the cadaveric specimens, and measuring inconsistencies surrounding the acetabular notch.

The primary difficulty one encounters whilst attempting to accurately measure the surface morphology of the acetabulum may be related to the presence of labrum on the cadaveric specimens while performing the measurements. The cadaveric measurements

attempted to quantify the bony acetabulum from the centre of the acetabulum to the outer acetabulum rim at each of the 12 degree points. However, the labrum attaches medially to the acetabular rim and extends outwards past the rim to deepen the acetabulum. An error may have occurred in the cadaveric measurements by the observers believing they were measuring to the acetabular rim, when in reality they were measuring only to the labral attachment point. Removing the labrum prior to measurement on cadaveric specimens could rectify this possible error.

Calcification of the labrum is a common finding in patients with degenerative hip disease, similar to other sites of chondrocalcinosis. Thus, another potential error may have been created by the presence of calcified labra. When measuring the cadaveric models it was easy to identify bone from labrum and it was easy to visualize where the labrum was calcified. However, due to the bone-like composition of the calcified labra, their imaging appearance can parallel bone in digital models making it difficult to distinguish labrum from bone. Degeneration of the acetabular labrum is often found early in the arthritic process [18]. It is suggested that this breakdown is caused by morphological variations of the joint leading to abnormal contact of the femur and the acetabular rim [9, 10].

Repeated impact causes damage to the labrum and underlying cartilage. Continued trauma may result in the ossification of the labrum and further ossification surrounding the acetabular rim itself [8-10]. Calcified labrum leads to excessive coverage of the acetabulum over the femoral head, limiting the femur's range of motion and creating abnormal contact, which leads to exacerbation of the problem [8-10, 19]. Understanding where the labrum is calcified may be clinically relevant as it likely reflects locally progressive arthropathy [20]. It is important to realize that labral chondrocalcinosis is a problem when digitally measuring the acetabulum and it would be ideal for a measurement approach of the acetabulum to be capable of distinguishing between bony acetabulum and calcified labrum.

Another potential error may have been created by the measurement approach itself. The shape of the acetabulum presented some challenges due to its concave surface. It is possible that the flexible ruler used to measure the concave acetabular surface did not adhere to all of the contours of the bony acetabulum, resulting in the cadaveric measures

being systematically lower than the digital measures. Utilizing a tool that more easily adheres to the contours of the concave acetabular surface may enable more accurate quantification of the surface morphology of the acetabulum.

Another area of difficulty, when measuring the acetabulum, is the acetabular notch. For this study measurements taken within the notch were recorded as 0mm. If a measurement of bony acetabulum was taken with one modality and it was established as part of the notch in another modality. This measurement inconsistency resulted in a large difference between measures and an artificially low mean of the two measures; creating obvious outliers on the Bland-Altman plots. Typically the notch is found anteroinferiorly between 180° and 300° on the measurement scale. In the cadaveric models the acetabular notch is filled with fat, whereas in the digital realm only bone is visualized and measured. Thus, the fatty notch in the cadaveric specimens may create a measurement error. To adjust for these inconsistencies, the notch, for each individual acetabulum, could be established prior to measurement and then measurements should only be taken outside of the notch. Another way to deal with this inconsistency would be to dissolve the fat from the cadaveric acetabuli prior to measurement. This error was also found in the intra- and interobserver measurements indicating that there may be a discrepancy in where each measurement is taken. The concave surface proved to be a challenge for the observers as they had difficulty ensuring they were measuring along the correct trajectory from the degree template.

The presence of the labrum in the cadaveric models resulted in two different lengths being measured in each modality, the length from the centre of the acetabulum to the attachment of the labrum in the cadaveric specimens and the length from the centre of the acetabulum to the acetabular rim in the digital realm. Thus, validity was not being assessed since the two measures were quantifying different structures. To further investigate the validity of this measurement approach a subset ( $n = 13$ ), of the cadaveric acetabuli, was re-measured with labra removed (see Appendix F). The removal of the labrum did decrease the mean difference between cadaveric and digital measures from -9.06mm with labrum to -6.22mm without labrum. However, the digital measurements were still systematically larger than the cadaveric measures. Although removing the

labrum did decrease the error created with this measurement approach, the inconsistencies between the measurements were not eliminated. Thus, the other three potential sources of error presented within may still be contributing to the disagreement between measures.

Other limitations to this measurement approach could be related to the creation of the model and the measurement approach in itself. The segmentation protocol used to create the 3D models may have created a small error due to partial-volume effects. Partial-volume effects occur when more than one tissue type falls within a single voxel (a 3D pixel). The voxel is expressed as an average of the attenuation properties of all contributing tissues, resulting in blurred tissue boundaries [21]. However, partial-volume errors are minimized with high resolution and thin CT slice thicknesses. The resolution of the CT scans used in this study was high with a matrix of 512 by 512 and the slice thickness was 0.6mm, thus error was minimized as it is less likely for multiple structures to occupy the same voxel. Once the model was created there were some surface voids in the bone created from a lack of cortical bone thickness in areas of the proximal femur. A cavity-fill process was performed manually to ensure that deviations in the model surface were filled; yet no excess bone was added to the surface. Although the cavity-fill was performed carefully and manually, this process may have created a source of error in the digital measurements. Error may have been created due to observer fatigue during the performance of the measurements and additional error may have been created via the placement of the measurement template. The angle template was applied to the centre of the acetabular floor; however, a slight change in location of the template may alter the measurement results. However, the high agreement between measurements indicates that the placement of the template produced minimal error. Lastly, it is ideal to run a Bland-Altman analysis with a minimum sample of 50. This study's sample of 45 may have produced slightly wider 95% confidence limits [22].

It is possible that measurement of the acetabulum could be improved by performing the measurements with MRI or magnetic resonance arthrogram (MRA) scans as opposed to CT scans. MRI and MRA allow for a greater visualization of soft tissues, including labra [23]. If the non-calcified labrum is visualized within the 3D model then it may be easier

to tell where the labrum is calcified. It is necessary to establish a measurement approach of the acetabulum that reliably and accurately quantifies the entire 3D surface morphology of the acetabulum. Future studies should be performed to establish such an approach and then normal and pathological values could be established. Creating pathological criteria values using a valid and reliable measurement modality may lead to earlier diagnoses and treatment of structural hip disease, presumably leading to a decrease in morbidity associated with OA [8, 9, 12-14]. Once criteria values have been created, the measurement approach could be automated for simple diagnosis on widely available advanced visualization stations. While it is important to examine the 3D morphology of the disarticulated hip for the presence of structural lesions that may be otherwise hidden while the hip is articulated [17], it would also be beneficial to assess the acetabular structural lesions in relation to the femoral structural lesions.

In conclusion, the presented measurement approach is reproducible; however, the differences between the measurements were relatively large from a clinical perspective. The presence of the labra on the cadaveric specimens did contribute to some of the differences between measures as presented in Appendix F. However, even with the removal of the labra, differences between the measurements modalities still existed. The presence of calcified labrum appearing as bone in the digital realm may have contributed to these differences. However, it is suspected that acetabular labral chondrocalcinosis contributes to degenerative disease and is a clinically relevant issue surrounding measurement of acetabular morphology; thus, it is essential to be able to identify and quantify calcified labrum. Other errors in the measurements may be attributed to the cadaveric measurement approaches inability to measure all of the contours of the concave acetabular surface, and measurement inconsistencies surrounding the acetabular notch. Future studies should be performed to establish a reliable and valid measurement approach that measures the entire 3D surface geometry of the acetabulum in order to assist in early diagnosis and treatment of early degenerative disease of the hip.

## 5.5 References

1. Gregory, J.S., J.H. Waarsing, J. Day, H.A. Pols, M. Reijman, H. Weinans, and R.M. Aspden, *Early identification of radiographic osteoarthritis of the hip using an active shape model to quantify changes in bone morphometric features: Can hip shape tell us anything about the progression of osteoarthritis?* Arthritis & Rheumatism, 2007. **56**(11): p. 3634-3643.
2. Clohisy, J.C., J.C. Carlisle, R. Trousdale, Y.J. Kim, P.E. Beaulé, P. Morgan, K. Steger-May, P.L. Schoenecker, and M. Millis, *Radiographic evaluation of the hip has limited reliability.* Clin Orthop Relat Res, 2009. **467**(3): p. 666-75.
3. Lynch, J.A., N. Parimi, R.K. Chaganti, M.C. Nevitt, and N.E. Lane, *The association of proximal femoral shape and incident radiographic hip OA in elderly women.* Osteoarthritis and Cartilage, 2009. **17**(10): p. 1313-1318.
4. Wiberg, G., *Studies on dysplastic acetabula and congenital subluxation of the hip joint. with special reference to the complication of osteo-arthritis.* Acta Chirurgica Scandinavica, 1939. **83**(Suppl 58): p. 1-135.
5. Murphy, S.B., R. Ganz, and M.E. Muller, *The prognosis in untreated dysplasia of the hip. A study of radiographic factors that predict the outcome.* J Bone Joint Surg Am, 1995. **77**(7): p. 985-9.
6. Lequesne, M. and S. de, *[False profile of the pelvis. A new radiographic incidence for the study of the hip. Its use in dysplasias and different coxopathies.]* Rev Rhum Mal Osteoartic, 1961. **28**: p. 643-52.
7. Delaunay, S., R.G. Dussault, P.A. Kaplan, and B.A. Alford, *Radiographic measurements of dysplastic adult hips.* Skeletal Radiol, 1997. **26**(2): p. 75-81.
8. Ganz, R., J. Parvizi, M. Beck, M. Leunig, H. Notzli, and K.A. Siebenrock, *Femoroacetabular impingement: a cause for osteoarthritis of the hip.* Clin Orthop Relat Res, 2003(417): p. 112-20.
9. Lavigne, M., J. Parvizi, M. Beck, K.A. Siebenrock, R. Ganz, and M. Leunig, *Anterior femoroacetabular impingement: part I. Techniques of joint preserving surgery.* Clin Orthop Relat Res, 2004(418): p. 61-6.
10. Beck, M., M. Kalhor, M. Leunig, and R. Ganz, *Hip morphology influences the pattern of damage to the acetabular cartilage: femoroacetabular impingement as a cause of early osteoarthritis of the hip.* J Bone Joint Surg Br, 2005. **87**(7): p. 1012-8.

11. Laude, F., T. Boyer, and A. Nogier, *Anterior femoroacetabular impingement*. Joint Bone Spine, 2007. **74**(2): p. 127-32.
12. James, S.L., K. Ali, F. Malara, D. Young, J. O'Donnell, and D.A. Connell, *MRI findings of femoroacetabular impingement*. AJR Am J Roentgenol, 2006. **187**(6): p. 1412-9.
13. Notzli, H.P., T.F. Wyss, C.H. Stoecklin, M.R. Schmid, K. Treiber, and J. Hodler, *The contour of the femoral head-neck junction as a predictor for the risk of anterior impingement*. J Bone Joint Surg Br, 2002. **84**(4): p. 556-60.
14. Kassarian, A., M. Brisson, and W.E. Palmer, *Femoroacetabular impingement*. European Journal of Radiology, 2007. **63**(1): p. 29-35.
15. Waarsing, J.H., R.M. Rozendaal, J.A.N. Verhaar, S.M.A. Bierma-Zeinstra, and H. Weinans, *A statistical model of shape and density of the proximal femur in relation to radiological and clinical OA of the hip*. Osteoarthritis and Cartilage, 2010. **18**(6): p. 787-794.
16. Beaulé, P.E., E. Zaragoza, K. Motamedi, N. Copelan, and F.J. Dorey, *Three-dimensional computed tomography of the hip in the assessment of femoroacetabular impingement*. J Orthop Res, 2005. **23**(6): p. 1286-92.
17. Audenaert, E., L. Vigneron, and C. Pattyn, *A method for three-dimensional evaluation and computer aided treatment of femoroacetabular impingement*. Computer aided surgery : official journal of the International Society for Computer Aided Surgery, 2011. **16**(3): p. 143-8.
18. Seldes, R.M., V. Tan, J. Hunt, M. Katz, R. Winiarsky, and R.H. Fitzgerald, Jr., *Anatomy, histologic features, and vascularity of the adult acetabular labrum*. Clinical Orthopaedics and Related Research, 2001(382): p. 232-40.
19. Beck, M., M. Leunig, J. Parvizi, V. Boutier, D. Wyss, and R. Ganz, *Anterior femoroacetabular impingement: part II. Midterm results of surgical treatment*. Clin Orthop Relat Res, 2004(418): p. 67-73.
20. McCarthy, J.C., P.C. Noble, M.R. Schuck, J. Wright, and J. Lee, *The Otto E. Aufranc Award: The role of labral lesions to development of early degenerative hip disease*. Clin Orthop Relat Res, 2001(393): p. 25-37.
21. Pham, D.L., C. Xu, and J.L. Prince, *Current methods in medical image segmentation*. Annu Rev Biomed Eng, 2000. **2**: p. 315-37.
22. Rankin, G. and M. Stokes, *Reliability of assessment tools in rehabilitation: an illustration of appropriate statistical analyses*. Clinical rehabilitation, 1998. **12**(3): p. 187-99.

23. Leunig, M., D. Podeszwa, M. Beck, S. Werlen, and R. Ganz, *Magnetic resonance arthrography of labral disorders in hips with dysplasia and impingement*. Clin Orthop Relat Res, 2004(418): p. 74-80.



## Chapter 6

### 6 General Discussion

#### 6.1 Introduction

The overarching aim of this dissertation was to explore three-dimensional (3D) modelling of the hip joint. Very few morphometric studies take advantage of the inherent 3D nature of magnetic resonance imaging (MRI) and computed-tomography (CT) data sets. Additionally, very few studies set out to assess the features of commercially available 3D reconstructive software programs used for morphometrics and knowledge transfer of 3D anatomy. This dissertation assessed, in detail, the advantages and challenges of quantifying the innately three-dimensional and complex geometry of the two articulating surfaces of the hip joint. Further, this dissertation objectively compared 3D reconstructive software programs available to perform these types of morphometric analyses.

#### 6.2 3D Modelling

3D modelling may have many advantages over traditional, two-dimensional (2D) imaging, techniques enabling visualization of complex 3D anatomical morphology [1]. As such, the use of 3D modelling for morphometrics, education, pre-operative assessment, and pre-surgical planning has become more prevalent [2-4]. Many of the current radiographic metrics used to quantify the bony anatomy of the hip joint are linear and are measured on 2D scans; these metrics do not allow for visualization of the entire 3D anatomy and often miss clinically relevant structures [5, 6]. 3D modelling and novel

3D measurement approaches enable complete visualization and quantification of the entire anatomical structures. Additionally, with changes in clinical practice relying more heavily on 3D acquisitions for visualization and measurement, educational tools follow suit. Transferring knowledge of anatomical morphology, measurement, and surgical techniques is also relying more on 3D modelling. 3D models enable learners to conceptualize complex anatomical structures and their spatial relationships with surrounding structures [7].

### 6.3 3D Reconstructive Software Programs

The 3D nature of the hip joint is complex and difficult to quantify in the 3D realm, let alone on 2D radiographic scans. There are many 3D reconstructive software programs available to researchers and educators; however, no program has become the standard [1, 12]. In Chapter Three, three affordable widely available programs, Amira, OsiriX, and Mimics, were assessed with respect to the software's ability to create 3D models, to conduct morphometric research, and to produce learning tools. There were two arms to the software assessment, the morphometric research weighting scale to assess the software's ability to perform anatomical measurement studies and the educational weighting scale to assess the software's ability to produce educational tools to be used to translate knowledge regarding human morphology and morphometrics. The results of the morphometric research weighting scale found that Mimics was the best-suited program for morphometric research studies. Mimics has a user-friendly interface, creates anatomical models quickly, and has a variety of measurement tools available to the user. The results of the educational weighting scale were less clear. Both Amira and OsiriX have educational features available such as the ability to make movies and stereo models. However, although Amira's end-product was high quality and the potential for dynamic learning tools was endless, the interface was challenging to manipulate. Additionally, while OsiriX's interface was user-friendly, the educational features had limited capabilities. Although, Mimics did not inherently have educational features, the software

did have educational potential if third party programs were integrated. This comparison may be used as a resource for morphometric researchers and educators to select the appropriate reconstruction program when starting a new 3D modelling project. Understanding the features available in each program may help to further the research in 3D surface measurement of the hip joint, leading to a valid and reliable measurement of the acetabulum. In addition, this information can assist educators in choosing the appropriate program to create educational tools, which may aid in transferring the knowledge of the complexities of measuring the hip joint on to other researchers and clinicians.

This software comparison utilized a decision-making concept selection tool commonly used in engineering. This type of analysis has not been used previously to select an appropriate anatomical software program. The decision matrix aids the decision-making process by transforming subjective rankings to meaningful scores. The decision matrix assisted in the comparison of the three software programs presented in Chapter Three, this novel method of transforming subjective ranks into more objective scores could be used for other studies comparing multiple tools or programs in future studies.

In Chapter Three, Mimics was identified as the best suited software for morphometric research. Thus, Mimics, was used in Chapters Four and Five to quantify the morphology of the femoral head and acetabulum, respectively. Mimics' ability to quantify lengths while adhering to the model's digital surface made it ideal for these morphometric research projects. Other programs, such as Amira and OsiriX, were unable to perform this quantification. Studies that establish the limitations of quantification of 3D morphology should be performed to present these challenges to the software developers. Understanding the complexities of measuring the hip joint can assist the software developers, of 3D reconstructive programs, to develop new measurement tools to quantify complex joints.

## 6.4 3D Modelling and Morphometrics of the Hip Joint

The current metrics used to diagnose hip instability and femoroacetabular impingement (FAI), have been identified as being unreliable [8, 9]. In addition to these metrics lacking reproducibility, they are also 2D linear measures attempting to quantify 3D anatomy on 2D scans. A valid and reliable measurement approach that quantifies the entire 3D morphology of the hip joint is necessary. Reliable identification and early detection of these structural lesions may lead to a better understanding of where the lesions occur along the spectrum of the degenerative disease process and may assist in early treatment preventing the progression of the disease.

A novel measurement approach was created to quantify the entire 3D surface morphology of each articulating bone of the hip joint. The hip joint is comprised of two bones, the spherical femoral head and the deep socket of the pelvis, the acetabulum. This complex morphology proved to be a challenge to measure, even in the 3D environment. When the measurement approach was applied to the femoral head, in Chapter Four, the results were very positive. The mean difference between the cadaveric and digital measures was - 2.04mm, with upper and lower 95% confidence limits of 13.67mm and 17.75mm respectively. Additionally, the digital femoral measurement approach had excellent intraobserver reliability (ICC = 0.99, CI 0.98 to 0.99) and interobserver reliability (ICC = 0.98, CI 0.93 to 0.99). Due to the elderly age of the proximal head specimens analyzed in this study, it is possible that structural hip pathologies may have been present. Bony calcifications were easily visualized on both the cadaveric specimens and the digital models and were included in the measurements, illustrating that the digital measurement approach is robust, valid, and reliable regardless of variation in femoral head anatomy.

When applying the measurement approach to the acetabular side of the hip joint some challenges were encountered (Chapter Five). Similar to the results found in Chapter Four, the digital measurement approach had high intraobserver reliability (ICC = 0.99, CI 0.98 to 0.99) and interobserver reliability (ICC = 0.97, CI 0.91 to 0.99). However, unlike the results found in Chapter Four the digital measurement approach for acetabular

morphometry had larger differences between the measurements. In Chapter Four it was established that the cadaveric approach and the digital approach for the femoral head had a mean difference of -2.04mm. The mean difference in measurements for the acetabulum was -9.06mm; however, the 95% confidence limits were wide and some differences between measurements were as large as 61.29mm. Differences this large are clinically significant considering the size of the acetabulum and its surrounding tissues. In addition to this divergence, the results in Figure 5.3 and 5.4 suggest that the digital measurements are systematically larger than the cadaveric measurements. These inconsistencies in the measurements may have potentially come from a variety of error sources, such as the presence of labrum on the cadaveric specimens, a partially calcified acetabular labrum measured as bone on the digital models, difficulty measuring along the concavity of the acetabulum in the cadaveric specimens, and measuring inconsistencies surrounding the acetabular notch.

The differences in results between the femoral and acetabular measurements bring to light the challenges and limitations surrounding measuring the acetabulum. The first limitation was associated with the presence of labrum on the cadaveric specimens leading to inaccurate cadaveric measurements. To further investigate this limitation, a subset of cadaveric specimens was re-measured with the labra removed (Appendix F). The removal of the labrum did decrease the mean difference between cadaveric and digital measurements from -9.06mm to -6.22mm; however, the digital measurements were still systematically larger than the cadaveric measures. Although removal of the labrum did decrease the error in the acetabular measurements, inconsistencies between the measurements remained. These inconsistencies may have been caused by calcified labra appearing as bone on the digital models, leading to increased digital measurements. Although, the calcified labrum represents a source of error in the measurements it is clinically relevant to know where the labrum is calcified as it likely reflects locally progressive arthropathy [10]. It is possible that the measurement approach could be improved in its ability to quantify the bony acetabulum and identify calcified labrum by performing the measurements on MRI, or even better, magnetic resonance arthrography (MRA) scans to better visualize the labrum and other soft tissues [11]. Another limitation is related to the shape of the acetabulum. The acetabulum is a concave structure, which

proves to be a more difficult morphology to quantify than the convex surface of the femoral head in Chapter Four. It is possible that the flexible ruler used to measure the surface of the cadaveric acetabulum did not follow all of the bony contours of the acetabulum, resulting in the digital measures being systematically larger than the cadaveric measures. Utilizing a tool that is more pliable and easily adheres to the bony contours within the acetabular concavity may assist in validating this measurement approach. Finally, the acetabular notch introduced difficulties when quantifying the acetabular morphology. If a measurement vector of a certain degree point fell within the acetabular notch, then the measurement was recorded as 0mm. The observer marking a degree point as part of the acetabular notch in one modality and measuring it as part of the bony acetabulum in the other modality created outlying points that were clearly represented by the Bland-Altman plots (Fig. 5.4, 5.6, 5.8, and Fig. 3 from Appendix F). This disagreement in measurement across modalities resulted in an artificially low mean of the two measurements and a large difference between the measurements. To rectify this source of error the location of the notches could be established prior to measurement and thus would not be included in the measurements. The majority of the morphological variations of the acetabulum, that are associated with early degenerative disease, affect the anterosuperior acetabular rim. Thus, removing measurements surrounding the acetabular notch should not affect quantification of the clinically relevant areas. Although, the measurement approach applied to the femoral head resulted in valid and reliable quantification of the proximal femur morphology, a similar approach may not be ideal to measure the complex morphology of the acetabulum.

## 6.5 Future Directions

With novel 3D measurement approaches of hip morphology such as those presented in Chapters Four and Five, greater use of 3D reconstructive software can be exploited to measure hip morphology. A reproducible measurement approach that accurately quantified the proximal femur within -2.04mm was created; however, a valid and reliable

measurement approach of the acetabulum, to be used in conjunction with the proximal femur approach, must be further established to quantify the entire surface morphology of the hip joint.

The measurement approach presented in Chapters Four and Five could be compared to geographical surface mapping. Displaying anatomical surface lengths measured every 30 degrees around the femoral head and acetabulum in polar diagrams represents the geometric surface of those articular surface areas in shape and size. Once a spectrum of normal values for articular surface lengths is established, surface lengths that extend outside normative values may indicate the presence of pathologies in specific areas of the articular surface. For instance, longer surface lengths at the anterosuperior-lateral aspect of the femoral head, between 150 and 240 degrees, may represent bony lesions at the femoral head neck junction and may be diagnostic of FAI (Fig. 4.3). Longer surface lengths located at the anterosuperior aspect of the acetabulum, between 0 and 60 degrees, may represent bony proliferation at the acetabular rim, and thus be diagnostic of FAI (Fig. 5.3). Conversely, shorter lengths at the anterosuperior aspect of the acetabulum, between 0 and 60 degrees, may represent an acetabular insufficiency and may be diagnostic of AD (Fig. 5.3).

Future studies should be performed to establish a range of normal and pathological values. These values can then be used to establish diagnostic criteria values to identify structural hip disease. Once diagnostic criteria values have been established, the measurement approach could be automated and widely available for use on imaging visualization stations. Thus, producing an automated measurement approach could decrease measurement error. Creating pathological criteria values using a validated and reliable measure may lead to earlier diagnoses and treatment of structural hip disease [14-16]. It is unlikely, that the consensus regarding treatment of one type of structural hip disease, FAI, will change with a reliable 3D measurement approach. However, reliable detection of the FAI structural lesions may lead to future discoveries surrounding the condition. It is essential to understand the role FAI plays in the degenerative disease process to provide a consensus regarding appropriate treatment [17]; however, further

discoveries cannot be achieved if the structural lesions themselves cannot be identified reliably.

Ideally, to establish the relationship between OA and morphological variations a natural history study would need to be done. A valid and reliable measurement approach could be applied to MR scans of a young cohort of individuals that present with the morphological variations and a young control cohort of individuals that present with normal anatomy of the hip joint. These individuals would be scanned periodically through their lives and monitored for the presence of degenerative disease markers; thus, indicating whether these morphological variations predispose individuals to degenerative disease or if the control group developed degenerative disease markers at the same rate.

## 6.6 Conclusion

In conclusion, 3D modelling is becoming more prevalent in morphometric research and education. 3D modelling can provide new insights into the advantages and challenges of quantifying human anatomy. Chapter Three may be used as a resource regarding the available features and tools available within 3D reconstructive software programs, researchers and educators can select the appropriate program to educate clinicians and researchers on the challenges of measuring the hip joint and to further study morphometrics of the joint. The hip joint is a complex joint that benefits from 3D visualization and quantification; however, challenges surrounding measuring the acetabulum remain. A valid and reproducible measurement approach that quantifies the acetabulum, along with the proximal femur measurement approach, is necessary to be able to identify early hip disease. Early identification of hip disease may lead to a further understanding of where these bony lesions fit in along the spectrum of the degenerative disease process. A better understanding of the degenerative disease process may enable appropriate treatment for these lesions, which may lead to a decrease in morbidity associated with osteoarthritis and improve quality of life.



## 6.7 References

1. Landes, C.A., F. Weichert, P. Geis, F. Helga, and M. Wagner, *Evaluation of two 3D virtual computer reconstructions for comparison of cleft lip and palate to normal fetal microanatomy*. The Anatomical Record Part A: Discoveries in Molecular, Cellular, and Evolutionary Biology, 2006. **288A**(3): p. 248-262.
2. Humbert, L., H. Carlloz, A. Baudoin, W. Skalli, and D. Mitton, *3D Evaluation of the acetabular coverage assessed by biplanar X-rays or single anteroposterior X-ray compared with CT-scan*. Computer Methods in Biomechanics and Biomedical Engineering, 2008. **11**(3): p. 257 - 262.
3. Rosse, C., *The potential of computerized representations of anatomy in the training of health care providers*. Academic Medicine, 1995. **70**(6): p. 499-505.
4. Bale, R. and G. Widmann, *Navigated CT-guided interventions*. Minimally Invasive Therapy & Allied Technologies, 2007. **16**(4): p. 196-204.
5. Waarsing, J.H., R.M. Rozendaal, J.A.N. Verhaar, S.M.A. Bierma-Zeinstra, and H. Weinans, *A statistical model of shape and density of the proximal femur in relation to radiological and clinical OA of the hip*. Osteoarthritis and Cartilage, 2010. **18**(6): p. 787-794.
6. Beaulé, P.E., E. Zaragoza, K. Motamedi, N. Copelan, and F.J. Dorey, *Three-dimensional computed tomography of the hip in the assessment of femoroacetabular impingement*. J Orthop Res, 2005. **23**(6): p. 1286-92.
7. Vernon, T. and D. Peckham, *The benefits of 3D modelling and animation in medical teaching*. The Journal of audiovisual media in medicine, 2002. **25**(4): p. 142-8.
8. Clohisy, J.C., J.C. Carlisle, R. Trousdale, Y.J. Kim, P.E. Beaulé, P. Morgan, K. Steger-May, P.L. Schoenecker, and M. Millis, *Radiographic evaluation of the hip has limited reliability*. Clin Orthop Relat Res, 2009. **467**(3): p. 666-75.
9. Carlisle, J.C., L.P. Zebala, D.S. Shia, D. Hunt, P.M. Morgan, H. Prather, R.W. Wright, K. Steger-May, and J.C. Clohisy, *Reliability of various observers in determining common radiographic parameters of adult hip structural anatomy*. The Iowa Orthopaedic Journal, 2011. **31**: p. 52-58.
10. McCarthy, J.C., P.C. Noble, M.R. Schuck, J. Wright, and J. Lee, *The Otto E. Aufranc Award: The role of labral lesions to development of early degenerative hip disease*. Clin Orthop Relat Res, 2001(393): p. 25-37.

11. Leunig, M., D. Podeszwa, M. Beck, S. Werlen, and R. Ganz, *Magnetic resonance arthrography of labral disorders in hips with dysplasia and impingement*. Clin Orthop Relat Res, 2004(418): p. 74-80.
12. Haas, A. and M.S. Fischer, *Three-dimensional reconstruction of histological sections using modern product-design software*. The Anatomical Record, 1997. **249**(4): p. 510-516.
13. Al-Najjar, B.a.A., Imad, *Selecting the most efficient maintenance approach using fuzzy multiple criteria decision making*. Int. J. Production Economics, 2003. **84**: p. 85-100.
14. Ganz, R., J. Parvizi, M. Beck, M. Leunig, H. Notzli, and K.A. Siebenrock, *Femoroacetabular impingement: a cause for osteoarthritis of the hip*. Clin Orthop Relat Res, 2003(417): p. 112-20.
15. Lavigne, M., J. Parvizi, M. Beck, K.A. Siebenrock, R. Ganz, and M. Leunig, *Anterior femoroacetabular impingement: part I. Techniques of joint preserving surgery*. Clin Orthop Relat Res, 2004(418): p. 61-6.
16. Notzli, H.P., T.F. Wyss, C.H. Stoecklin, M.R. Schmid, K. Treiber, and J. Hodler, *The contour of the femoral head-neck junction as a predictor for the risk of anterior impingement*. J Bone Joint Surg Br, 2002. **84**(4): p. 556-60.
17. Palmer, W.E., *Femoroacetabular impingement: caution is warranted in making imaging-based assumptions and diagnoses*. Radiology, 2010. **257**(1): p. 4-7.

## Appendices

### Appendix A: 3D Reconstructive Software Assessment Form and Final Questionnaire

Evaluator: \_\_\_\_\_

Software Program: \_\_\_\_\_

#### 3D Modeling

		Strongly Disagree					Strongly Agree		Not Available
		1	2	3	4	5	6	7	
1.	Creating a surface-rendered model is easy								N/A
2.	Esthetics of a surface-rendered model are pleasing								N/A
3.	I perceive the anatomical accuracy of the surface-rendered model to be high								N/A
4.	Creating a volume-rendered model is easy								N/A
5.	Esthetics of a volume-rendered model are pleasing								N/A
6.	I perceive the anatomical accuracy of the volume-rendered model to be high								N/A
7.	Overall this software has useful 3D modeling tools for research purposes								N/A
8.	I would use this software to build 3D models for research purposes								N/A
9.	Overall this software has useful 3D modeling tools for educational purposes								N/A
10.	I would use this software to build 3D models for educational purposes								N/A

Comments: -

---



---

Evaluator: \_\_\_\_\_

Software Program: \_\_\_\_\_

**Measurement Tools**

		Strongly Disagree						Strongly Agree	Not Available
11.	Utilizing the 2D measurement tools is easy	1	2	3	4	5	6	7	N/A
12.	I perceive the 2D measurement tools to be accurate	1	2	3	4	5	6	7	N/A
13.	Overall this software has useful 2D measurement tools for research purposes	1	2	3	4	5	6	7	N/A
14.	Utilizing the 3D measurement tools is easy	1	2	3	4	5	6	7	N/A
15.	I perceive the 3D measurement tools to be accurate	1	2	3	4	5	6	7	N/A
16.	Overall this software has useful 3D measurement tools for research purposes	1	2	3	4	5	6	7	N/A
17.	I would use this software for clinical measurement research	1	2	3	4	5	6	7	N/A

Comments: -

---



---

Evaluator: \_\_\_\_\_

Software Program: \_\_\_\_\_

**Educational Tools**

		Strongly Disagree						Strongly Agree	Not Available
18.	Quality of the movie function is high	1	2	3	4	5	6	7	N/A
19.	Utilizing the movie function is easy	1	2	3	4	5	6	7	N/A
20.	Quality of the stereo capabilities is high	1	2	3	4	5	6	7	N/A
21.	Utilizing the stereo capabilities is easy	1	2	3	4	5	6	7	N/A
24.	Overall this software has useful 3D educational tools for creating learning tools	1	2	3	4	5	6	7	N/A
25.	I would use this software to create an educational tool	1	2	3	4	5	6	7	N/A

Comments: -

---



---

**3D Reconstructive Software Comparison Final Questionnaire**

Which program would you use if you based your judgment on interface only?

---

Which program would you use to build a 3D model?

---

Which program would you use to conduct clinical measurements?

---

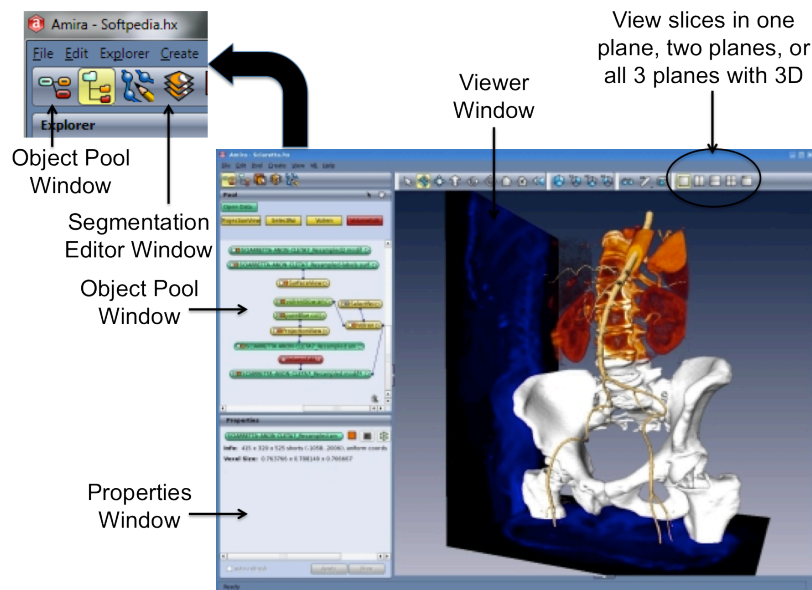
Which program would you use to create an educational tool?

---

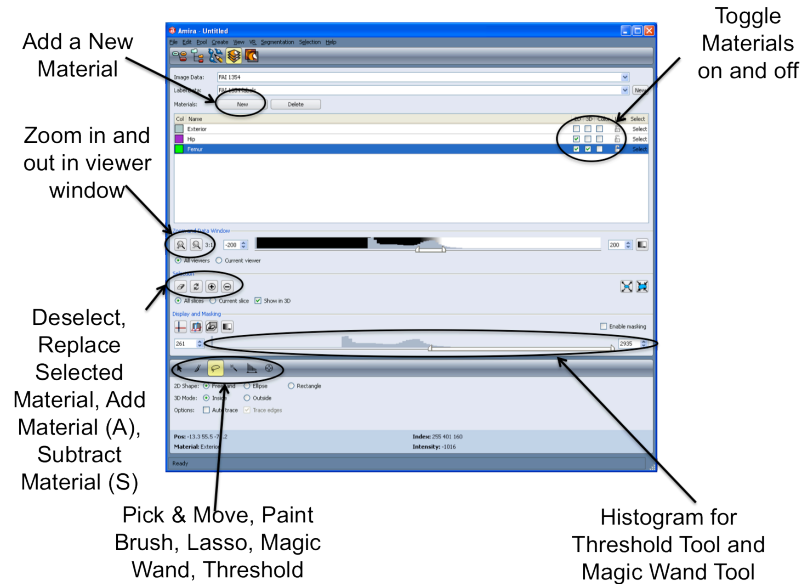
## Appendix B: Amira Instructional Guide

### Amira Instructional Guide

#### Main Viewer Screens:



## Segmentation Editor Window:



- Note that on your workstation the *Viewer Window* will appear on the LEFT Screen and the *Object Pool Window* and *Properties Window* will appear on the Right Screen

### Amira Keyboard Shortcuts:

Ctrl – Erase

F – Fill

A – Add to Material

S – Subtract from Material

### Step 1: Importing Data

- Select *Open Data*
  - o Go to *C:/Documents and Settings/User/Desktop*
    - Find the *Hip CT Data Folder*
      - Select all data files
  - o Select *Load* to load the sequences
    - Select *OK* to load the data to Amira



- You should now see a *FAI 1354* label in your pool window
  - Note that you can move the labels around in the object pool window to your desired location
- To save your model select *File* from the main menu bar
  - Select *Save Network As...*
  - Choose a location to save your data (desktop is easiest)
    - Ensure the File Type is selected as *All Files (\*)* and *Amira Script and Data Files (pack & go)(.hx)*

### Step 2: Creating 3D Models

- In the *Object Pool Window*:
  - Select your dataset
    - Select the *Isosurface button*
      - Select *Apply* in the *Properties Window*
        - Note in the *Object Pool Window* you can toggle structures on and off by using the orange square on the label
        - Note the isosurface model contains all structures found on the CT Scan

### Step 3: Separating Structures

- Delete the Isosurface you created in the *Object Pool Window*
- Right click the data set
  - Select *labeling* from the pull-down menu
    - Select *Labelfield*
      - Note you can also get to the *Segmentation Editor Window* by clicking the Segmentation Editor Button above the *Object Pool Window*
- You are now working within the *Segmentation Editor Window*
  - All materials are labeled as *Exterior*
  - Change the *Inside* material label to *Hip* as we need to segment all bone first
    - Note you can toggle the *Materials On and Off*, in 2D and 3D, in the *Segmentation Editor Window*
    - Note in the *Viewer Window* you can toggle between 4 screens: single plane, two planes, or all 3 planes with 3D
- Tools you can use for Segmentation are found in the *Segmentation Editor Window*
  - Paintbrush: can highlight voxels individually
  - Lassou: Can outline a shape of differing pixel intensities

- Threshold: Uses a histogram of structure intensities to select one structure type
    - Use the slider in the *display and masking* box to find the correct threshold
    - Need to hit *select* after you have found the appropriate threshold
  - Magic Wand: When you click a certain intensity it will select
    - Once you have selected the region of interest you can Add or Subtract from the materials slice by slice
    - Can use a threshold to increase or decrease the voxels include in the magic wand selection
- To add a selected structure to a highlighted Material select “+” in the Segmentation Editor Window or hit the “A” button on the keyboard
- To remove a selected structure from a highlighted Material select “-” in the Segmentation Editor Window or hit the “S” button on the keyboard
  - To deselect a selected structure select the *Clear Current Selection* button
- To isolate all bone use the *Threshold* button to isolate the bone voxels
    - You can do this using the slider in the *Display and Masking Window*
    - Zoom in using the *Zoom* button in the *Segmentation Editor Window*
    - Select *Select* after you have found the appropriate threshold
      - Ensure *All Slices* under *Options* is selected
        - Note a change in colour
      - Add your selected structures to your *Hip* material by selecting the “+” button in the segmentation editor window or by pressing “A” on the keyboard
        - Note the bone is now the same colour as your ‘hip’ material
  - To separate the femur from the acetabulum
    - Add another Material Label select *New* from the Segmentation Editor Window
      - Repeat the steps above to add all bone to the *Femur* Material Label
        - Now work with the other segmentation tools to remove the acetabulum from the *Femur* Material Label
        - Remove your selected structures from the *Femur* material by selecting the “-” button in the segmentation editor window or by pressing “S” on the keyboard
    - Select the *Lassou* tool to select large areas of the acetabulum for removal

- You can remove structures slice by slice or you can remove them in 3D, via the 3D model in the bottom right hand corner, in the *4 viewers window*
- Select the *Magic Wand* tool to remove parts of the acetabulum when the femur is present on the slice
  - You can change the threshold that the Magic Wand selects in the Segmentation Editor Window
  - If the Magic Wand selects both the femur and the acetabulum re-add the femoral head to the material label by using the *Brush* tool

#### Step 4: Create A 3D Model of the Femur

- Ensure the 3D button is selected next the *Femur* Material Label in the Segmentation Editor Window
  - Go back to the *Object Pool Window*
    - Right-click the data set
      - Select *SurfaceGen*
    - Choose level of smoothing
      - None: does not smooth at all and structure will look like the voxels that make it up
      - Constrained Smoothing: takes away the rough edges of the voxels without adding too much error
      - Unconstrained Smoothing: Ensures a smooth surface good for esthetics but not necessarily good for anatomical accuracy
    - Select *Apply*
    - Select the *labelssurf* tab the *SurfaceGen* created and select *Surface View*
      - If the entire 'Exterior' material or 'Hip' material is visible select the material(s) you want to remove from the *Material* pull-down menu in the *Properties Window* and select *Remove*
      - If the 'Femur' material is not present select 'Femur' from the *Material* pull-down menu in the *Properties Window* and select *Add*
- Note you can only create a surface-rendered model in Amira
  - **Please rate all of the 3D modeling criteria and make any necessary comments**

### Step 5: Measurements

- On your 3D model
  - o Select the *2D Length* button
    - Measure the diameter of the femoral head
    - Move the model around
      - Note that the 2D measure is not associated with the 3D model
      - Note that all measurements can be toggled and named in the properties box
  - o Select the *2D Angle* button
    - From the center of the femoral head measure the angle of the fovea
    - Move the model around
      - Note that the 2D measure is not associated with the 3D model
  - o Select the *2D Annotate* button
    - Label the Lesser Trochanter
      - Note that you change the text of the annotation in the *Properties Box*
    - Move the model around
      - Note that the 2D measure is not associated with the 3D model
  - o Select the *3D Length* button
    - Measure the diameter of the femoral head
    - Move the model around
      - Note that the 3D measure is associated with the 3D model and can only be measured within the confines of the model
      - Note that the 3D measure does not measure the surface of the model but measures directly from point A to point B
  - o Select the *3D Angle* button
    - From the center of the femoral head measure the angle of the fovea
    - Move the model around
      - Note that the 3D measure is associated with the 3D model and can only be measured within the confines of the model
      - Note that the 3D angle does not measure the surface of the model but measures directly from point A to point B
  - o Select the *3D Annotate* button
    - Label the Lesser Trochanter
      - Note that you change the text of the annotation in the *Properties Box*

- Move the model around
    - Note that the 3D measure is associated with the 3D model and can only be added within the confines of the model
- Note that all measurements are listed in the *Properties Box*
  - On the *Object Pool Window* right-click the data *labelsurf\** file
    - Select *Measure*
      - Select *Surface Area*
        - Select *Apply* in the *Properties Box*
        - Ensure the *labelsurfstatistics\** label is clicked
          - Select *Show* in the *Properties Box*
            - Note that this screen calculates the area and volume of your model and other materials
- Note that measurement tools can only be used on the 3D model and not the 2D scans
  - **Please rate all of the measurement criteria and make any necessary comments**

#### Step 7: Creating a Movie

- In the *Object Pool Window* Right-click the original data file (not the data file from the model you created)
  - Select *BoundingBox* and *Orthoslice* to the data
    - Click on the *Orthoslice* label
      - Note that in the *Properties Box* you can scroll through the 2D slices using the *Slice Number* slider
        - Note the *Slice Number* that correlates to the top and bottom of your 3D model
- To animate scrolling through the slices select *Create* from the main menu bar
  - Select *Animation/Demo/Demomaker* from the pool down menu
    - Click on the Blue *Demomaker* label that appeared in the *Object Pool Window*
      - To animate an element of your model you must select it the *GUI element* pull-down menu
        - Find the *OrthoSlice/Slice Number* element from the *GUI element* pull-down menu
      - The start and end value, that appear below the *GUI element* pull-down menu, will specify the values in which the *OrthoSlice* slider will be moved
        - Set the desired start and end values for your *OrthoSlice* animation from the top to the bottom of your model
        - Set the desired time to 0 and .2

- Note your time frame always has to be between 0 and 1
  - Select *Add* to add the animation to the *Event List*
    - Note you can test your animation by pressing the play button on the *Time* slider, just ensure that the slider is at the beginning
- To animate the bone to come up segmentally with the *OrthoSlice* slider select *DemoMaker*
  - Select *SurfaceView/Viewer mask/Viewer 0* from the *GUI element list*
    - Select *Toggle* to *on* and a trigger time to *.3*
    - Click *Add* in the *Event List*
  - Select *SurfaceView/Clip using OrthoSlice* from the *GUI element list*
    - Select *Toggle* to *on* and a trigger time to *.3*
    - Click *Add* in the *Event List*
  - Now, select *OrthoSlice/Slice Number* from the *GUI element* pull-down menu
    - Enter your desired start and end values for your *OrthoSlice* animation but now we want to go from the bottom to the top of your model
    - Enter *.3* and *.5* as the start/end time
      - Click *Add* to the *Event List*
        - Note: you can press play on the time slider to check your animation at any time
- To animate a rotation of your model
  - Select *Create/CameraRotate* from the main menu
    - Try the rotation of your model using the time slider in the *Camera Rotate Properties* Box
      - If you are satisfied with the rotation add it to the event list; if not, change the orientation of the model and try again
        - Click on the *DemoMaker* label;
        - Click *Update* to update the GUI elements
        - Select *CameraRotate/Time* from the *GUI element* list
          - Enter 0 and 360 as the start and end value
          - Enter *.5* and *.7* as the start and end time
          - Click *Add* to add the animation to the *Event List*
- Press the play button on the time slider to watch your completed animation
  - Note: If you need to edit any portions of your animation use the *Event List* pull-down menu and make any necessary changes
    - Once the changes are complete select the *Replace* Button under the *Event List*
  - Note: The features completed in this animation can be modified and changed to provide a variety of model manipulations for animations

- To save the movie as movie file right click on *DemoMaker* and select *MovieMaker*
  - o In the *MovieMaker* module:
    - Choose a file name and location (desktop is easiest) for your movie file (ensure it is an .mpg file)
    - You can change the parameters of the movie to your liking ie. *number of frames, image size, or compression quality*
      - For your movie file select 100 frames and leave other parameters untouched
        - o Select *Apply* to record
- Find your movie file on the desktop and review it.
  - **Rate the quality of the movie function for educational purposes**
  - **Rate the usability/ease of use of the movie function**

### Step 8: 3D Visualization

- Using the Red/Blue 3D glasses play with your model in 3-dimensions
    - o Select the *Stereo* Button
    - o Select *Red/Cyan Stereo* from the pull-down menu
    - o Ensure the stereo box is checked
  - Using the Amber/Blue 3D glasses play with your model in 3D
    - o Select the *Stereo* Button
    - o Select *Blue/Yellow Stereo* from the pull-down menu
    - o Ensure the stereo box is checked
      - Note: you can also visualize the 3D models in stereoscopic display using dual projectors and a silver screen
- **Rate the quality of the stereo capabilities**
  - **Rate the usability/ease of use of the stereo capabilities**
  - **Please complete the ratings for the educational criteria and make any necessary comments**

## Appendix C: OsiriX Instructional Guide

### Osirix Instructional Guide

Navigation Windows:



Database Window:

The screenshot shows the OsiriX Database Window with the following components labeled:

- Toolbar**: Located at the top of the window, containing icons for various functions like Import, Export, and Anonymize.
- Patient list**: A table listing patient information, including Patient name, Patient ID, Accession Number, Study Description, Modality, ID, and Comments.
- Thumbnails**: A small grid of image thumbnails on the left side of the window.
- Preview**: A large central area displaying a 2D axial CT scan of a chest.

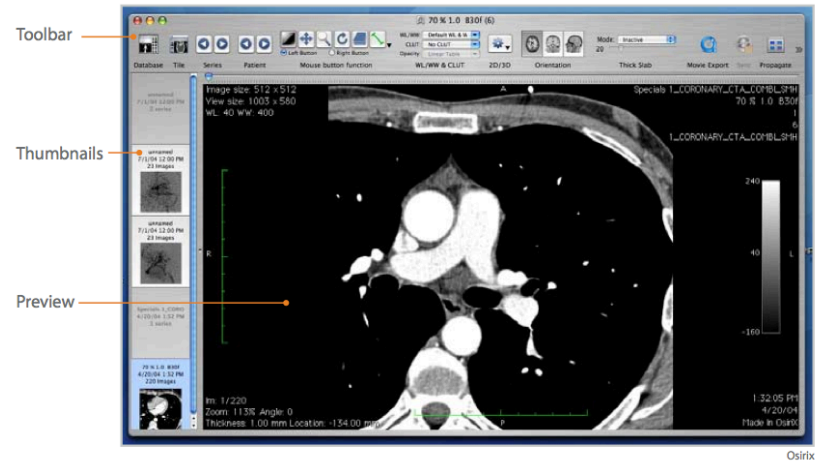
To the right of the screenshot is a list of tools available in the software:

#### TOOLS YOU CAN USE

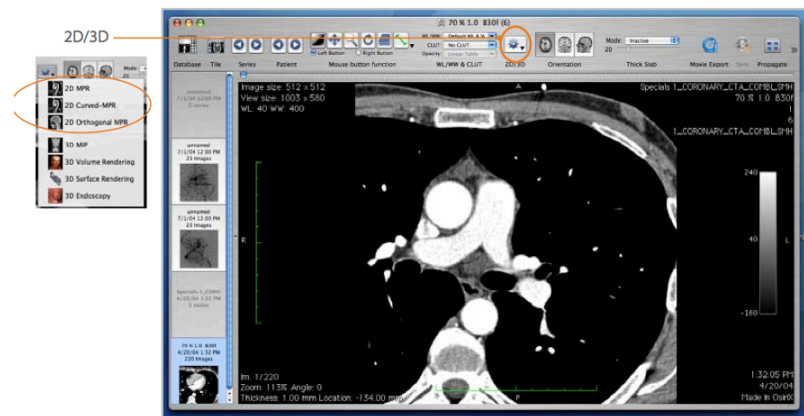
- Import**: Import data
- CD-Rom**: Import from cd
- Export**: Export data
- Anonymize**: Anonymize remove ID
- iPod**: Export to iPod
- 2D-3D Viewer**: Open window
- 4D Viewer**: Sync PET and CT scans
- Burn**: Burn cd
- Albums & Sources**: Create data sets




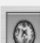

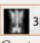
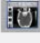
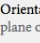
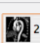


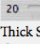
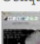
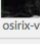



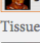

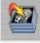





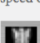


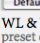

## Viewer Window:



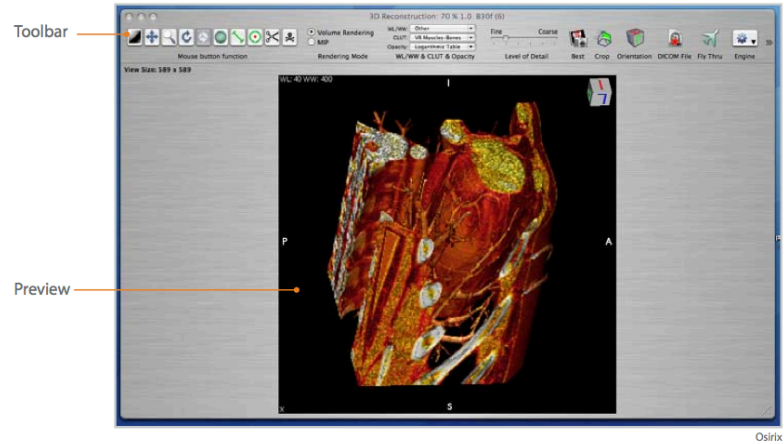
Osirix



Osirix

TOOLS YOU CAN USE		TOOLS YOU CAN USE		TOOLS YOU CAN USE		TOOLS YOU CAN USE	
	<b>Database</b> return to window		<b>Orientation</b> plane of reference		<b>2D/3D</b> open 3D window		<b>3D MIP</b>
	<b>Tile</b> tile view		<b>Thick Slab</b> change slab thickness		<b>2D MPR</b> Oblique planes across data		Contrast (vasculature) <a href="http://osirix-viewer.com/Snapshots.html">osirix-viewer.com/Snapshots.html</a>
	<b>Series</b> previous/next		<b>Movie Export</b> create a Quicktime movie		<b>2D Curved-MPR</b> Curved planes across data		<b>3D Volume Rendering</b> Tissue intensity values <a href="http://osirix-viewer.com/Snapshots.html">osirix-viewer.com/Snapshots.html</a>
	<b>Patient</b> previous/next		<b>Browse</b> display cine images		<b>2D Orthogonal MPR</b> Axial, coronal, sagittal planes		<b>3D Surface Rendering</b> Rendering volume for 3D programs <a href="http://osirix-viewer.com/Snapshots.html">osirix-viewer.com/Snapshots.html</a>
	<b>Contrast Adjustment</b> contrast & intensity		<b>Loop</b> 10.0 im/s speed of browse button		<b>3D Panel</b> data in 3D		<b>3D Endoscopy</b> Navigate through lumen <a href="http://osirix-viewer.com/Snapshots.html">osirix-viewer.com/Snapshots.html</a>
	<b>Move and Pan</b> command key		<b>Print</b> print image				
	<b>Zoom</b> shift key		<b>Sync</b> applies changes to all images				
	<b>Rotate</b> horizontally move		<b>Propagate</b> ROI to all images in stack				
	<b>Scroll</b> through image set						
	<b>Length</b> measure distance						
<b>Default WL &amp; W</b> <b>WL &amp; WW</b> preset contrast and intensity <b>No CLUT</b> <b>CLUT</b> Color Look Up Tables assign color							

### 3D Volume Rendering Window:



TOOLS YOU CAN USE	
	<b>Contrast Adjustment</b> contrast & intensity
	<b>Move and Pan</b> command key
	<b>Zoom</b> shift key
	<b>Rotate</b> horizontally move
	<b>Manipulate</b> around center of gravity
	<b>Angle of View</b> camera position
	<b>Length</b> measure distance
	<b>Tag Reference Points</b> specific feature
	<b>Sculpt 3D Object</b> scissors cut out
	<b>Bone Removal</b> removes bone
WL/WW: Other	
preset contrast and intensity	
CLUT: VR Muscles-Bones	
Color Look Up Tables assign color	
Opacity: Logarithmic Table	
Opacity preset opacities	
Fine Coarse Detail fine course	
TOOLS YOU CAN USE	
	<b>Best Rendering</b> resolution
	<b>Crop Volume</b> frame to crop
	<b>Orientation</b> toggles box in corner on/off
	<b>DICOM file</b> export DICOM
	<b>Fly Thru</b> animated movie
	<b>Engine</b> Ray cast 3D texture
<input checked="" type="radio"/> Parallel <b>Perspective</b> <input type="radio"/> Perspective advanced <input type="radio"/> Endoscopy	
<input checked="" type="checkbox"/> <b>Shading</b> Ambient: 0.2 Edit Diffuse: 0.9 Specular: 0.3-15.0 <b>Shading advanced</b>	

### Step 1: Importing Data

- *Import* the Hip CT Data from the desktop

### Step 2: Creating 3D Models

- Select the *2D Viewer* button to view the 2D Viewer Screen:
  - o Create a 3D volume-rendered model of the hip bones
    - Using the *2D/3D* pull-down menu create volume-rendered model
      - If more than bone appears in the 3D model (soft tissue) select *high contrast* from the *3D presets* pull-down menu
    - Use the *delete key* button to clean up the model
      - Highlight what you want to keep and press *Return*
  - o Create a 3D surface-rendered model of the hip bones
    - Using the *2D/3D* pull-down menu create volume-rendered model

### Step 3: Separating Structures

- Close the 3D viewer screen(s)
- In the 2D viewer screen:
  - o To isolate bone use the *window level (WL)* button to change the contrast
    - Adjust the contrast while holding the right click on the mouse
    - Adjust until bone is really white and all other structures are black
  - o To select the femur as your Region of Interest (ROI) select the *Grow Region (2D/3D Segmentation)* tab from the *ROI* pull-down menu, **from the main menu**
    - Select *3D Growing Region (entire series)* to select your region of interest throughout the entire CT dataset
    - Set the *interval* to 2000 to select the threshold
    - Click a point on the femur that is solid white
    - Select *Compute*
      - Scan through dataset to ensure the entire femur (and not pelvis) is highlighted as a region of interest
        - o If not increase/decrease *interval* as necessary
      - Note: that the majority of the femur has now been highlighted
  - o In the *ROI* menu select *ROI manager*
    - Change the name of the region of interest to reflect the structure
  - o To isolate **ONLY** the femur

- In the *ROI* pull-down menu, **from the main menu**, select *Set Pixel Values to...*
  - Make sure the *ROIs with same name as the selected ROI* is selected
  - Make sure the *Outside ROIs* button is selected
  - Make sure the *To this new value:* is selected
    - This value should be the default number for black -3024)
  - Click OK

#### Step 4: Create A 3D Model of the Femur

- Create a 3D Surface rendered model of the femur
  - Select *2D/3D* Button
  - Select *3D Surface Rendering*
  - Uncheck *Decimate*
  - Select *CT bone* from the *Predefined Values* drop-down menu
- Create a 3D volume rendered model of the femur
  - Using the *2D/3D* pull-down menu create volume-rendered model

#### Step 5: Fixing Void Defects in Model

Note the 3D model had holes and voids to get rid of them we need to fill in the voids for the femoral head

- Close the 3D viewer screen
- In the 2D viewer screen:
  - Using the scroll function find the scan at the most inferior aspect of the femoral head
  - Using the *Zoom* button increases the size of the slice so that you can see the voids in the model accurately
  - On the *ROI Tool* pull-down menu, **on the 2D viewer screen**, select the *brush* tool (Click and Drag)
    - Select a small size for the *brush* tool
    - Use the *brush* tool to add pixels to the voids on each slice
      - For anatomical accuracy do not place the pixels outside of the current highlighted pixels
    - Add pixels to complete the outline of the femur on each slice, working your way up until you complete the femoral head
  - To fill-in your ROI automatically select *Brush ROI's* from the *ROI* pull-down menu, **from the main menu**
    - Select *Closing* to close in the majority of the area
  - Select *OK*

### Step 6: Create a 3D Model of your ROI

- Select *ROI Volume* from the *ROI* pull-down menu, **from the main menu**
    - o Select *Compute Volume*
      - Note: the choppy/blocky appearance of the model
        - Play with the features of the *ROI Volume* to see how this changes the model
          - o *Power Crust* vs. *Delaunay*
          - o *Show Surface*, *Show Wireframe*, *Show Points*, *Textured*, *Opacity*
            - Ensure *Power Crust* is checked
    - o To visualize your ROI in the standard 3D window create a surface-rendered 3D model of the femur using the instructions from **Step 4**
      - Select *ROI Manager* and check the box to make your ROI appear
        - Note: the ROI shows up on top of the original 3D surface-rendered model
        - Note: this feature is useful for materials that show up black in CT ie. Lungs
        - Note: there is not an easy way to fill-in the holes of an 3D model in Osirix
- **Please rate all of the 3D modeling criteria and make any necessary comments**

### Step 6: 2D Plane Measurements

- Select the *ROI Tool* button, **on the 2D view screen**
  - o Select the *Length* button
    - Measure the diameter of the femoral head on a center cut scan
  - o Select the *Oval* button
    - On the center cut scan create a best fit circle around the femoral head
      - Note OsiriX automatically calculates the area of the oval
  - o Select the *Angle* button
    - From the center of the femoral head measure the angle of the fovea
  - o Select the *Rectangle* button
    - Form a rectangle around the femoral head
      - Note OsiriX automatically calculates the area of the rectangle
  - o Select the *Text* button
    - Create a text box to label the fovea
  - o Select the *Open Polygon* Button
    - Create an open polygon outlining the femoral head leaving the polygon open at the fovea

- Note OsiriX automatically calculates the area of the Polygon
- Select the *Closed Polygon* Button
  - Create a polygon outlining the femoral head
    - Note OsiriX automatically calculates the area of the Polygon
- Select the *Pencil* Button
  - Outline the femoral head using the *Pencil* function
    - Note OsiriX automatically calculates the area of the shape created by the pencil
- Select the *Point* Button
  - Place a point on a recognizable part of the femoral anatomy, ensure it is placed on the outer surface of the anatomy.
  - Create a 3D Surface Rendered model following Step 4.
    - Note the point you placed on the 2D scan appears on the 3D model
    - Note that point is the only measurement tool available in the 3D Volume Rendering Window
  - Create a point on a recognizable part of the femoral anatomy on the 3D model
    - Note the point you placed on the 3D model appears on the 2D scan
      - Note that these points could be used to mark a structure in either 2D or 3D
- **Please rate all of the measurement criteria and make any necessary comments**

#### Step 7: Creating a Movie

- In the 3D Volume Rendering Window create a movie using your 3D model
  - Use the *Fly Thru* button to create the points of interest for your movie
    - Ensure that you capture each orientation of your model using the *Orientations* buttons
    - Under the *Movie* tab within the *Fly Thorough* pop-up menu select *Compute* and then *Play* to visualize your movie
  - Export your movie as a Quicktime Movie
    - Under the *Movie* tab select *Save*
    - Save the movie to a known location (desktop is easiest)
      - Watch your quicktime movie from the saved file
- **Rate the quality of the movie function for educational purposes**
- **Rate the usability/ease of use of the movie function**

**Step 8: 3D Visualization**

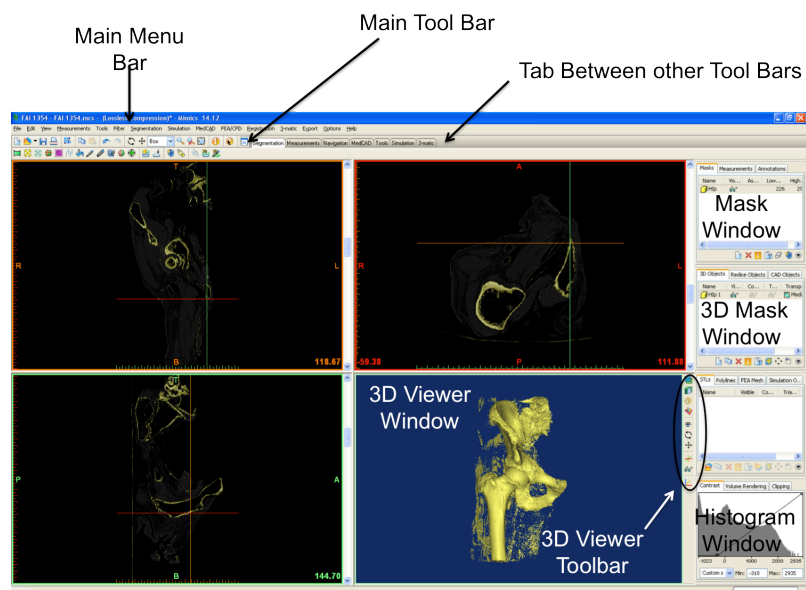
- While viewing a surface rendered model of your femur select the *Stereo* Button
    - o Using the Red/Blue 3D glasses play with your model in 3-dimensions
      - Note: Osirix only has stereo anaglyph capabilities
- **Rate the quality of the stereo capabilities**
  - **Rate the usability/ease of use of the stereo capabilities**
  - **Please complete the ratings for the educational criteria and make any necessary comments**



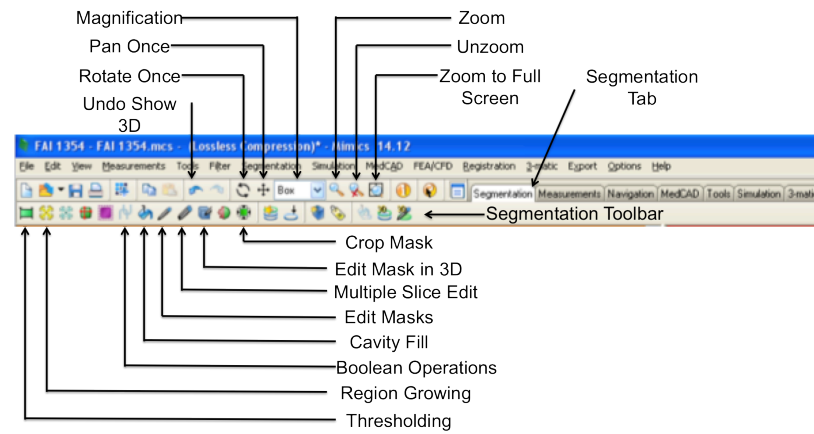
## Appendix D: Mimics Instructional Guide

### Mimics Instructional Guide

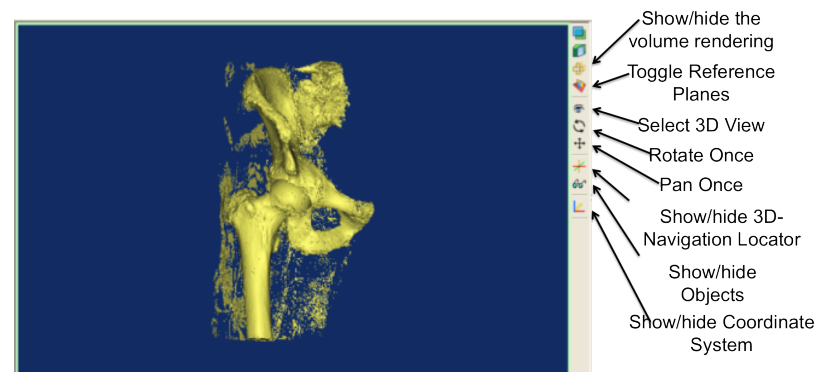
#### Mimics Main Windows:



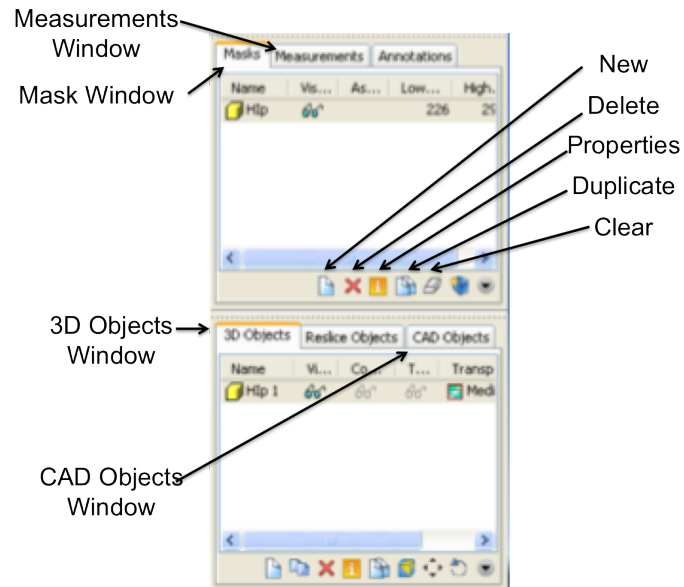
### Mimics Toolbars:



### 3D Viewer Window and Toolbar



### Mask and 3D Object Windows



### Step 1: Importing Data

- Select *File*
  - o Select *New Project Wizard*
    - Find the *Hip CT Data* Folder from the desktop
      - Select all data files
  - o Select *Next* to load the data
    - Select *Convert* to load the data to Mimics
      - Note a screen will show up displaying the orientations of all of the slices
  - o Select *OK*
- To save your model select *File* from the main menu bar
  - o Select *Save Project As...*
  - o Choose a location to save your data (desktop is easiest)
    - Name your file
  - o Select *Save*

### Step 2: Creating 3D Models

- Note that you automatically visualize your data in all 3 planes and there is a 3D viewer window
  - o To visualize one plane/or 3D viewer in full-screen select the *Zoom to Full Screen* from the *Main Tool Bar*
- To create a 3D model of the bone select *New* in the *Mask Window*
  - o A *Thresholding Window* will pop-up select the *Bone (CT)* element from the *Predefined thresholds sets*: pull-down menu
  - o Check the *Fill Holes* Box
  - o Select *Apply*
    - Name your new Mask in the *Mask Window* to '*Threshold*'
- To eliminate all extra material segmented via thresholding select the *Region Growing* button from the *Segmentation Toolbar*
  - o A *Region Growing* window will pop-up
    - Note we will be growing the region from the *Source: 'Threshold'* to a new mask
      - Click on a highlighted portion of the bone
        - o Name your new Mask in the *Mask Window* to '*Hip*'
        - o Note you can toggle your masks on and off by clicking the sunglasses next to each mask in the *Mask Window*
- To create a surface-rendered 3D model select *New* in the *3D Objects Window*
  - o A *Calculate 3D* Window will pop-up ensure *Optimal Quality* is checked
  - o Select *Calculate*
    - Ensure you are visualizing all 4 windows or the *3D viewer window* to visualize your model
      - Use the *Rotate Once* or *Pan Once* buttons found in the *3D Viewer Toolbar* to move your model around within the window
        - o Or hold the right-click button to rotate and scroll to zoom in and out
        - o Hold the left-click button and the wheel to pan
- To create a volume-rendered model toggle off your surface-rendered model by clicking the sunglasses next to '*Hip*' in the *3D Objects Window*
  - o In the *Histogram Window* select the *Volume Rendering* tab
    - Select *Bone* from the pull-down menu
      - Ensure you have the *Show/hide the volume rendering* button clicked in the *3D Viewer Toolbar*

### Step 3: Separating Structures

- Uncheck the *Show/hide the volume rendering* button from the *3D Viewer Toolbar*
- Choose a 2D plane to work within by selecting the *Zoom to Full Screen* button from the *Main Toolbar*

Segmentation Tools from the *Segmentation Toolbar*:

- *Thresholding*
  - o Used to first create a mask
  - o Applies a threshold to an entire mask
- *Region Growing*
  - o Allows you to select a connecting region of similar attenuation/threshold
  - o You must select a source (mask) that you are going to grow your region from and a target (existing or new mask)
  - o You can grow a region on ONE slice or MULTIPLE slices throughout the entire dataset
- *Boolean Operations*
  - o Allows you to subtract one mask from another to make a new mask
  - o Or add multiple masks together to make a new mask
- *Cavity Fill*
  - o Allows you to fill in a closed object
  - o You can make the fill the same mask as the mask you are filling or a different mask
  - o You can cavity fill ONE slice or MULTIPLE slices throughout the entire dataset
- *Edit Masks*
  - o Allows you add (*draw*), remove (*erase*) and *threshold* specific regions
    - Lasso – everything you circle will be added, subtracted to your selected mask
      - thresholding everything you circle that falls within the desired threshold will be added to your selected mask
- *Multiple Slice Edit*
  - o Similar to *Edit Masks* this function allows you to add, remove and threshold specific regions on multiple slices
  - o You can manually apply your selection buy using the up and down *Green Arrows* or you can *Interpolate* between to selections
- To separate the femur from the pelvis duplicate your '*Hip*' mask by selecting the *Duplicate Mask* button from the *Mask Window Toolbar*
  - o You can either remove the pelvis from this mask or remove the femur
    - In this case let's remove the pelvis from the mask thus name your new mask '*Femur*'
  - o Find the scan with the largest spherical portion of the femoral head
    - Select the *Multiple Slice Edit* Button from the *Segmentation Toolbar*

- Select *Lasso* from the *Type*: pull-down menu
- Ensure *Select* is checked
- Select *Remove* from the *Operation on active mask*: pull-down menu
  - With the mouse draw a large region around the bony pelvis avoiding the femoral head (it is ok if you miss some of the bony pelvis close to the femoral head)
  - Scroll 'down' through the slices to the slice where you can see the bottom of the bony pelvis
  - Highlight a similar area that you highlighted earlier once again avoiding the region of the femur
  - Select the *Interpolate* button
  - Select *Apply*
    - Note that you have now removed a large region of the bony pelvis from the '*Femur*' mask
  - Now scroll 'up' through the slices to the slice where you can no longer see the femoral head
  - Highlight the entire CT scan
  - Scroll 'up' through the slices to the slice where the bony pelvis ends
  - Once again highlight the entire CT scan
  - Select the *Interpolate* button
  - Select *Apply*
    - Note that you have once again removed a large region of the bony pelvis from the '*Femur*' mask
    - Note that now you only have slices surrounding the femoral head that contain any bony pelvis
- You can now use *Edit masks* to remove (*erase*) the remaining pelvis slice by slice or you can continue to use *Multiple Slice Edit*
  - When using *Multiple Slice Edit* you can highlight an area and then use the up and down *Green Arrows* to apply that highlight to the next slice
  - You can add to your selected area on each slice, whatever you add will NOT be added to your previous slices
    - If you accidentally highlight a portion of the femur, remove that region of the highlight by checking the *Deselect* button on the *Multiple Slice Edit* pop-up window and then continue

- Continue until you have completed segmented the femur

#### Step 4: Fixing void Defects in Model

- Now that you have completed segmenting the femur from the pelvis we need to fix the femoral head of defects
  - o Select the *Edit Masks* button
    - Ensure the *Draw* button is checked
    - Use this tool to complete the outer perimeter of the femoral head
    - Complete this process with all slices of the femoral head
- To fill in the femoral head to make it a solid structure select the *Cavity Fill* button
  - o Ensure the *Source* mask is '*Femur*' and ensure the *Target* mask is '*Femur*'
  - o Ensure *Multiple Slice* is UNCHECKED
  - o Apply the cavity fill to any large gaps within the femoral head

#### Step 4: Create A 3D Model of the Femur

- To create a surface-rendered 3D model of your femur select *New* in the *3D Objects Window*
  - o A *Calculate 3D* Window will pop-up ensure '*Femur*' and *Optimal Quality* is checked
  - o Select *Calculate*
    - Ensure you are visualizing all 4 windows or the *3D viewer window* to visualize your femur model
      - Note any time you make any changes to your *Mask* you will have to create a new 3D Model of that mask to visualize the changes in 3D
- **Please rate all of the 3D modeling criteria and make any necessary comments**

#### Step 5: Measurements

2D Measurements:

- On a 2D slice select the *Measurements* tab from the top of the *Mask Window*
  - o Select the *Measure Distance* button
    - Measure the diameter of the femoral head
      - Note that all measurements can be toggled via the sunglasses button and named in the *Measurements Window*
  - o Select the *Measure Angle* button

- From the center of the femoral head measure the angle of the fovea
- Select the *Measure Diameter* button
  - Measure the diameter of the femoral head
    - Note that the *Measure Diameter* tool measures the diameter via a best fit circle as opposed to using the *length* tool
- Select the *Measure Density in Rectangle* button
  - Draw the rectangle around the femoral head
    - Note that this tool measures the area of the rectangle over all scans
- Select the *Measure Density in Ellipse* button
  - Draw the ellipse around the femoral head
    - Note that this tool measures the area of the ellipse over all scans
- Select the *Annotations* tab from the top of the *Measurement Window*
  - Label the Fovea
    - Note that your annotation remains associated with that slice
- Note that all measurements/Annotations are listed in the *Measurements/Annotations Window*
  - You can toggle the measurements on and off via the sunglasses button

### 3D Measurements:

- On your 3D model select the *Measurements* tab from the top of the *Mask Window*
  - Select the *Measure Distance* button from the *New* pull-down menu
    - Measure the diameter of the femoral head
      - Note that the measurement is a length taken directly from point A to point B through the 3D model, but the points are directly associated with the part of the model you clicked
  - Select the *Measure Angle* button from the *New* pull-down menu
    - While looking at a medial view of the fovea with the femur in an upright position, measure the angle between the fovea and the lesser trochanter from the most inferior mid-shaft
      - Note that the measurement is taken directly from point A to point B, which can be through the 3D model, but the points are directly associated with the part of the model you clicked
  - Select the *Measure Diameter* button from the *New* pull-down menu
    - Measure the diameter of the femoral head
      - Note that the *Measure Diameter* tool measures the diameter via a best fit circle as opposed to using the *length* tool



- Note that the diameter is measured at the location on the femoral head that you clicked
  - Select the *Measure Distance Over Surface* button from the *New* pull-down menu
    - Measure the distance over the surface from the center of the fovea to your *Measure Diameter* best fit circle
      - Note that the measurement is taken over the surface mesh of the 3D model
- Select the *Annotations* tab from the top of the *Measurement Window*
  - Label the Fovea
    - Note that your annotation remains associated with the fovea on the 3D slice
- Note that all of these measurements are visible in 3D but not on the corresponding 2D slices

#### Cad Module Objects:

- Using the 4 viewer main window select the *CAD Objects* Tab from the *3D Objects Window*
  - Note all of the features from the *New* pull-down menu with the *CAD Objects* Tab are visible in 3D and on the corresponding 2D slice
    - For instance select *Point* from the *New* pull-down menu
    - Select *Draw*
    - Click to drop the point in the middle of the fovea
      - Find the corresponding 2D slices where this point is visible
    - Play with the other features within the CAD module as you feel necessary

**Please note that Mimics software does not have any educational tools.**

## Appendix E: Decision Matrix

	A	B	C	D	E	F	G
1	Criteria #	Criteria	Rating	Ed weight	Ed Score	M Weight	M Score
2		<b>3D Modeling</b>					
3	1	Creating a surface-rendered model is easy	3.00	7.07	21.21	6.98	20.93
4	2	Esthetics of a surface-rendered model are pleasing	4.33	6.06	26.24	0.00	0.00
5	3	I perceive the anatomical accuracy of the surface-rendered model to be high	4.67	5.05	23.59	8.14	38.01
6	4	Creating a volume-rendered model is easy	0.00	2.02	0.00	5.81	0.00
7	5	Esthetics of a volume-rendered model are pleasing	0.00	1.01	0.00	0.00	0.00
8	6	I perceive the anatomical accuracy of the volume-rendered model to be high	0.00	1.01	0.00	8.14	0.00
9	7	Overall this software has useful 3D modeling tools for research purposes	5.67	0.00	0.00	8.14	46.15
10	8	I would use this software to build 3D models for research purposes	4.00	0.00	0.00	8.14	32.56
11	9	Overall this software has useful 3D modeling tools for educational purposes	5.00	7.07	35.35	0.00	0.00
12	10	I would use this software to build 3D models for educational purposes	4.00	7.07	28.28	0.00	0.00
13		<b>OVERALL</b>	<b>30.67</b>	<b>36.36</b>	<b>134.68</b>	<b>45.35</b>	<b>137.65</b>
14		<b>Mesurement Tools</b>					
15	11	Utilizing the 2D measurment tools is easy	6.00	3.03	18.18	6.98	41.86
16	12	I perceive the 2D measurement tools to be accurate	3.67	3.03	11.12	8.14	29.87
17	13	Overall this software has useful 2D measurement tools for research purposes	3.67	3.03	11.12	8.14	29.87
18	14	Utilizing the 3D measurment tools is easy	6.00	3.03	18.18	6.98	41.86
19	15	I perceive the 3D measurement tools to be accurate	4.33	3.03	13.12	8.14	35.24
20	16	Overall this software has useful 2D measurement tools for research purposes	4.00	3.03	12.12	8.14	32.56
21	17	I would use this software for clinical measurement research	2.67	3.03	8.09	8.14	21.73
22		<b>OVERALL</b>	<b>30.34</b>	<b>21.21</b>	<b>91.94</b>	<b>54.65</b>	<b>233.00</b>
23		<b>Education Tools</b>					
24	18	Quality of the movie function is high	5.00	7.07	35.35	0.00	0.00
25	19	Utilizing the movie function is easy	3.00	7.07	21.21	0.00	0.00
26	20	Quality of the stereo capabilities is high	4.33	7.07	30.62	0.00	0.00
27	21	Utilizing the stereo capabilities is easy	6.00	7.07	42.42	0.00	0.00
28	22	Overall this sorftware has useful 3D educational tools for creating learning tools	5.00	7.07	35.35	0.00	0.00
29	23	I would use this software to create an educational tool	3.67	7.07	25.95	0.00	0.00
30		<b>OVERALL</b>	<b>27</b>	<b>42.42</b>	<b>190.91</b>	<b>0.00</b>	<b>0.00</b>
31			<b>88.01</b>	<b>100.00</b>	<b>644.14</b>	<b>100.00</b>	<b>741.30</b>

## Appendix F: Cadaveric Acetabular Measurements with Labra Removed

### Appendix A: Further Investigation of Validity of a Novel 3D Measurement

#### Approach for the Morphology of the Acetabulum

##### **Methodology**

A random subset of 13 hemi-sectioned pelvises, from the 45 pelvises used in chapter four, were collected for this study. The 13 specimens (9 right; 4 left) were all male and had an average age of  $74.69 \pm 9.28$  years (age range 51-85 years).

Each acetabulum was individually dissected to remove the labrum from the acetabular rim. The angle templates used previously were still intact on the specimens and the cadaveric measurements from chapter four were repeated. To establish the  $0^\circ$  angle a line was drawn from the most anteroinferior portion of the anterior inferior iliac spine to the center of the acetabulum (Fig. 1A). Measurements were made from the acetabular center to the acetabular rim and labrum at each of the 12-degree markers using a bendable ruler (Fig. 1B).



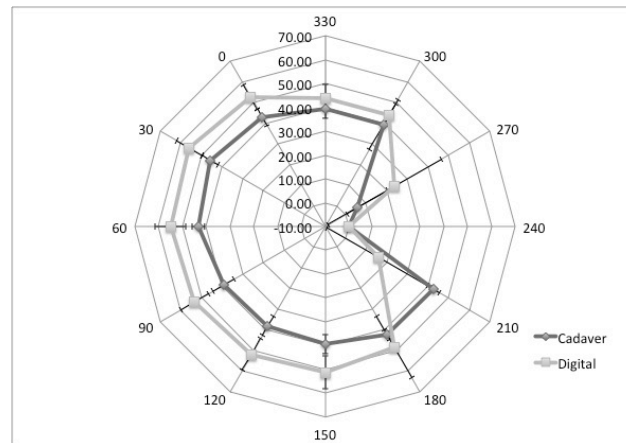
**Figure 1:** Measurement of the cadaveric specimens. A) Establishment of the center of the acetabulum and the  $0^\circ$  angle marker. B) Measurement of the acetabulum from the center

of the acetabulum to the acetabular rim/labrum. Measurements are taken at each of the 12 angle markers.

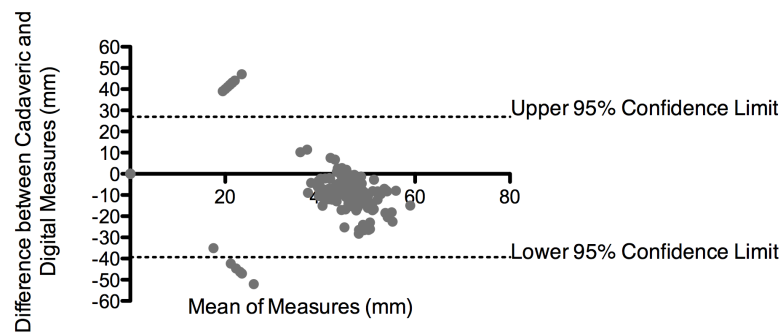
To assess validity of the measurement approach the measurements taken in the study were compared to the first set of digital measurements taken in chapter four, by the same observer (CM). Statistical analysis was performed using *SPSS 16 (SPSS Inc., Chicago, Illinois, USA)* and *Prism 5 (GraphPad Software Inc. La Jolla, California, USA)*. The mean difference between measurements and confidence limits were calculated using the Bland-Altman method.

## **Results**

The radar graph, Figure 2, displays mean acetabular measurements for each modality, cadaveric and digital, at each of the 12 degree points. The points on the radar graph correspond to the points measured on the femoral head (Fig. 1C). Figure 3 illustrates the difference between the mean cadaveric measures and the mean digital measures; the average difference was -6.22mm. The upper and lower 95% confidence limits were 26.92mm and -39.36mm respectively.



**Figure 2:** Radar graph of mean cadaveric measures vs. mean digital measures. The 12 axes represent the 12-degree ( $^{\circ}$ ) points (see Figure 5.1C) where the measurements were taken and the mean measurement ( $\text{mm} \pm \text{SD}$ ) for each degree point is plotted for the cadaveric and digital measures.



**Figure 3:** Bland-Altman plot of the difference between the cadaveric measurements and the digital measurements. The x-axis plots the mean of the measurements produced by each modality against the difference between the measurement modalities (cadaveric - digital) on the y-axis.

## Appendix G: Permissions

### Permission for Figure 2.1

#### WOLTERS KLUWER HEALTH LICENSE TERMS AND CONDITIONS

Aug 21, 2012

is a License Agreement between Charys M Martin ("You") and Wolters Kluwer Health ("Wolters Kluwer Health") provided by Copyright Clearance Center ("CCC"). The license consists of your order details, the terms and conditions provided by Wolters Kluwer Health, and the payment terms and conditions.

**Payments must be made in full to CCC. For payment instructions, please see information listed at the bottom of this invoice.**

License Number	2973791037113
License date	Aug 21, 2012
Licensed content publisher	Wolters Kluwer Health
Licensed content publication	Current Orthopaedic Practice
Licensed content title	Anterior Femoroacetabular Impingement: Part I. Techniques of Joint Preserving Surgery
Licensed content author	Martin Lavigne, Javad Parvizi, Martin Beck, et al
Licensed content date	Jan 1, 2004
Volume Number	418
Type of Use	Dissertation/Thesis
Requestor type	Individual Account
Title of your thesis / dissertation	EXPLORATION OF THREE-DIMENSIONAL MORPHOMETRICS OF THE HIP JOINT AND RECONSTRUCTIVE TECHNOLOGIES
Expected completion date	Oct 2012
Estimated size(pages)	200
Billing Type	Invoice
Billing address	[REDACTED]
Customer reference info	None
<b>Total</b>	<b>0.00 USD</b>
Terms and Conditions	

#### Terms and Conditions

1. A credit line will be prominently placed and include: for books - the author(s), title of book, editor, copyright holder, year of publication; For journals - the author(s), title of article, title of journal, volume number, issue number and inclusive pages.
2. The requestor warrants that the material shall not be used in any manner which may be considered derogatory to the title, content, or authors of the material, or to Wolters Kluwer.
3. Permission is granted for a one time use only within 12 months from the date of this invoice. Rights herein do not apply to future reproductions, editions, revisions, or other derivative works. Once the 12-month term has expired, permission to renew must be submitted in writing.
4. Permission granted is non-exclusive, and is valid throughout the world in the English language and the languages specified in your original request.
5. Wolters Kluwer cannot supply the requestor with the original artwork or a "clean copy."



## Permission for Figure 2.2

# American Roentgen Ray Society

Trys Martin

07/30/12

Invoice No: C 07777

ada

Thank you for your request for permission to reproduce the following material from the *American Journal of Roentgenology*.

0

JR  
38:1540-  
552

Tannast M., Siebenrock  
K.A., Anderson S.E., et al.

Femoroacetabular Impingement: Radiographic  
Diagnosis—What the Radiologist Should Know  
Figure 2

1

0

Order Total \$0.00

Permission is effective when signed below by ARRS authorized representative. Payment if applicable, may be made by check or credit card. Tax is not included in the price, if your country requires a tax, you will have to calculate the tax separately. Permission will not be granted until invoice is paid in full. Please return this form with payment.

The following conditions apply:

Use of the following credit line: Reprinted with permission from the *American Journal of Roentgenology*.  
One-time, non-exclusive use only to include on-line versions and/or CD-ROMS. This permission does not include revisions or future editions.  
Translations of copyrighted text is prohibited.

We regret that ARRS cannot supply original or digital material for reproduction.

ARRS authorized signature: \_\_\_\_\_

Date 8/1/12

Payment Options

Check (made out to ARRS in U.S. funds drawn on a U.S. bank)

\_\_\_\_ Visa \_\_\_\_ American Express \_\_\_\_ Master Card

Card # \_\_\_\_\_ Exp. Date \_\_\_\_\_

Signature: \_\_\_\_\_ Phone # \_\_\_\_\_

Send remittance to: 44211 Slatestone Court Leesburg, VA 20176-5109  
Or fax Credit Card # to 703-729-5913



## Permission for Figure 2.3 and 2.4

### SPRINGER LICENSE TERMS AND CONDITIONS

Aug 21, 2012

This is a License Agreement between Charys M Martin ("You") and Springer ("Springer") provided by Copyright Clearance Center ("CCC"). The license consists of your order details, the terms and conditions provided by Springer, and the payment terms and conditions.

**Payments must be made in full to CCC. For payment instructions, please see information listed at the bottom of this**

License Number	2954880826475
License date	Jul 23, 2012
Licensed content publisher	Springer
Licensed content publication	Skeletal Radiology
Licensed content title	Radiographic measurements of dysplastic adult hips
Licensed content author	S. Delaunay
Licensed content date	Feb 1, 1997
Volume number	26
Issue number	2
Type of Use	Thesis/Dissertation
Portion	Figures
Author of this Springer article	No
Order reference number	None
Title of your thesis / dissertation	EXPLORATION OF THREE-DIMENSIONAL MORPHOMETRICS OF THE HIP JOINT AND RECONSTRUCTIVE TECHNOLOGIES
Expected completion date	Oct 2012
Estimated size(pages)	200
<b>Total</b>	<b>0.00 CAD</b>
Terms and Conditions	

**Introduction**  
The publisher for this copyrighted material is Springer Science + Business Media. By clicking "accept" in connection with completing this licensing transaction, you agree that the following terms and conditions apply to this transaction (along with the Billing and Payment terms and conditions established by Copyright Clearance Center, Inc. ("CCC"), at the time that you opened your Rightslink account and that are available at any time at [REDACTED]).

**Limited License**  
With reference to your request to reprint in your thesis material on which Springer Science and Business Media control the copyright, permission is granted, free of charge, for the use indicated in your enquiry.  
Licenses are for one-time use only with a maximum distribution equal to the number that you identified in the licensing process.  
This License includes use in an electronic form, provided its password protected or on the university's intranet or repository, including UMI (according to the definition at the Sherpa website: <http://www.sherpa.ac.uk/romeo/>). For any other electronic use, please contact Springer at [REDACTED].

The material can only be used for the purpose of defending your thesis, and with a maximum of 100 extra copies in paper. Although Springer holds copyright to the material and is entitled to negotiate on rights, this license is only valid, provided permission is also obtained from the (co) author (address is given with the article/chapter) and provided it concerns original material which does not carry references to other sources (if material in question appears with credit to another source,

authorization from that source is required as well).

Permission free of charge on this occasion does not prejudice any rights we might have to charge for reproduction of our copyrighted material in the future.

Altering/Modifying Material: Not Permitted

You may not alter or modify the material in any manner. Abbreviations, additions, deletions and/or any other alterations shall be made only with prior written authorization of the author(s) and/or Springer Science + Business Media. (Please contact Springer at [permissions.dordrecht@springer.com](mailto:permissions.dordrecht@springer.com) or [permissions.heidelberg@springer.com](mailto:permissions.heidelberg@springer.com))

Reservation of Rights

Springer Science + Business Media reserves all rights not specifically granted in the combination of (i) the license details provided by you and accepted in the course of this licensing transaction, (ii) these terms and conditions and (iii) CCC's Billing and Payment terms and conditions.

Copyright Notice/Disclaimer

You must include the following copyright and permission notice in connection with any reproduction of the licensed material: 'Springer and the original publisher /journal title, volume, year of publication, page, chapter/article title, name(s) of author(s), figure number(s), original copyright notice) is given to the publication in which the material was originally published, by adding: with kind permission from Springer Science and Business Media'

Warranties: None

Example 1: Springer Science + Business Media makes no representations or warranties with respect to the licensed material.

Example 2: Springer Science + Business Media makes no representations or warranties with respect to the licensed material and adopts on its own behalf the limitations and disclaimers established by CCC on its behalf in its Billing and Payment terms and conditions for this licensing transaction.

Indemnity

You hereby indemnify and agree to hold harmless Springer Science + Business Media and CCC, and their respective officers, directors, employees and agents, from and against any and all claims arising out of your use of the licensed material other than as specifically authorized pursuant to this license.

No Transfer of License

This license is personal to you and may not be sublicensed, assigned, or transferred by you to any other person without Springer Science + Business Media's written permission.

No Amendment Except in Writing

This license may not be amended except in a writing signed by both parties (or, in the case of Springer Science + Business Media, by CCC on Springer Science + Business Media's behalf).

Objection to Contrary Terms

Springer Science + Business Media hereby objects to any terms contained in any purchase order, acknowledgment, check endorsement or other writing prepared by you, which terms are inconsistent with these terms and conditions or CCC's Billing and Payment terms and conditions. These terms and conditions, together with CCC's Billing and Payment terms and conditions (which are incorporated herein), comprise the entire agreement between you and Springer Science + Business Media (and CCC) concerning this licensing transaction. In the event of any conflict between your obligations established by these terms and conditions and those established by CCC's Billing and Payment terms and conditions, these terms and conditions shall control.

Jurisdiction

All disputes that may arise in connection with this present License, or the breach thereof, shall be settled exclusively by arbitration, to be held in The Netherlands, in accordance with Dutch law, and to be conducted under the Rules of the 'Netherlands Arbitrage Instituut' (Netherlands Institute of Arbitration). **OR:**

**All disputes that may arise in connection with this present License, or the breach thereof, shall be settled exclusively by arbitration, to be held in the Federal Republic of Germany, in accordance with German law.**

Other terms and conditions:

v1.3

If you would like to pay for this license now, please remit this license along with your payment made payable to "COPYRIGHT CLEARANCE CENTER" otherwise you will be invoiced within 48 hours of the license date. Payment should be in the form of a check or money order referencing your account number and this invoice number RLNK500823726. Once you receive your invoice for this order, you may pay your invoice by credit card. Please follow instructions provided that time.

Make Payment To:

[REDACTED]  
[REDACTED]  
[REDACTED]

## Curriculum Vitae

<b>Name:</b>	Charys Martin (nee Raynor)
<b>Post-secondary Education and Degrees:</b>	<p>The University of Western Ontario London, Ontario, Canada 2002-2006 B.Sc.</p> <p>The University of Western Ontario London, Ontario, Canada 2006-2008 M.Sc.</p> <p>The University of Western Ontario London, Ontario, Canada 2008-2012 Ph.D.</p>
<b>Honours and Awards:</b>	<p>The University of Western Ontario Graduate Student Teaching Award 2011/2012</p> <p>Ontario Graduate Scholarship Science &amp; Technology (OGSST) 2009/2010</p> <p>Dean's Award for Research Excellence for Third Place Oral Presentation. "The Presence of Femoroacetabular Impingement in an Asymptomatic Population" in the Biological Sciences Session at the 22<sup>nd</sup> Annual Western Research Forum 2009</p>
<b>Related Work Experience:</b>	<p>Teaching Assistant The University of Western Ontario Anatomy/Exercise Physiology 2006-2012</p> <p>Sessional Instructor University of Optometry Human Gross Anatomy 2009/2010</p>

Instructor  
 London College of Healthcare and Technology  
 Anatomy and Physiology/Nutrition  
 2008/2009

### **Publications:**

**Martin, C.M.**, Turgeon, J.G., Rice, C.L., Goela, A., and Wilson, T.D.  
 Validity and Reliability of a Novel 3D Measurement Approach of the  
 Acetabulum (*Work in Progress*).

**Martin, C.M.**, Turgeon, J.G., Rice, C. L., Goela, A., and Wilson, T.D.  
 Validity and Reliability of a Novel 3D Measurement Approach of the  
 Proximal Femur (*Under Review with Acta Orthopaedica*).

**Martin, C.M.**, Roach, V.A., Nguyen, N., Rice, C.L., and Wilson, T.D. Comparison of 3D  
 Reconstructive Technologies used for Morphometric Research and the Translation  
 of Knowledge (*Will be submitted to Journal of Digital Imaging*).

**ABSTRACT – Martin, C. M.**, Turgeon, J. G., Rice, C. L., and Wilson, T. D. Validity  
 and Reliability of a Novel 3D Measurement Approach of the Acetabulum. *Poster*  
*Presentation*, AAA at FASEB. San Diego, California. April 2012.

**ABSTRACT – Martin, C.**, and Wilson, T.D. 3D Surface and Volumetric Analysis of  
 Hip Morphometrics. *Poster Presentation*, AAA at FASEB. Washington D.C. April 2011.

**ABSTRACT - Raynor, C.**, Willits, K., Bryant, D., and Spouge A. The Presence of  
 Markers for Femoroacetabular Impingement in Asymptomatic Individuals. *Poster*  
*Presentation*. AAA at FASEB. New Orleans, Louisiana. April 2009.